Alterations of CCSP Expression and Macrophages Metabolism in the Development of Silica-Induced Pulmonary Inflammation and Fibrosis

by

Antonella Marrocco

Laurea Specialistica in Medicina e chirurgia, Seconda Università degli studi di Napoli, Italy, 2008

Diploma di Specializzazione in Medicina del Lavoro, Seconda Università degli studi di Napoli, Italy, 2015

Submitted to the Graduate Faculty of the

Department of Environmental and Occupational Health

Graduate School of Public Health in partial fulfillment

of the requirements for the degree of

Doctor of Philosophy

University of Pittsburgh

2020

UNIVERSITY OF PITTSBURGH

GRADUATE SCHOOL OF PUBLIC HEALTH

This dissertation was presented

by

Antonella Marrocco

It was defended on

June 5, 2020

and approved by

Linda L. Pearce, PhD, Assistant Professor, Department of Environmental and Occupational Health, Graduate School of Public Health, University of Pittsburgh

James Peterson, PhD, Associate Professor, Department of Environmental and Occupational Health, Graduate School of Public Health, University of Pittsburgh

Stacy L. Wendell, PhD, Assistant Professor, Department of Pharmacology & Chemical Biology Director, Health Sciences Metabolomics and Lipidomics Core, School of Medicine, University of Pittsburgh

Bruce Pitt, PhD, Professor, Department of Environmental and Occupational Health, Graduate School of Public Health, University of Pittsburgh

Dissertation Director: Luis A. Ortiz, MD, Professor, Department of Environmental and Occupational Health, Graduate School of Public Health, University of Pittsburgh

Alterations of CCSP Expression and Macrophages Metabolism in the Development of Silica-Induced Pulmonary Inflammation and Fibrosis

Antonella Marrocco, PhD

University of Pittsburgh, 2020

Abstract

Silicosis is a lethal pneumoconiosis, for which no therapy is available. Silicosis is a public health threat: more than 2.2 million people/year in the US and 230 million/year worldwide, are exposed to silica, and consequently are at increased risk of active mycobacterial tuberculosis (TB), and lung cancer. The initial response to silica is mediated by the innate immunity in a two-stage process: 1)injury of conducting epithelium at distal lung, loss of Club cells secretory protein (CCSP), and impairment of regenerative capacity; 2)phagocytosis of silica by macrophages, metabolic alterations, oxidative stress, and release of reactive-oxygen-species (ROS) and inflammatory cytokines, such as Interleukin-(IL-)1β, Tumor necrosis factor-(TNF-)α, Interferon-(IFN-)β. However, the specific role of airway epithelium and macrophage in the pathogenesis of silicosis in humans is poorly understood.

This study focuses on whether silica-induced inflammation compromises the Club cells ability to regenerate bronchiolar and/or alveolar epithelium and on the macrophages metabolic alterations that occurs upon phagocytosis of silica, leading to chronic inflammation.

Using wild-type and CCSP-deficient (CCSP-/-) mice we exhibit that the development of the silicotic nodules in the lung is characterized by peri-bronchiolar inflammatory cell recruitment and tissue fibrosis, that compromises the expression and proliferation of CCSP-expressing progenitor cells and limits the reparative properties of the distal airway epithelium, resulting in

exacerbation of silicosis. We reveal an immunomodulatory role for CCSP in response to silica both in mice and in human lungs.

Subsequently, using murine RAW 264.7 macrophage cell lines, and state- of- art techniques, such as high-resolution respirometer and liquid chromatography-high resolution mass spectrometry (LC-HRMS), to determine the effects of silica on mitochondrial respiration, and the changes in central carbon metabolism of silica-exposed macrophages, we demonstrate that in contrast to the prevalent view, crystalline silica alone induces an innate immune response without previous macrophage activation with LPS, and yet different from the one LPS-induced, since they affect differently the CII of ETC, which plays a crucial role in macrophages survival and silica-induced inflammation.

Our data highlight the urgency to validate these concepts and elucidate the mechanisms underlying the silica-induced impairment of macrophages, development of inflammation and fibrosis, and consequent increased TB risk.

Table of Contents

List of Tables

List of Figures

Preface

I would like to express my deep and sincere gratitude and appreciation to Dr. Ortiz for having allowed me to work in his lab, which has been fundamental in my personal and professional growth. In addition, I would like to thank the members of my committee, Dr. Linda Pearce, Dr. Jim Peterson, Dr. Stacy Wendell and Dr. Bruce Pitt for their commitment, and guidance, and for sparing their valuable time to give me useful comments and suggestions that improved my scientific skills and professional competency.

I would also like to thank, Ariana Detwiler and Dr. Kristyn Frawley, and the entire current and past team of the Ortiz's Lab for their assistance with this work.

I would like to thank Dr. Barchowsky for having been my advisor during the entire journey, and for having given me the possibility to serve as his teaching assistant for many years, the Environmental and Occupational Health Department and the Graduate School of Public Health for having supported me in the last years.

Finally, I would also like to sincerely express my appreciation to my family, my mom, and my brothers, without whom nothing of these would have been possible. Their love, support, patience, and understanding during my entire career allowed me to push myself beyond my limitation, giving me the strength and courage to persevere and always look ahead following my dream.

I want to dedicate my achievement to all of you. We made it!

1.0 Introduction

1.1 Crystalline silica occupational exposure

Crystalline silica, also known as silicon dioxide (SiO_2), is one of the most abundant minerals on Earth. It is an essential component of soil, sand, granite, and many other minerals. The most common form of crystalline silica is quartz; two other forms are cristobalite and tridymite. All three forms may become respirable size particles (silica <10 μm in diameter) when workers chip, cut, drill, or grind objects that contain crystalline silica [1].

More than 2 million workers in the United States and more than 230 million around the world are exposed to silica every year [2-4]. Occupational exposure has been historically associated with work in mining, construction, sandblasting, masonry, foundry operations, glass manufacturing, ceramic and pottery production, and cement and concrete production and with work with specific materials in dental laboratories. However, newly emerging occupations and tasks are increasing the risk of exposure: including fabricating and installing quartz-containing engineered stone products and extraction of natural gas by hydraulic fracturing [3, 5-9]

Inhalation of crystalline silica leads to the development of silicosis, a progressive pneumoconiosis characterized by lung inflammation and fibrosis, for which no specific therapy is available. Silicosis is associated with increased risk of tuberculosis, lung cancer, chronic obstructive pulmonary disease (COPD), kidney disease, and autoimmune disease, with these risks remaining high even when exposure to silica dust has ceased [3, 10, 11].

Silica-related diseases are preventable by avoiding or reducing the exposure to silica dust in the workplace, implementing the ventilation system, the use of wet methods, and the use of

personal protective equipment. Although preventive measures have decreased the mortality attributable to silica exposure in the past decade, this occupational lung disease still kills about 100 people every year in the United States, according to the National Institute for Occupational Safety and Health (NIOSH). Between 1999 and 2013, silicosis was the underlying or contributing cause of death for about 2000 people, and 300 deaths occurred each year between 1991 and 1995, while it decreased to about 100 per year in 2012 and 2013 [5]. Data from NIOSH show that a large number of workers are at increased risk for silicosis because the levels of exposure to silica exceed the current regulatory standards. Therefore, regulatory agencies have been forced to further reduce the permissible exposure levels (PEL) to 25 $\mu g/m^3$ (micrograms of silica per cubic meter of air) over an 8-hour shift, to improve prophylaxis. Despite these efforts, silicosis remains a global health threat.

1.2 Crystalline silica health effects

Silica exposure has been associated with several disorders. Silicosis is the direct consequence of silica exposure, and it is one of the most common occupational lung diseases worldwide [12]. Pathological varieties include simple (nodular) silicosis, progressive massive fibrosis, silico-proteinosis, and diffuse interstitial fibrosis [3].

Increased risk of tuberculosis (TB) has been reported among exposed miners and stone crushers [4, 13, 14]. In agreement, nowadays, it has been estimated that silicosis increases the risk of active TB by up to four-fold, and exposure to silica dust of healthy or paucisymptomatic individuals also has been demonstrated to increase the life-long risk for TB [15]. Reducing exposures to silica decreases the likelihood of developing silicosis, and subsequently, tuberculosis.

Chronic obstructive pulmonary disease (COPD) has also been associated with silica exposure, independent of smoking. In 1997, the International Agency for Research on Cancer (IARC) and subsequently NIOSH and the National Toxicology Program (NTP) classified crystalline silica inhaled in the form of quartz or cristobalite from occupational sources as a human carcinogen (Group 1), due to the correlation between silica exposure and lung cancer.

The presence of silicosis increases the risk of other mycobacterial, fungal, and bacterial lung infections, as well as renal and autoimmune diseases.

1.3 Pathogenesis of silicosis

The understanding of the pathogenesis of silicosis is incomplete, and almost no data exist in humans [16, 17]. The initial response to silica in the lung is mediated by the innate immunity, and it consists of two stages: disruption of the regenerative program in the conducting epithelium, and phagocytosis of silica particles by macrophage [18], followed by the establishment of oxidative stress, release of ROS [19-23], and the transcription and release of inflammatory cytokines such as interleukin (IL)-1β, tumor necrosis factor (TNF)-α and interferons (IFN) [19, 20, 23-25]. Therapeutic antagonism of these mediators has been proposed in silicosis [19, 20, 23-25].

1.4 Silica damages the BADJ and decreases the release of CCSP

The distal portion of bronchi, the transition from bronchioles to alveolar sacs in the lung, is known as the bronchoalveolar duct junction (BADJ). It is lined by different types of cells, including Club Cells, which are non-ciliated, non-mucous, secretory cells, that represent a primary progenitor cell population for ciliated and secretory epithelial cells in the terminal bronchiole, and secrete many essential glycoproteins, lipids, and proteins providing chemical and physical protection for both pulmonary surfactant and small airways [26]. Specifically, Club cells are the source of the immune-modulatory protein Club Cell Secretory Protein (CCSP, also known as uteroglobin/blastokinin, CC16, or SCGB1A1) [27-30]. Club Cells are absent in the proximal segment of the bronchioles, while in the BADJ they represent the 11-22% of the entire cell population, and the 15-44% of all proliferating cells [26, 31]. Other location of Club Cells in the human body consists of the gravid uterus, hence the name uteroglobin for the CCSP, kidneys, and prostate [26].

The CCSP gene is located on chromosome 11, p12-q13, a region involved in allergy and inflammation [32]. Even though the exact role of CCSP is not completely clear, there is evidence supporting the protective role of CCSP in the respiratory tract against oxidative stress and inflammatory response. CCSP inhibits the activation of phospholipase A2 and modulates the production of inflammatory cytokines, including IFN gamma and TNF-α [33]. Lack of CCSP in mice induces exaggerated inflammatory response to viral infection [34] and exhibit increased expression of TNF-α when compared to CCSP competent mice [35].

Club cells are also involved in the biotransformation of many inhaled xenobiotic and toxic compounds, including furans, hydrocarbons (including aromatic hydrocarbons), naphthalene and its derivatives, tobacco smoke, and many other substances, which are mainly detoxified through

cytochrome P-450 [30], in a process that can also generate toxic metabolites and lead to cell damage and necrosis [30].

The peculiar role of CCSP in the regeneration and protection of the epithelial cells is also supported by the evidence that decreased levels of this protein in human serum are associated with reduced lung function either in childhood and in adulthood [36]. Moreover, the lack of CCSP exacerbates the alveolar cell damage and inflammation induced by cigarette smoke and increases the risk of mortality for lung cancer [36]. While patients suffering interstitial lung diseases, such as sarcoidosis and idiopathic pulmonary fibrosis (IPF), show an increase of CCSP level in serum and bronchoalveolar lavage (BAL) [37-39], workers exposed to silica report decrease serum concentration of CCSP protein, without any correlation with the time and dose of exposure [40, 41], suggesting that the decreased serum levels of CCSP could be used as a sensitive prognostic indicator of disease progression.

The exact mechanism that leads to the silica-induced decreased serum levels of CCSP is still unclear. Silica particles can directly damage the Club cells membrane since they are very sensitive to toxic compounds [42], alveolar macrophages can engulf silica particles and release dangerous cytotoxins, or silica particle can impair the regenerative program of the progenitor Club cells. Thus, the decreased level of CCSP in serum mirrors the silica-induced damage of Club cells in the lung [43].

1.5 Metabolic activation of macrophages

In 2008, Cassel et al. revealed that the development of silicosis is dependent upon the activation of the NLRP3 inflammasome [19]. The inflammasome is a complex of proteins

composed of multiple subunits, that once activated and assembled with pro-caspase-1, it prompts the activation of caspase-1 and the release of mature IL-1β. This process, however, requires two different starting signals; the first one is represented by the interaction of Toll-Like Receptor (TLR) 4 and its ligand, the lipopolysaccharide (LPS), which activates the transcription factor NF-κB, and in turn of inflammatory cytokines precursors pro-IL-1β and pro-IL-18. The second signal is represented by phagocytosis of silica into phagolysosomes, damage of mitochondria, ROS production, assembly of the NLRP3, activation of caspase-1, and releases of mature IL-1β and IL-18 [19, 20, 23, 44].

However, this mechanism implies that LPS is a determinant factor in the immune response because macrophage exposed to silica alone cannot be activated and consequently cannot develop inflammation and IL-1β release; in contrast, cells primed with LPS can have an enhanced response to silica particles. Moreover, it does not explain the high TNF-α secretion during silicosis.

Previous studies have shown that LPS-activated bone marrow-derived macrophage (BMDM) undergoes the "Warburg effect" or aerobic glycolysis [45]. LPS activation increases the rate of glycolysis and decreases mitochondrial respiration, accompanied by a defective tricarboxylic acid (TCA) cycle and accumulation of succinate [46]. The latter plays a crucial role as proinflammatory signal acting via succinate dehydrogenase (SDH) and Reverse Electron Transport (RET) through complex I and is responsible for stabilization of HIF-1α and consequent secretion of IL-1β. In contrast, inhibition of glycolysis with 2-deoxyglucose (2DG) downregulates HIF-1α protein and consequently blocks the release of LPS-induced IL-1β. [47]

The remodeling of mitochondrial electron-transport chain (ETC) complexes in macrophage are required for optimal responses to bacterial infection. Specifically, viable *Escherichia coli* bacteria encountered by macrophages are engulfed in phagosomes, which become

surrounded by mitochondria that are adaptively remodeled in response to infection. The adaptation consists of changes in mitochondrial super-complexes in the mitochondrial inner membrane that result in diminished complex I (CI) and increased complex II (CII) activities, production of toxic products such as reactive oxygen species (ROS), fumarate, itaconic acid and perhaps others that are delivered locally at high concentrations. This pathway elicits many antibacterial responses, several of which are augmented by this upregulation of CII's activity [48].

More recently, in 2017, a study performed by Saborano et al. indicated metabolic reprogramming induced by silica nanoparticles in RAW 264.7 macrophages, which is characterized by increased glycolytic activity, altered TCA cycle, reduced ATP generation and increased TNF-α production, consistent with a pro-inflammatory phenotype.

1.6 Scope of dissertation and statement of hypothesis

The present study aimed to elucidate the two particular aspects of the silica-induced inflammation and lung fibrosis mentioned above: to clarify the mechanism by which silica damages Club cells and compromise the regenerative properties of stem cells of the distal lung epithelium, and to determine the immune-metabolic responses induced by silica in macrophage that leads to the secretion of cytokines and perpetuation of inflammation. We hypothesize that silica induces macrophage metabolic reprogramming characterized by alteration of glycolysis, and mitochondrial respiration, mediated by adaptation of ETC, which is necessary for the cell survival through the release of inflammatory cytokines.

2.0 Club Cell Secretory Protein (CCSP) Regulates the Innate Immune Response in Silicosis

2.1 Introduction

Occupational or environmental exposure to silica is associated with the development of silicosis, a lung disease characterized by progressive granulomatous inflammation and pulmonary fibrosis, autoimmune disease, mycobacterial infection, and lung cancer [3]. Despite significant progress in its prevention, silicosis remains a major global health problem associated with high morbidity and mortality for which no specific therapy is available [10, 11].

The pathogenesis of silica-induced lung disease is not entirely understood, almost no data exist in humans [16, 17], and most of our knowledge focuses on the role that immune cells play in this process. Consequently, the current hypothesis indicates that the initial response to silica in the lung is mediated by innate immunity. Phagocytosis of silica particles by alveolar macrophages [18] is followed by the establishment of oxidative stress, the release of ROS [19-21, 23], activation of the NLRP3 inflammasome and the transcription and release of inflammatory cytokines such as IL-1β and TNF-α [19, 20, 23-25].

However, this hypothesis does not take into account the role that lung epithelium plays in the pathogenesis of silicosis and the disruption of the regenerative program in the conducting epithelium.

In transgenic mice expressing an epithelial-restricted IκB (nuclear factor kappa-light-chain-enhancer of activated B cells inhibitor) moiety that cannot be phosphorylated, we previously demonstrated a role for the epithelium in that inhibition of the pro-survival NF-κB (nuclear factor kappa-light-chain-enhancer of activated B cells) in Club cells or type II alveolar epithelial cells is

associated with enhanced apoptosis of these cells and significantly worse silica-induced lung inflammation and fibrosis [10].

As mentioned above, the BADJ is lined by different types of cells, including Club cells secretory cells that represent an abundant progenitor cell population and the source of the immune-modulatory protein CCSP [27-29].

Studies in crystalline silica or asbestos-exposed workers demonstrated that decreased serum levels of CCSP could be used as a sensitive prognostic indicator of disease progression [43, 49]. These studies suggest that the reduced CCSP levels in asymptomatic patients are the result of damaged Club cells associated with diminished secretory function regardless of the dose of silica exposure [43]. In sharp contrast to silicosis, BAL, and serum concentrations of CCSP were markedly increased in IPF, although most of the studied IPF patients were smokers [37]. The serum concentration of CCSP is also augmented in other fibrotic lung diseases like hypersensitivity pneumonitis and those associated with some connective tissue diseases [37-39]. A significant reduction in CCSP levels is identified, as early as three days, after exposures of rats to silica [50]. In mice, injuries specifically targeted to stem and transit-amplifying cells of conducting airways have a profound impact on alveolar homeostasis, suggesting that crosstalk between bronchiolar and alveolar compartments has a critical role in modulating lung function and tissue remodeling [51, 52]. Based upon these known functions of Club cells and the changes in CCSP described in silica-exposed miners, we hypothesize that silica exposure directly affects the reparative properties of the distal airway epithelium leading to Club cell deficiency and associated immunomodulatory perturbations that promote macrophage activation and exacerbation of fibrotic remodeling.

Consistent with an immune-regulatory role for Club cells and CCSP in lung injury, we previously reported that exposure of Club cell-depleted or CCSP-deficient (CCSP-/-) mice

modulate the *in vivo* response to LPS by enhancing expression of TLR4 and inducing the production of TNF-α by macrophages [53]. TNF-α plays a fundamental role in the pathogenesis of silica-induced lung injury and human, as well as mouse lungs exposed to silica, demonstrate enhanced macrophage TNF-α production in a manner that precedes the inflammatory response and the accumulation of lung collagen [16].

Despite the ample evidence that the toxic action of silica on the lung structures is closely linked to the ability of silica particles to damage cell membranes, the exact molecular process and progression are still not wholly understood, and different mechanisms have been proposed. Decreased secretion of CCSP by Club cells might be due to direct cell damage by silica, might be consecutive to lesions of other cell types within the respiratory epithelium which are sensitive to lung irritants, or Club cells are damaged by cytotoxic mediators released from activated macrophages that have engulfed silica particles [43].

The present study was designed to determine whether the altered CCSP expression described following silica exposure is the result of inflammatory cell recruitment and fibrosis that involves the BADJ, a region that represents a niche for maintenance of lung tissue stem cells, thus compromising the ability of the Club cells to regenerate the bronchiolar and/or alveolar epithelium. Furthermore, using CCSP-/- mice, we studied the mechanism by which Club cell secretory protein dysfunction accelerates silica-induced lung injury. Our results in wild type mice indicate that silica induces remodeling of the bronchiolar/alveolar duct region with apparent disorganization of CCSP-immunoreactive cells, reduced CCSP content, and decreased proliferation within the CCSP-expressing cells suggesting that silica compromises the ability of these stem and/or progenitor cells to restore homeostasis. Our studies using CCSP-/- mice indicate that CCSP exerts anti-inflammatory properties by inhibiting TLR responses and suppressing macrophage activation in

response to silica through a mechanism involving the release of Type I alpha interferon and early TNF-α production thus contributing to pathological lung remodeling during silica exposure**.**

2.2 Materials and Methods

Animals. All experiments were approved by the University of Pittsburgh Institutional Animal Care and Use Committee. Eight to ten-week-old male C57BL/6 mice and mice lacking the Club cell secretory protein (CCSP-/-) gene congenic to C57BL/6J mice (Jackson Laboratory, Bar Harbor, ME) were given a single intratracheal (i.t.) instillation of 0.2 mg/kg freshly-fractured crystalline silica in 60 μl of sterile 0.9% saline. Control mice were treated with 60 μl of saline alone. Mice were sacrificed at 0, 3, 7, 14, and 28 d post-silica instillation.

Bronchoalveolar Lavage (BAL) Analysis. Total protein in BAL fluid was determined by a Coomassie Blue-based protein assay (ThermoScientific, Pittsburgh, PA). White blood cell counts and differential cell counts were analyzed as described previously [54]. Levels of TNF-α in the lavage fluid and cultured macrophages were assayed by ELISA (ThermoScientificThermo Scientific, Pittsburgh, PA).

Lung Sample Preparation. Mice were administered pentobarbital (50 mg/kg) intraperitoneal (i.p.), and lungs were either gently lavaged with PBS to assess secreted CCSP abundance by ELISA as described previously [53] followed by fixation (naphthalene/silica exposure experiment) or directly open-cavity inflation fixed at 10 cm H_20 using 10% formalin. Whole lungs were fixed overnight in 10% formalin and placed in 70% EtOH (for paraffin embedding) or washed in PBS/0.02% azide (for whole-mount microdissection).

Naphthalene and BrdU Exposure. Following silica exposure, groups of 10 female C57BL/6 were injected i.p. with naphthalene (225 mg/kg) dissolved in corn oil. Mice were inspected and weighed before and 24-48 h post-injection to assess injury severity. Subsequently, mice were given 6 mg/ml BrdU in sterile saline i.p. every 12 h for a total of 7 d. For animals sacrificed at 14 and 28 d after silica exposure, BrdU (50 mg/kg) was administered 2 h prior to sacrifice. Following euthanasia, lungs were inflation fixed using 10% formalin, degassed in 30% sucrose, and cryopreserved using optimal cutting temperature (OCT) solution.

Immunostaining and Whole-Mount Microdissection. Murine CCSP (in house), CGRP (Sigma), acetylated tubulin (ACT) (Sigma), Ki67 (Novocastra), and GFP (Abcam) antibodies were used for immunostaining following citrate buffer antigen retrieval. Secondary antibodies included appropriate species-specific Alexa488, Alexa555, and Alexa633 dyes (Invitrogen). Frozen sections were stained for BrdU plus airway markers, as previously described [55]. Left lung lobes were inflation fixed and dissected using a brightfield microscope, fine forceps, and micro-dissecting scissors to expose the airway network to terminal bronchioles and antibody stained. Microdissected lungs were incubated in 10% bovine serum/0.25% fish skin gelatin for 2–3 h to block nonspecific antigen reactivity. Primary antibodies were added in blocking solution overnight (O/N) at room temperature, followed by PBS/0.2% Tween20 washes. Secondary antibodies were also added O/N at room temperature and washed extensively. Immunostained lung lobes were imaged up to 2 weeks post-staining.

Image Acquisition and Analysis. Whole lung images were collected as previously described [56] using an 8000-Hz resonance detector-equipped Leica TCS confocal microscope. X–Y field size and Z-thickness were determined based on total lung size (≈2 cm × 1 cm × 500 μm) to produce a single 3D image projection. High-resolution images were collected at 400–700 Hz.

Digitally flattened, 3D lung images were analyzed using Volocity based on GFP signal intensity and patch boundary continuity to determine CCSP abundance and expression in the distal 200 square micrometers of 14 terminal bronchioles. Regions of interest (ROI) were drawn on each lung image that encompassed the entire conducting airway and GFP channel intensity was used to distinguish GFP(+) and (−) cells. The average pixel surface area (square micrometers) of single cells was determined empirically and used to exclude subcellular debris. A negative reference of the CCSP abundance was derived from the staining of the airways of CCSP-/- mice. All contiguous cells within our defined ROI were scored automatically using these parameters to determine BrdU labeling and/or CCSP expression. Total cell number vs. CCSP expressing/BrdU labeled frequency was plotted using Microsoft Excel frequency/bins parameters. In all figures, error bars represent the standard error of the mean (SEM). Statistical significance was considered when $P < 0.05$ based on Student's t-test.

Hydroxyproline analysis. Dried lung tissue was acid-hydrolyzed in sealed, oxygen-purged glass ampoules containing 2 ml of 6 N HCl for 24 h at 110 ºC and analyzed for hydroxyproline content using chloramine T as previously described [54].

Quantitative real-time polymerase chain reaction (qRT-PCR) assay. To adequately cover the TNF-α, NF-κB, Toll receptor pathways, and targeted cytokines, 84 transcripts selected were analyzed by qRT-PCR (Super Array Bioscience Corporation, Frederick, MD). Total RNA was isolated with TRIzol reagent (Invitrogen, Carlsbad, CA) and quantity was assessed by absorbance (NanoDrop, Thermo Scientific, Pittsburgh, PA). RNA (100 ng) was reverse transcribed (High Capacity cDNA Archive Kit, Applied Biosystems Inc., Foster City, CA) and cDNA was PCR amplified with primers and TaqMan Universal PCR Master Mix (Applied Biosystems). Arranged into functional groups, primers (SABiosciences, Frederick, MD) included:

A. TNF-α ligands and receptors pathway group (20 transcripts); B. NF-κB pathway group (10 transcripts); C. Cytokine group (15 transcripts); TLR receptors (10 transcripts); Transcription Factors (16 transcripts); other (13 transcripts). All abbreviations are current Entrez Gene official symbols and official full names are presented in **Appendix A table 1**. The analysis was performed with an Applied Biosystems 7900HT System (95°C 10 min; 40 cycles 95°C, 15 s; 60°C, 1 min). The expression of each transcript relative to Heat shock protein 90kDa alpha (cytosolic), class B member 1 (HSP90AB1) transcript level was determined using the $2^{-\Delta\Delta C}$T method and normalized to strain-matched mice exposed to saline.

Silica-exposed subject population. The University of Pittsburgh Institutional Review Board approved the procedures used in this study, and written informed consent was received from the subjects before inclusion in this study. Patient information was minimized to comply with HIPPA regulations. We identified patients that received lung transplantation at the University of Pittsburgh from May 1986 to July 2009. From this database, we selected patients that received lung transplantation for the diagnosis of silicosis (n=13). The diagnosis of silicosis or usual interstitial pneumonia (UIP) was unequivocally established by blind re-evaluation (S.Yousem). Characterization of the TNF-α, CCSP, and TLR7 and TLR9 expression in the human lungs was conducted by immunohistochemistry in paraffin-embedded lung tissues (4 μm) isolated from silicosis patients at the time of lung transplantation.

Specific TLR and CCSP RNA expression profiling in the human lung. RNA was isolated from human lung (six silica exposed subjects and morphologically normal regions of lungs retrieved from 15 patients at the time of surgical intervention to treat their lung cancer) tissue using Trizol (Invitrogen, Carlsbad, CA) and purified using the RNeasy Mini kit (Qiagen). Microarray experiments were carried out, as described previously [57]. Briefly, RNA quantity was determined

on an Agilent Nanodrop and quality assessed on an Agilent 2100 Bioanalyzer, according to the manufacturer's instructions. Five hundred nanograms of total RNA meeting quality control criteria were Cy3 labeled using the Agilent Low RNA Input Linear Amplification Kit PLUS (One-Color). After purification and fragmentation, aliquots of each sample were hybridized to an Agilent Whole Human Genome 4 x 44 K microarray, sequentially washed, and scanned on an Agilent DNA microarray scanner. RNA expression data were analyzed with Agilent Feature Extraction Software.

Microarray data analysis. Processed microarray data were log2-transformed and cyclic loss normalized, and then expressed as the difference of log of g processed signal (Agilent Feature Extraction) and log of geometric mean of controls. A two-fold difference in normalized expression value was used to estimate differential expression. Hierarchical clustering analysis was carried out using Scoregene statistical package (available at http://compbio.cs.huji.ac.il/scoregenes/) and visualized using the TreeView program [58]. The q-value, computed using the SAM (significance analysis of microarrays) package [59] in the R statistical environment (R Development Core Team. R: A Language and Environment for Statistical Computing. Vienna: R Foundation for Statistical Computing, 2006), was used to identify differentially expressed genes. The q-value represents the minimal false discovery rate at which an individual hypothesis test may be called significant. A gene was declared to be differentially expressed if the gene had a q-value < 5% in a two-way SAM analysis (healthy controls vs. silica) and also had a q-value < 1% in at least one of the three pairwise SAM analyses.

2.3 Results

2.3.1 Silica induces remodeling of the bronchiolar-alveolar duct region in a mouse model of silicosis

To follow remodeling events within the lung and to investigate the role of CCSP-expressing progenitor cells in the development of silicosis, we exposed C57BL/6J mice to 200 mg/kg of freshly fractured crystalline silica intratracheally (i.t.) and assessed tissue injury at 1, 3, 7, 14 and 28 days post-instillation.

Figure 1 shows terminal bronchiolar lesions associated with intratracheal silica exposure (200 mg/kg) in mice. C57BL/6J mice were exposed to **(A, B)** intratracheal saline or **(C-F)** crystalline silica and tissue obtained at **(A-D)** 3 d or **(E, F)** 28 d. Corresponding low magnification (10x left) and high magnification (20x right) photomicrographs of trichrome stained lung tissue sections revealing either (**A, B**) normal terminal bronchioles, or **(C-F)** typical nodular lesions induced by silica exposure that localize to bronchoalveolar duct junctions.

In contrast to saline-treated mice **(Figure 1A, B)** silica exposure of C57BL/6J mice resulted in the development of clearly identified lesions at 3d following silica exposure, that were localized at the terminal bronchiole/alveolar duct regions **(Figure 1C, D)**. These lesions consisted of dense accumulations of peribronchiolar and perivascular inflammatory cells. Lesions evolved rapidly with time, leading to a dramatic increase in peribronchiolar collagen deposition at 28 d post-exposure **(Figure 1E, F)**.

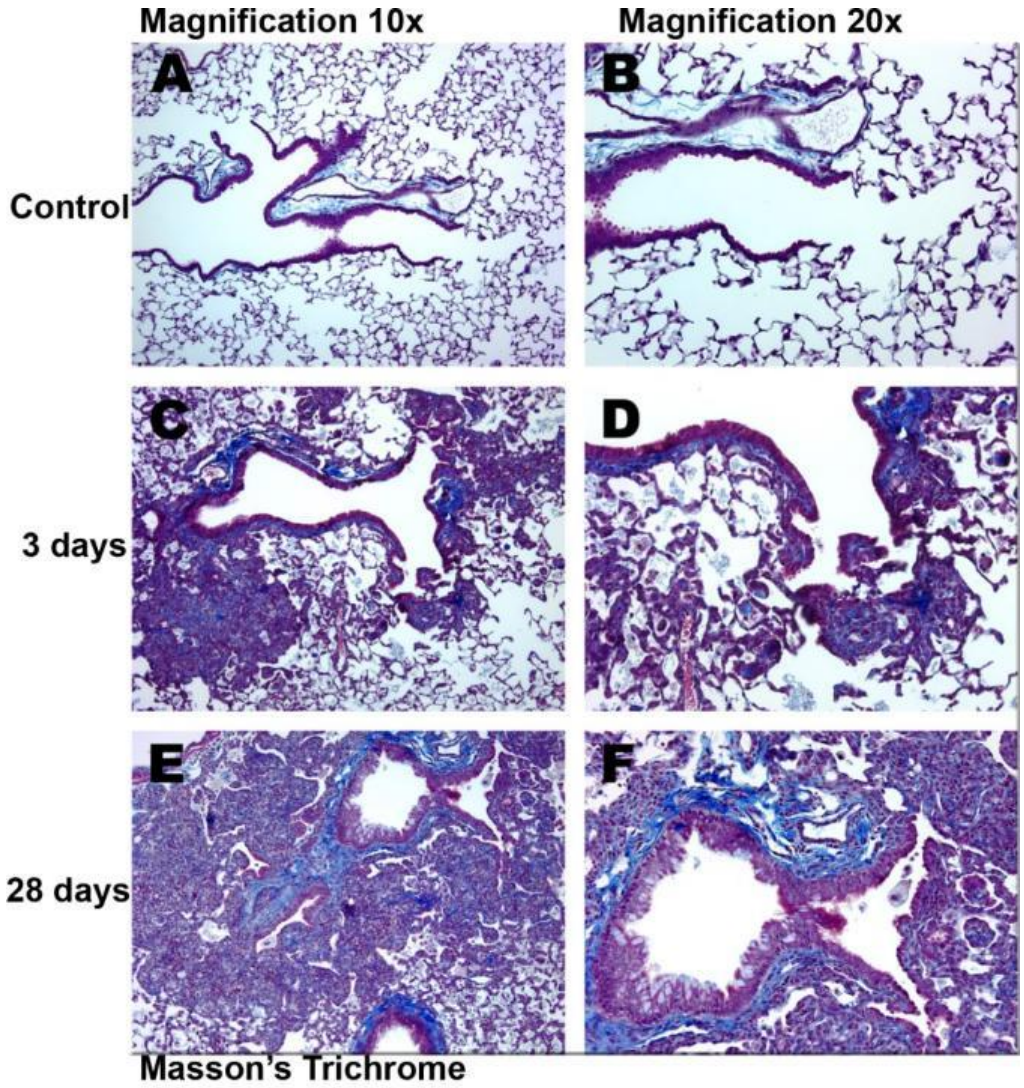

Figure 1 Silica induces remodeling of the bronchiolar alveolar duct and lung fibrosis in C57BL/6J mice

Progression to fibrotic lung disease was assessed through measurement of collagen gene expression, hydroxyproline content within total lung homogenate, and by histochemical identification of collagen deposition through trichrome staining of lung tissue **(Figure 1)**. Silica exposure was accompanied by increased collagen mRNA and hydroxyproline content in the lung at all post-exposure times. Specifically, collagen mRNA showed a peak 7 days post-treatment, while hydroxyproline showed significant differences ($p<0.005$) at 14 and 28 d post silica exposure as compared to control **(Figures 2A, B)**.

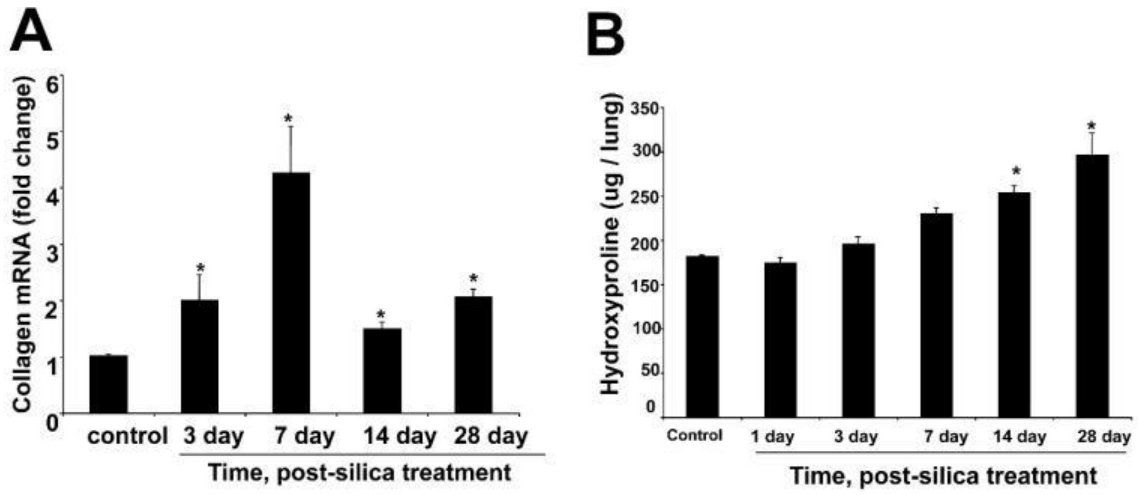

Figure 2 Measure of collagen gene expression and hydroxyproline content within total lung homogenate after silica exposure

These changes were consistent with the results of collagen content assessed by the trichrome staining of lung tissue sections **(Figure 1E, F)**.

2.3.2 Altered CCSP expression in the lungs of silica-treated mice

The impact that progressive silicotic lesions have on epithelial cells within terminal bronchioles and on cell proliferation within the entire lesion was assessed through analysis of CCSP immunoreactive cells, as a measure of the stem and progenitor cells, and the incorporation of BrdU into nascent DNA of proliferative cells.

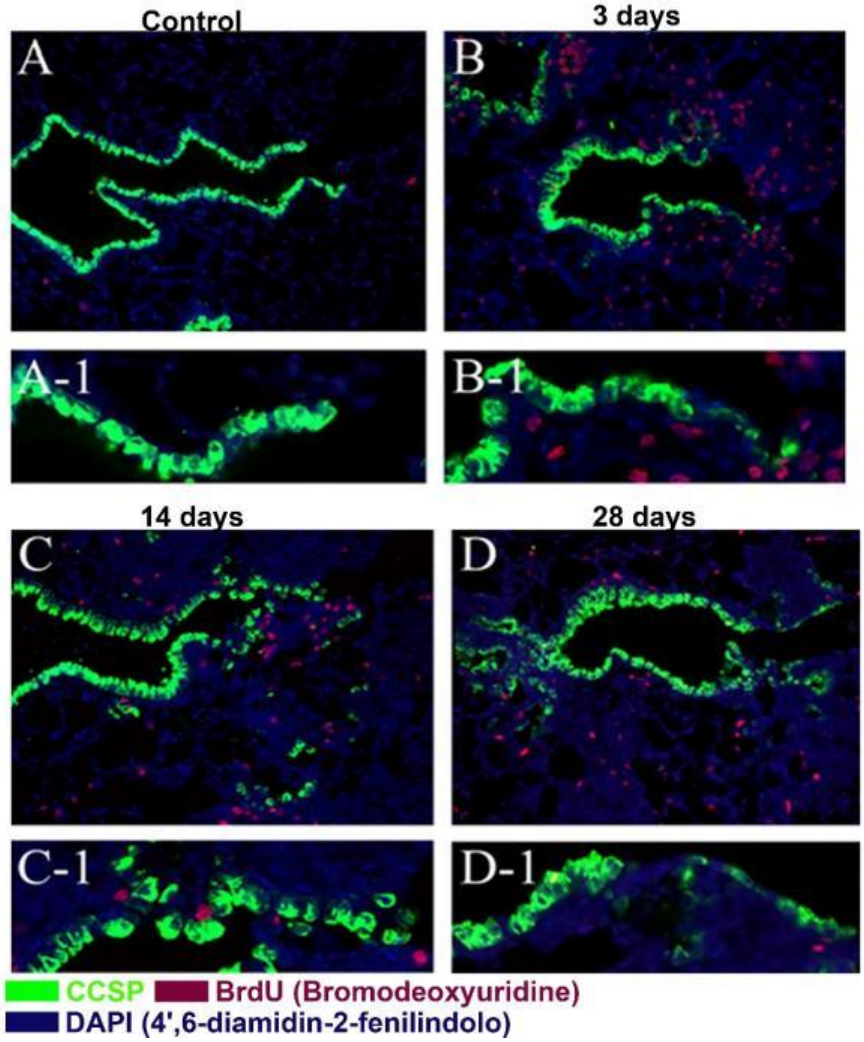

Figure 3 Altered CCSP expression during the silica-induced remodeling of the terminal bronchioles

In F**igure 3**, silica-induced remodeling of terminal bronchioles revealed by immunofluorescent colocalization of CCSP (Green) and BrdU (Red), with DAPI nuclear counterstain (Blue). Corresponding low (10x) and high (20x) magnification photomicrographs representing airways of (**A**, **A-1**) control mice or mice receiving i.t. silica (200 mg/kg) and tissue were obtained at (**B**, **B-1**)3 d, (**C**, **C-1**), 14 d, or (**D**, **D-1**) 28 d.

Profound effects of silica exposure on the integrity of terminal bronchiolar airways were evident early after silica exposure, when airway epithelial cells demonstrated reduced CCSP-immunoreactive content and interruptions on the continuous expression of CCSP were identified

3 d after silica exposure **(Figure 3, compare control A and A-1 with 3 d silica B and B-1)**. These changes into terminal bronchioles occurred concurrently with the development of inflammatory nodules and early establishment of fibrotic lesions, and include extensive BrdU labeling of cells within the parenchyma (mitotic index for control-treated mouse 0.008 increased to 0.14 after 3 d following silica exposure), but not the bronchiolar epithelium (average mitotic index of 0.006 in control mice versus 0.005 in silica exposed mice). At 14 and 28 d, silica-treated lungs demonstrated persistent increases in the BrdU labeling of parenchymal regions (mitotic index of 0.10 and 0.07 respectively) suggestive of fibroblast proliferation within developing fibrotic lesions **(Figure 3, C, C-1, D, and D-1)**.

Loss of CCSP-expression in terminal bronchioles was associated with modest incorporation of BrdU in the epithelium (mitotic index 0.04) and persistently decreased whole lung CCSP mRNA levels **(Figure 4A)**, while a significant increase in CCSP protein levels in the BAL fluid of silica-treated mice was noted **(Figure 4B)**.

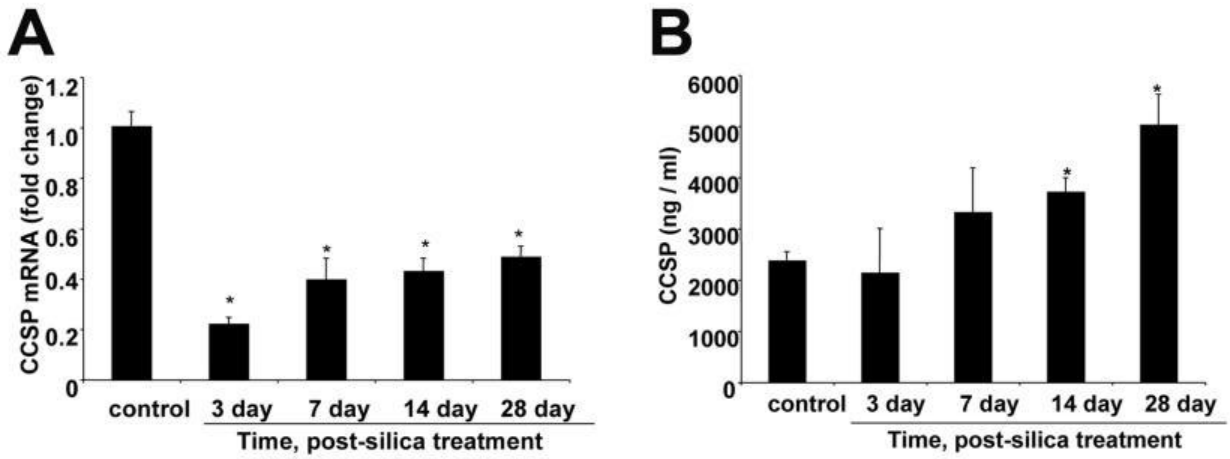

Figure 4 Measurement of CCSP mRNA levels in the lung and CCSP protein level in the BAL

These observations suggest that silica induces secretion of CCSP into airway lining fluid with an associated decrease in the intracellular pool of CCSP content.

Silica-induced injury in C57BL/6J mice was also associated with a significant ($p<0.001$) increase in BAL total protein **(Figure 5)**. Protein levels in BAL peaked 3 d after silica exposure and then decreased, although they remained significantly elevated **(Figure 5)**.

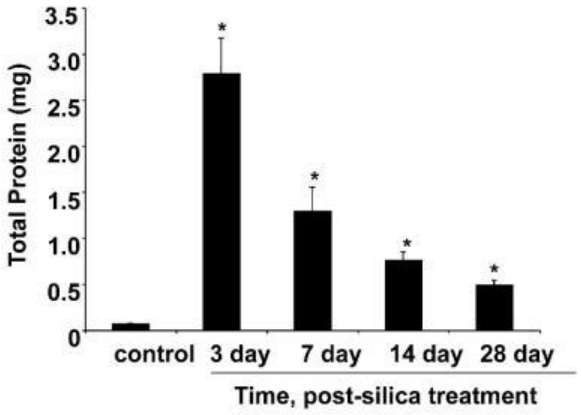

Figure 5 Total protein retrieved from BAL of C57BL/6J mice after silica exposure

To further characterize the effect of silica on the CCSP expression in the mouse lung, we quantified CCSP-expressing cells within the terminal bronchioles adjacent to BADJ of control or silica exposed mice. This analysis demonstrated that compared to control-treated mice (with an average of 18 $\pm$ 2 CCSP/cells) silica induces a significant ($p<0.05$) reduction (6 ± 3 cells at 3 d; 8 ± 1 cell at 7 d; and 12 ± 2 cells at 28 d) in the number of CCSP immunoreactive cells in the distal 200 μm of the terminal bronchioles. This decrease in the number of CCSP-expressing cells was associated with a corresponding increase (from 0 ± 2 cells in unexposed or saline-treated mice) in the number of non-CCSP expressing cells (7 ± 1 cell at 3 d; 9 ± 1 cell at 7d; 6 ± 1 cell 28 d) in silica-exposed mice (data not shown).

2.3.3 Defective epithelial repair in terminal bronchioles of silica-exposed mice

The absence of BrdU incorporation within the CCSP-expressing population of bronchiolar epithelial cells following silica exposure suggests that either the proliferative capacity of the stem and/or progenitor pool has been compromised, or that there is a lack of mitogenic stimuli for these cells. However, although silica decreased CCSP expression, it did not appear to abolish the population of Club cells. Combined exposures of naphthalene, that specifically ablates Club cells and promotes epithelial repair response by inducing proliferation of naphthalene resistant CCSP expressing cells, and silica were used to determine whether silica exposure compromises the regenerative capacity of airways. Mice were sequentially exposed to naphthalene (250 mg/kg) **(Figure 6A,B)**, i.t. silica (200 mg/kg, i.t.) alone (**Figure 6C**,**D**), or naphthalene (250 mg/kg) followed by silica (200 mg/kg, i.t.) (**Figure 6E**,**F**). Epithelial proliferation was assessed by measuring the BrdU-labeling index. Adjacent sections were either stained with hematoxylin and eosin (H&E, left panels) or dual immunofluorescence for CCSP (Green) and BrdU (Red), with DAPI nuclear counterstain (Blue) (right panel).

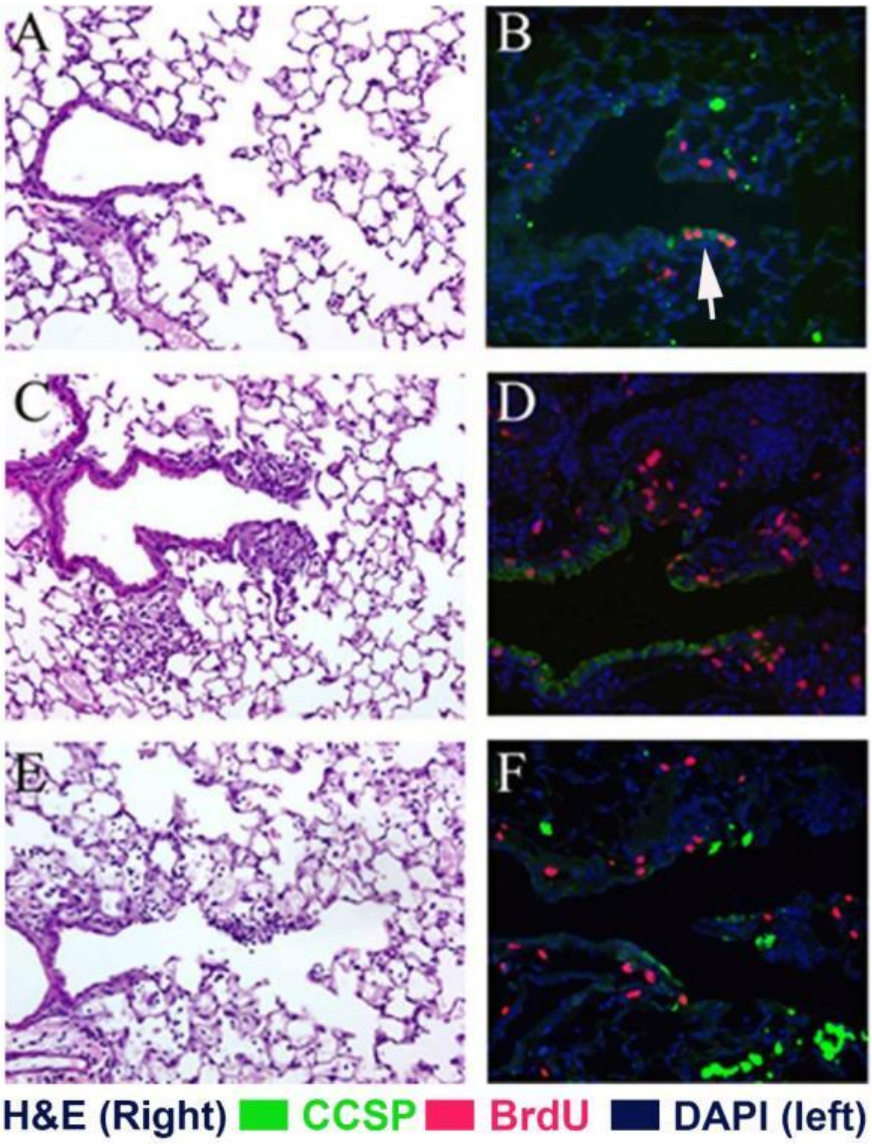

Figure 6 Silica inhibits epithelial repair. Silica inhibits the naphthalene-induced proliferation of resistant CCSP cells

Naphthalene exposure resulted in the depletion of CCSP-immunoreactive progenitor cells **(**compare **Figure 3A,A-1, with Figure 6A and B)** and proliferation of naphthalene-resistant stem cells (BrdU index increased from 0.005 to 0.5) for partial restoration of the depleted progenitor pool by the 3 d post-exposure **(Figure 6B)**. Exposure of mice to silica alone led to bronchiolar epithelial disorganization, and parenchymal proliferation after 3 d that was similar to that observed

previously **(**compare **Figure 3B, B-1, and Figure 6D).** Combined exposure of mice to naphthalene followed by silica resulted in a pattern of progenitor cell depletion similar to that observed with naphthalene alone (compare CCSP immunofluorescence in **Figure 6B, F),** an extensive parenchymal proliferation that was similar to silica-exposed mice (compare BrdU-labeling in **Figure 6D, F)**, yet was not associated with BrdU-labeling of naphthalene-resistant CCSP-immunoreactive cells (BrdU index was 0) (compare bronchiolar epithelial BrdU-labeling of CCSP-immunoreactive cells in **Figure 6B, F).** These data support our hypothesis that silica exposure induces epithelial disorganization in the absence of epithelial proliferation that compromises the reparative capacity of epithelial cells within terminal bronchioles.

2.3.4 Silica induces an enhanced inflammatory response in CCSP-/- mice

Previous reports indicate that Club cells function in an anti-inflammatory capacity, and CCSP-/- mice mount an exacerbated inflammatory response to infectious or environmental agents [53, 60]. Therefore, we sought to determine the role of the airway epithelium in modulating the silica-induced inflammation by contrasting the nature of inflammatory cells recovered from BAL of silica-exposed C57BL/6 and CCSP-/- mice. Silica exposure of C57BL/6J mice resulted in significantly ($p<0.001$) increased levels of total inflammatory cells, retrieved from the lung via BAL, at 3d post-treatment as compared to untreated controls **(Figure 7)**. BAL inflammatory cell counts remained elevated at 7, 14, and 28d post-silica exposure as compared to control **(Figure 7)**. Compared to their congenic C57BL/6J mice, CCSP-/- mice demonstrate a lower number of cells recovered by BAL at baseline and the numbers of cells retrieved from the lungs of C57BL/6J mice were greater than in CCSP-/- mice at each time tested **(Figure 7)**. Compared to control, silica treatment increases the number of cells in both mouse strains **(Figure 7)**.

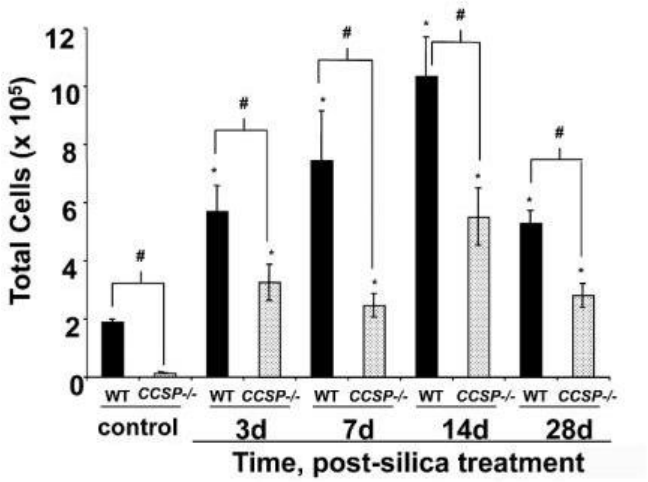

Figure 7 Total cells retrieved from the lung via BAL from C57BL/6J mice and CCSP-/- after silica exposure

Silica exposure induced the rapid recruitment of polymorphonuclear leukocytes (PMN's) within the first 24 h, and adaptation of this response to include elevated levels of macrophage/monocytes and lymphocytes by 3 d post-exposure and beyond **(Figure 8A-F)**.

Silica treatment also altered cell types recovered by BAL, shifting it from >99% macrophages in control mice to polymorph-nuclear (PMN) leukocytes that persisted throughout the 28 d after silica exposure in both C57BL/6J and CCSP-/- mice **(Figure 8A-F)**. The percent PMN in BAL from CCSP-/- mice was higher than that in BAL from C57BL/6J mice at 3, 7, and 14 d after silica. For example, CCSP-/- BAL consisted of >70% PMN as compared to ~40% in C57BL/6J BAL at 3 d after silica. In contrast to PMNs, lymphocytes were identified in BAL from silica-exposed C57BL/6J mice, whereas these cells were not identified in silica-exposed CCSP-/- mice **(Figure 8A-F).**

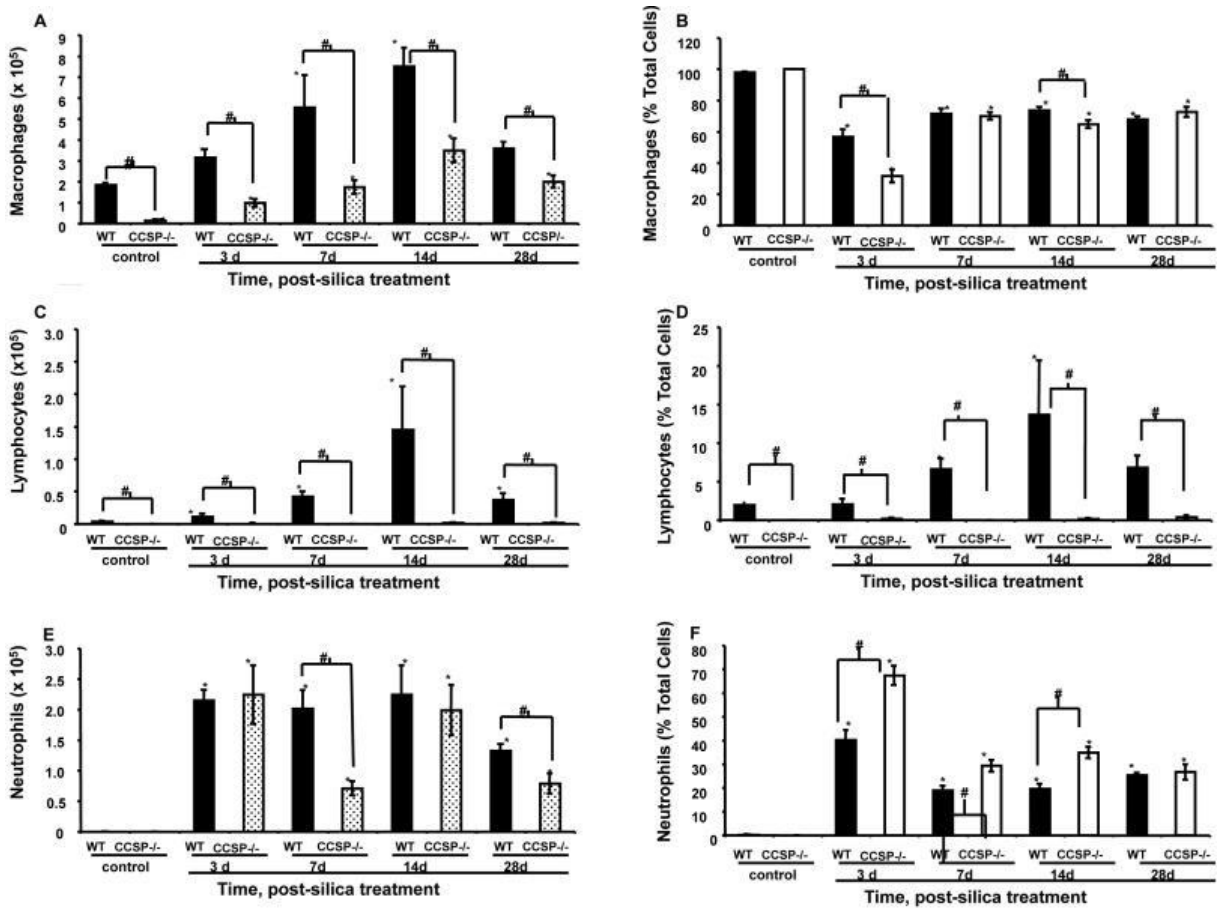

Figure 5 Cells retrieved from the BAL of C57BL/6J mice and CCSSP-/- after silica exposure differentiated for type, absolute number and relative number

As we described above, C57BL/6J mice showed a time-dependent increase in lung collagen deposition in response to silica exposure **(Figure 1)**. Therefore, we contrasted, by real-time PCR, the effects of silica exposure on the rate of collagen, type I, alpha 1 (COL1A1) mRNA in the lungs of C57BL/6J and CCSP-/- mice. Mice (n=7) were exposed to intratracheal silica (200mg/kg) and recovered for the times indicated. Collagen mRNA levels were determined by qRT-PCR from the lungs obtained at the indicated time after silica exposure. Silica increased COL1A1 mRNA that peaked 7 d after silica exposure and the increase was greater in CCSP-/- mice **(Figure 9)**. The asterisk indicates a significant difference by ANOVA ($p < 0.05$) between the CCSP-/- and the C57BL/6 wild type mice at the time point indicated **(Figure 9)**.

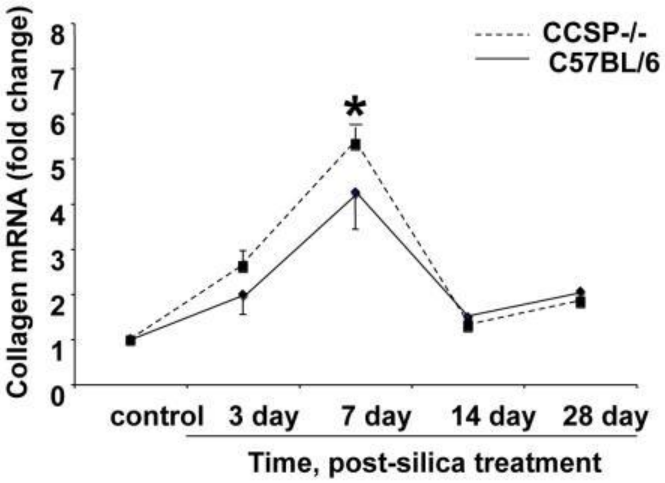

Figure 6 Increased collagen type I, alpha 1 mRNA in the lungs of CCSP-/- mice

2.3.5 Microarray analysis identifies enhancement of specific TLR expression in the lungs of silica-exposed CCSP-/- mice

Our previous work characterizing the inflammatory response of Club cell-depleted or CCSP-/- mice to LPS indicates that, compared to wild type mice, lung macrophages from CCSP-/- mice had enhanced TLR4 expression and increased TNF-α and IL6 production [53]. Similarly, we have recently reported that macrophages from the lung of silica-exposed subjects express TNF-α protein [61]. In addition, TNF-α-mediated effects in the lung of silica-treated animals required activation of the transcription factor NF-κB [61]. Therefore, to ascertain whether variations in TNF-α, TLR or NF-κB signaling pathways and targeted cytokines, characterize the observed differences in the response against silica between C57BL/6J and CCSP-/- mice, we used a custom microarray to assess 84 gene transcripts **(Appendix A Table 1)** that comprehensibly represents the TNF-α and TLR pathways leading to NF-κB activation, in the lung of C57BL/6J or CCSP-/- mice following silica exposure.

Mice (n= 7 C57BL/6J or CCSP-/- mice/group) were treated with silica, lung mRNA was obtained at 3, 7, 14, and 28 d, and 40 transcript levels were assessed by qRT-PCR. In **Figure 10**, the left panel shows self-organizing map visualization of transcripts in Tree View; the right panel is the visualization of Mean Tendency of the transcripts measured. Values are mean + standard error and *$p<0.05$ as determined by One-way analysis of variance with all pairwise multiple comparison procedures (Holm-Sidak method).

Overall, 40 of the 84 transcripts tested, including TNF-α, CCL2, IKβKG, increased within 3 d in silica-exposed mice **(Figure 10)**. At 28 d post-silica exposure, 39 of these 40 transcripts were increased (only GR1 was not significantly increased). Of the 40 transcripts measured, TNF-α mRNA abundance increased the most (~90-fold). mRNA levels of the TNF-α receptors, TNFRSF1B and TNFRSF1A increased, as did transcripts TNFAIP3 and RIPK2, that are rapidly induced by TNF-α. All 19 TNF-α signaling pathway transcripts increased by 28 d post-silica exposure, and the levels of expression were similar in both C57BL/6J as well as CCSP-/- mice **(Figure 10).**

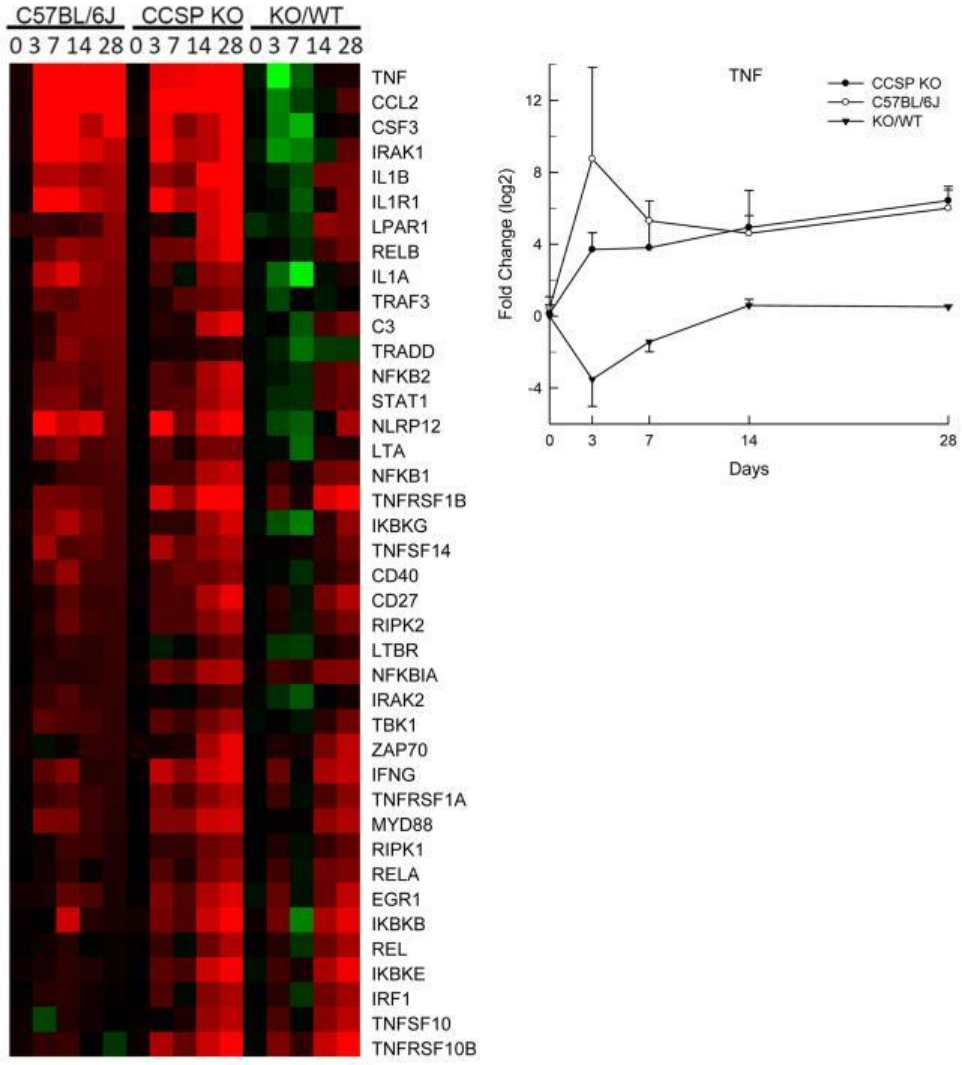

Figure 7 TNF-α, NF-κB and associated cytokines in mouse lung following silica treatment

NF-κB signaling pathway transcripts also increased in C57BL/6J and CCSP-/- mouse lung following silica exposure, although somewhat less than the TNF-α signaling pathway. At 28 d post-silica, NFKB1 (p50) increased ~5-10 fold, and Rel/NF-κB family transcription factors (REL, RELA, RELB) increased ~5-15 fold **(Figure 10)**.

Also, levels of 11 out of 12 cytokine transcripts encoding factors known to control the production, differentiation, and function of monocytes/macrophages (CCL2 a.k.a. MCP1), and granulocytes (CSF3: a.k.a. G-CSF) increased significantly with disease progression, and they had

similar levels of expression regardless of CCSP genotype. Furthermore, transcripts encoding IL-1β, IFN-γ, and the downstream transcription activator, STAT1, were increased markedly (~8-20 fold at 28 d) by silica exposure independently of CCSP genotype.

Twenty transcripts, including members of the TLR, significantly increased in the lungs of silica exposed CCSP-/- mice; most of them were not found to change in C57BL/6 mice in response to silica **(Figure 11A)**. Prominent among these transcripts were TLR 6, 7, 8, 9, MYD88, SLC20A1, ICAM1, SMAD3, JUN markedly increased (~10-35 fold at 14 and 28 d respectively) **(Figure 11A)**. TLR9 transcript levels increased more in CCSP-/- mouse lung than in strain-matched C57BL/6J mouse lung **(Figure 11B).**

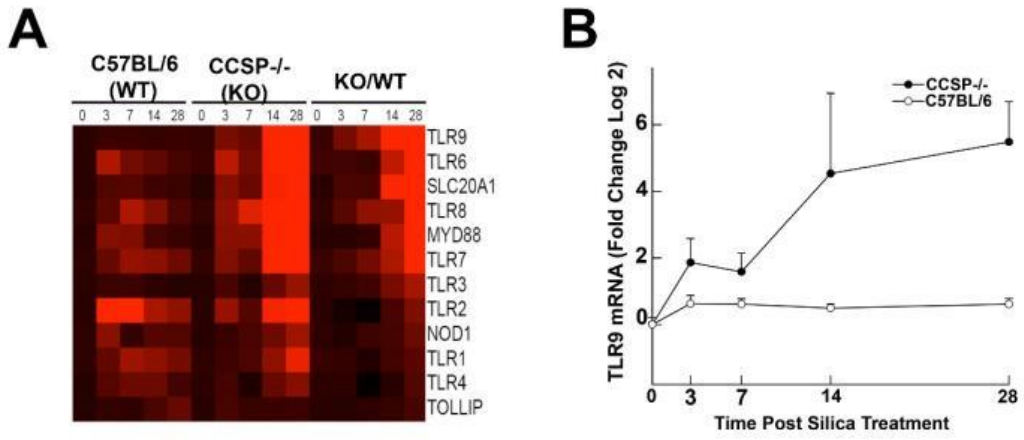

Figure 8 Toll receptor expression increased in CCSP-/- mouse lung following silica treatment

Immunohistochemistry was used to validate the altered expression of these proteins in the lung of CCSP-/-, but not in C57BL/6J, mice exposed to silica. Among the TLR's showing CCSP-dependent silica-induced changes in their expression, TLR7 and TLR9 immunoreactivity was dramatically increased in macrophages located in areas of inflammation surrounding the terminal bronchioles **(Figure 12A, B)** as described in **Figure 1**.

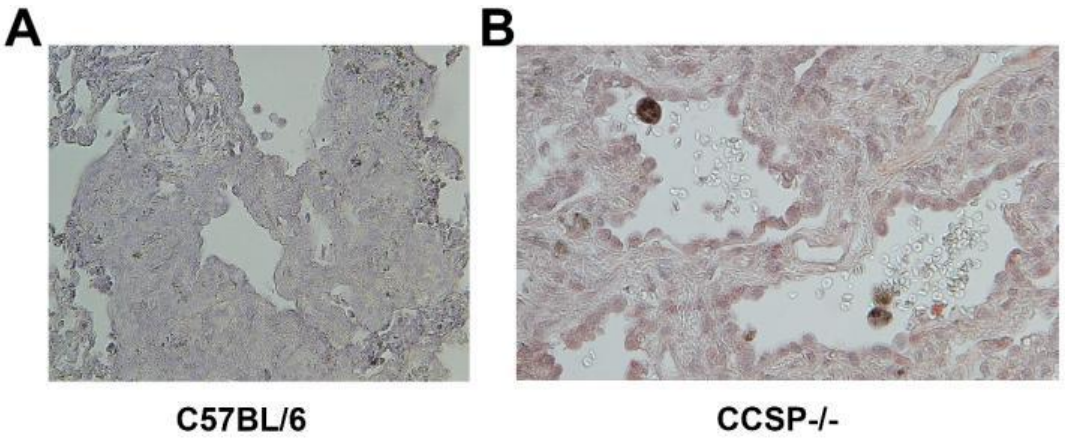

Figure 9 Immune-histological staining of the lungs of silica exposed CCSP-/- localized expression of TLR7 and TLR9 proteins to macrophages in the lungs of these mice

To determine whether the in vivo responses to silica were due to intrinsic differences in the response of macrophages from CCSP-/- mice to silica exposure, we cultured macrophages from BAL or bone marrow of wild type and CCSP-/- mice and expose them to silica in vitro. Western blot analysis of silica-exposed macrophages coupled with the detection of TLR proteins (4,6,7,8,9) revealed that silica-induced expression of TLR 7 and 9 proteins in primary macrophages **(Figure 13)** and that the level of induction was higher in macrophages from BAL of CCSP-/- than C57BL/6 mice.

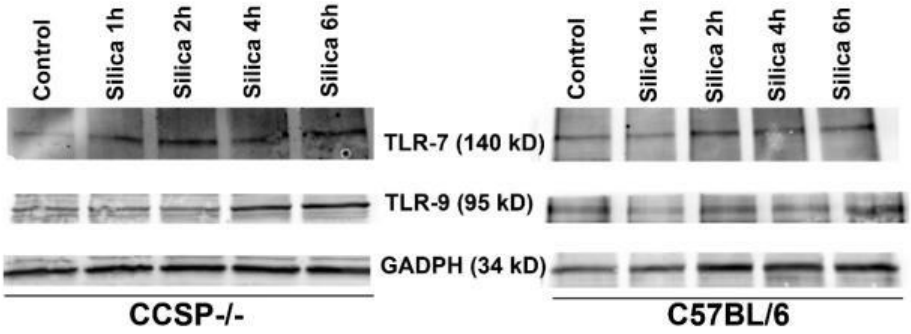

Figure 10 Western blot analysis of proteins isolated from CCSP-/- or C57BL/6 macrophages from BAL

2.3.6 CCSP-/- macrophages demonstrate enhanced Interferon I alpha and TNF-α production in response to silica

Our previous work identified the lung macrophage as the principal source of TNF-α in the lung in response to silica [61]. However, recent publications investigating the role of the inflammasome in the pathogenesis of silicosis indicate that exposure of unprimed macrophages to silica does not result in TNF-α production and that these cells would require priming (i.e., LPS) prior to the release of this cytokine [19, 62]. Our current data show that, although we identify similar increases in TNF-α RNA expression in the lungs of silica exposed mice from both mouse strains, we find that TNF-α release is significantly elevated in BAL fluid from CCSP-/- mice relative to exposed wild type mice 24 h after silica exposure **(Figure 14)**.

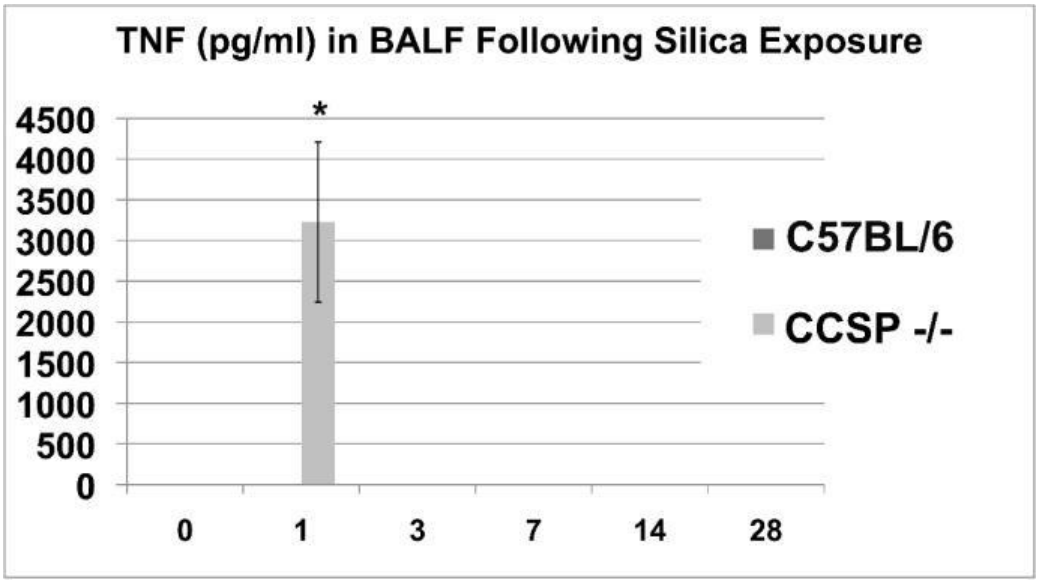

Figure 11 Silica induces TNF-α production in lungs of CCSP-/- but not in C57BL/6J wild type mice

Thus, compared to control-treated mice**,** CCSP-/- mice, but not C57BL/6J mice, release TNF-α protein (3200 ± 500 pg/ml) in BAL obtained at 24 h following silica exposure, **(Figure**

14). Consistent with an enhanced ability by non-primed CCSP-/- macrophages, we find that these cells release significant ($p<0.001$) amounts of TNF-α when challenged *in vitro* 4 h with a broad range concentration (from 50 to 200 μg/cm^2) of silica **(Figure 15)**. In contrast, C57BL/6J derived macrophages do not release TNF-α at 4 h after exposure to a broad range of silica concentrations, although they release significant concentrations of TNF-α in response to LPS **(Figure 15)**.

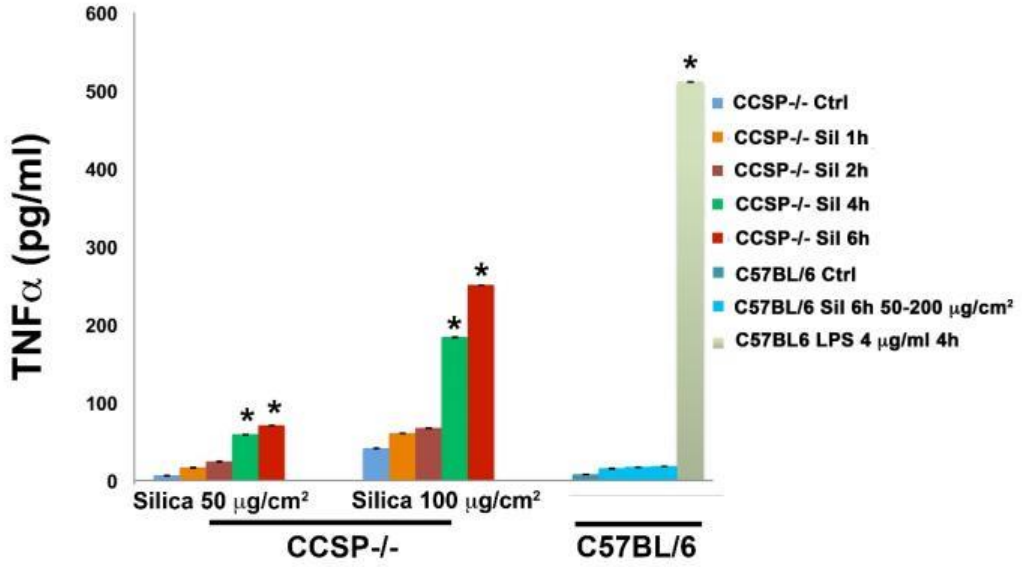

Figure 12 Enhanced production of TNF-α by CCSP-/- and C56BL/6J macrophages

But how does CCSP deficiency impact TNF-α release by macrophages? Our data show that silica predominantly enhances expression, in lungs and macrophages of CCSP-/- mice, of members of the TLR receptors family, such as TLR7 and TLR9, that are localized exclusively in the endosomal compartment [63]. Therefore, we reasoned that CCSP-/- macrophages could use a TLR7/9-mediated mechanism to induce the release of inflammatory mediators such as TNF-α in non-primed macrophages. TLR 7/9-mediated signaling, leading to the production of inflammatory mediators, is dependent on the recruitment of adaptor protein MyD88 expression of which is increased in the lungs of CCSP-/-, but not C57BL/6J mice (**Figure 11**). We speculate that elevated

MyD88 expression in macrophages of CCSP-/- mice promotes the activation of transcription factors, the production of type I IFN (alpha and beta) proteins, and the subsequent stimulation of IFN-sensitive genes such as TNF-α [63]. We find that CCSP-/-, but not C57BL/6J macrophages, exhibit a time-dependent release of type Iα IFN starting at 1 h after stimulation with silica **(Figure 16**). Importantly, no changes were observed in the expression of type I β IFN by macrophages from either mouse strain following silica exposure (data not shown). These data suggest that endosomal TLR receptors mediate the altered inflammatory response observed in CCSP-/- macrophages to silica.

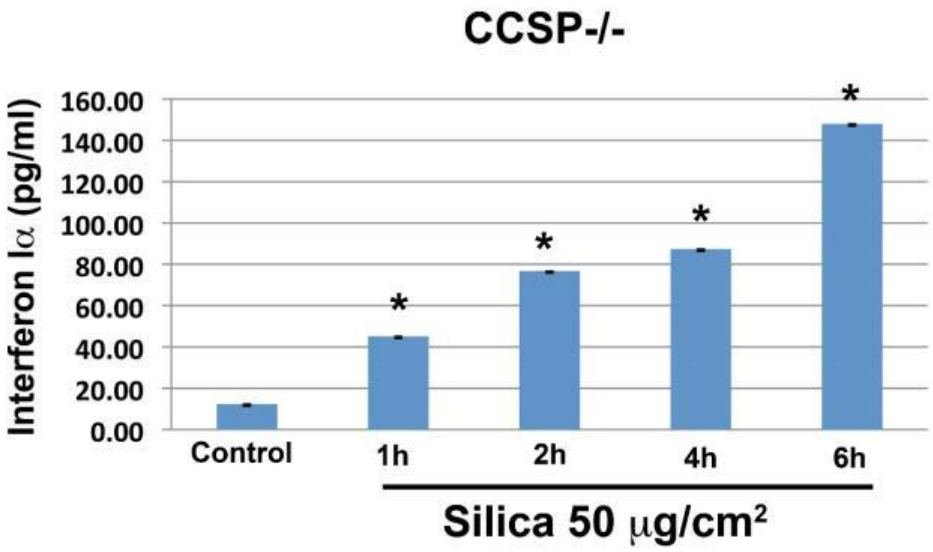

Figure 13 Enhanced production of Interferon Iα by CCSP-/- macrophages

2.3.7 CCSP expression is reduced, and TLR receptor expression is enhanced in the lungs of silica-exposed human subjects

To determine the relevance of the data observed in the lungs of silica-exposed CCSP-/- mice in the pathogenesis of silicosis, we studied the expression of members of the secretoglobin

and TLR family of genes within explanted lung tissue of 13 patients with silicosis at the time of lung transplantation. Of these samples, total RNA was isolated, and gene expression evaluated by microarray analysis. Total RNA isolated from the silicotic lung tissue of six patients was contrasted with total RNA isolated from morphologically normal regions of lungs retrieved from 15 patients at the time of surgical intervention to treat their lung cancer. Microarray analysis revealed that compared to healthy lungs, the expression of secretoglobin proteins and CCSP (SCG1A1) in particular is decreased in the lungs of silica-exposed subjects **(Figure 17A)**. In addition, our analysis of the TLR expression in the lungs of silica exposed subjects closely resembles the pattern of expression identified in the lungs of CCSP-/- mice and TLR 1, 2, 6, 7, and 8 transcripts increased in silicosis subjects when compared to controls **(Figure 17B)**. Although TLR9 transcript levels were greater than those of control, these levels did not achieve statistical significance ($p<0.05$).

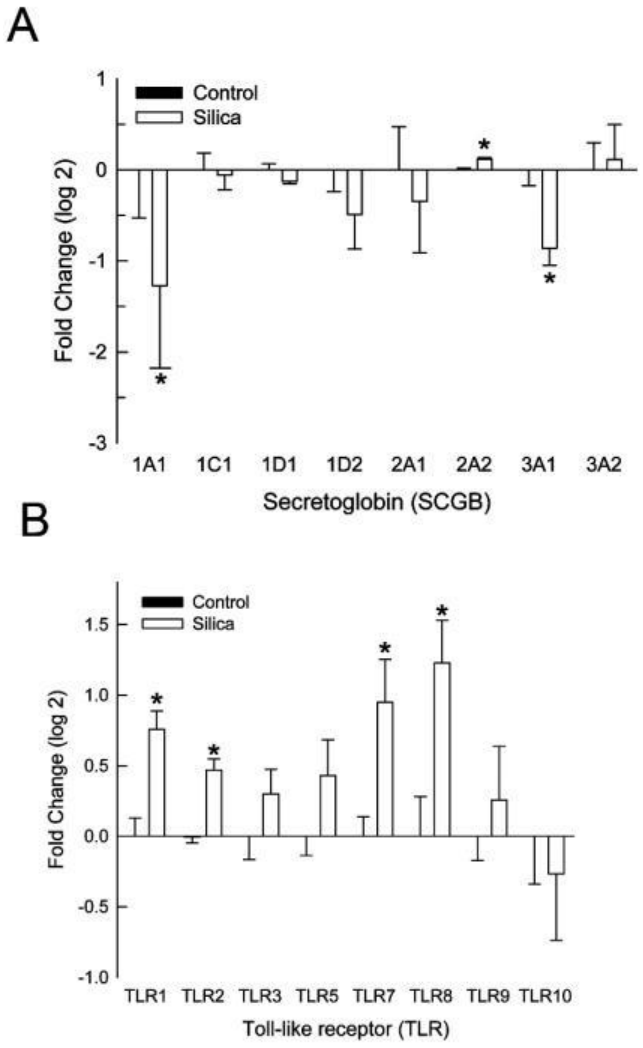

Figure 14 CCSP expression is reduced, and TLR receptor expression is enhanced in the lungs of silica-exposed human subjects

Subsequently, TNF-α and TLR7 localization were determined by performing immunostaining of lung tissues isolated from subjects suffering from silicosis at the time of lung transplantation. In all 6 silicosis patients, large areas of the lung parenchyma were replaced by coalescence of silicotic nodules **(Figure 18)**. These nodules contain fibrous material, had few cells and did not demonstrate TNF-α or TLR7 immunostaining.

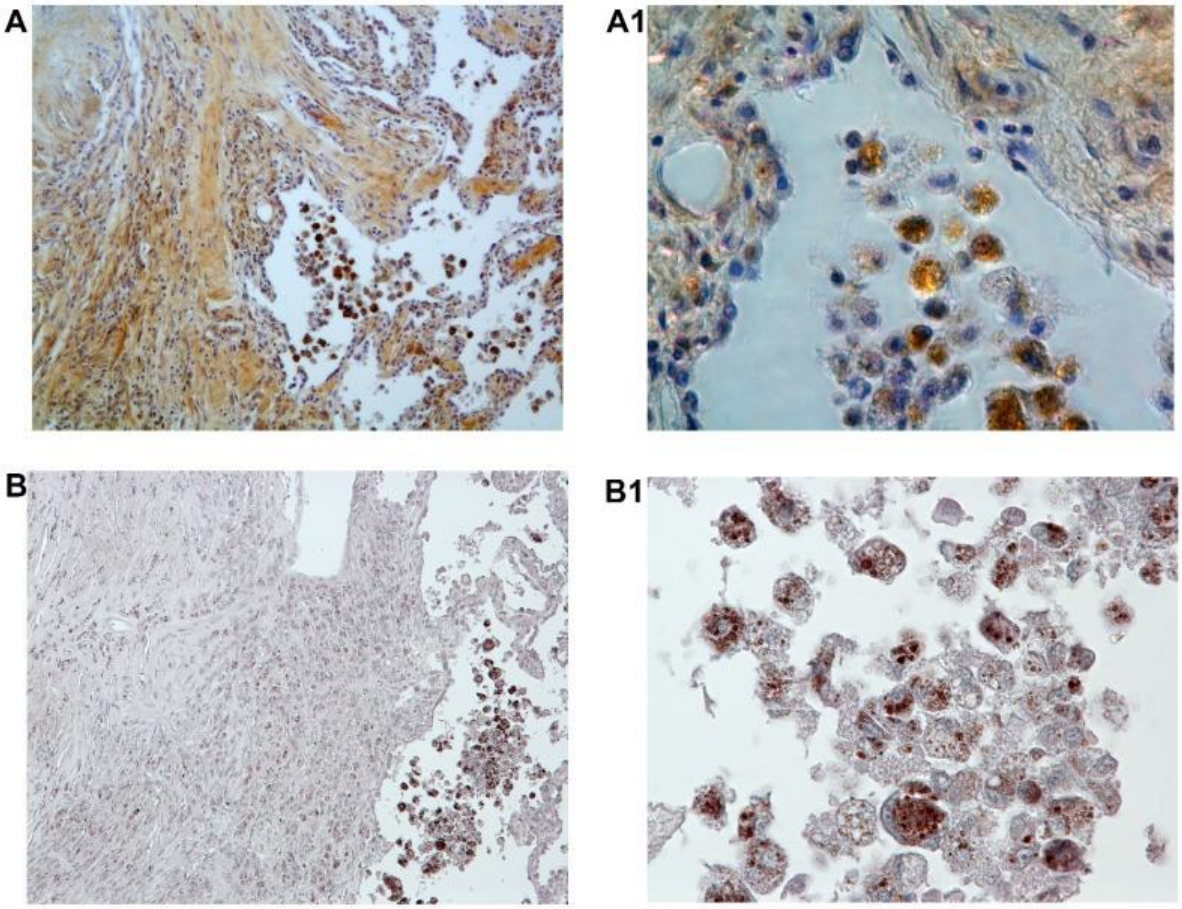

Figure 15 Characterization of the TNF-α and TLR7 expression in the human lungs conducted by immunohistochemistry

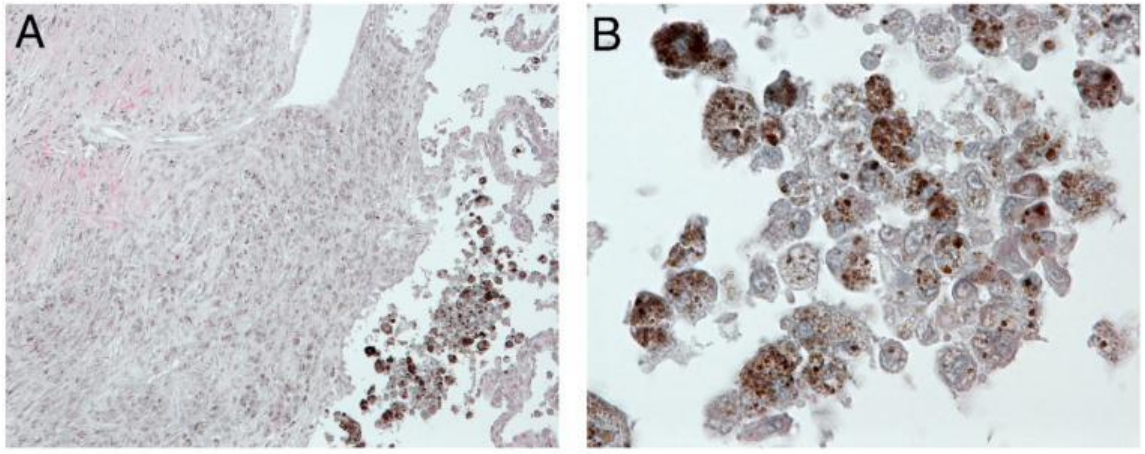

Figure 16 TLR 9 expression in the lung of silica exposed subjects

In contrast, TNF-α immunostaining was evident in preserved regions of the lung parenchyma adjacent to the silicotic nodules, where the expression was confined primarily to silica-laden macrophages **(Figure 18A,A1)**. Sequential section localized the expression of TLR7 **(Figure 18B,B1)** and TLR9 **(Figure 19)** to the same macrophages that expressed TNF-α. Therefore, these findings closely reproduce the TLR expression observed in the CCSP-/- mice. **Figure 18** shows the immunochemistry signal with the anti-TNF-α antibody at (A) low (x200) and (A1) high (x400) magnification and with the anti-TLR7 antibody at (B) low (x200) and (B1) high (x400) magnification. **Figure 19** shows the immunochemistry signal with anti-TLR9 antibody at (A) Low (x200) and (B) high (x400) magnification.

2.4 Discussion

Silicosis remains a serious occupational and environmental lung disease [10]. The worldwide incidence and prevalence of silicosis is uncertain but is increasing in developing countries [64]**.** For example, the silicosis burden in China is growing (with ~7-10,000 new cases/yr) and is extensive (>500,000 cases resulting in ~24,000 deaths/yr) [64]. In the United States, the incidence and prevalence of silicosis are under-estimated, as silicosis is not a reportable disease and under-recognized [65]. Approximately 1.7 million people in the US are occupationally exposed to silica [66-69], and as many as 119,000 are exposed above permissible levels [66-69] with the majority of these individuals employed in mining, construction, or maritime activities. The economic burden of silicosis to our society is enormous and recent studies by the National Institute for Occupational Safety and Health (NIOSH) tracking the death rates of silicosis patients

across the nation calculated that the near 2000 deaths (1968-2005) in patients under 65 years of age account for a loss of 17,130 years of potential life [70].

Although preventive measures have significantly decreased the mortality attributable to silica, no specific therapy, including lung transplantation, appears to be successful in these patients [66, 70]. Therefore, understanding the pathogenic mechanisms of silicosis is fundamental to identify targets that predict individual susceptibility or provide a window of opportunity for therapeutic intervention.

CCSP has been identified as a biomarker to screen the early toxic effects of environmentally-induced lung injury, including in silicosis [71]. CCSP is the main secreted product of Club cells, and under normal conditions, it achieves high concentrations in respiratory secretions [49]. BAL concentration of CCSP in healthy subjects average between 1-2 mg/l, but because BAL techniques result in a 100-fold dilution approximately of the epithelial lining fluid, CCSP concentrations at the surface of the airways can be estimated at 100 mg/l [49]. CCSP is produced as a homodimer of 70 amino acid subunits, with a molecular weight of 15,840 Da, and diffuses from the lung into the peripheral circulation. Although CCSP mRNA is present in tissues outside the lung, such as the prostate, there is consensus that the bulk of the circulating protein is produced by the airway epithelium of the lung [72]. Serum CCSP levels in healthy, non-smoker, individuals are reported in the range of 10-15 μg/l; thus a large concentration gradient is responsible for the movement of this protein from the lung into the blood [73]. The integrity of the alveolar-capillary membrane is a crucial determinant of this equilibrium, and the situation in which this barrier is disrupted (i.e., acute lung injury) results in increased serum concentrations [49]. An example of this is the rapid increased in serum CCSP observed on cyclist exposed to low concentrations of ozone [60] or the increase in serum concentration of CCSP in LPS treated rats

at a time point when CCSP concentrations in BAL and lung homogenates, as well as CCSP mRNA levels, were depressed [74]. These observations indicate that the assay of serum CCSP is a possible indicator of defects in the lung epithelial barrier permeability [60].

Serum CCSP concentration is decreased in a dose-dependent manner by tobacco smoking. Similarly, serum concentrations of CCSP are decreased in chronic diseases such as sarcoidosis, asthma, and pulmonary fibrosis [49]. A significant reduction in CCSP has been identified as early as 3 d after the exposures of rats to silica [50]. A significant reduction in serum CCSP is present in workers exposed to crystalline silica for less than 2 years and without clinical evidence of lung impairment [43]. Similar to these findings, we identify a decreased mRNA for CCSP in the lungs of silica-exposed subjects. However, large variations were observed in the level of expression between the individuals, and the number of silica-exposed subjects (n= 6) was small. Taken together, these data support the utility of serum CCSP as a suitable biomarker in silicosis; still, they do not clarify the mechanisms by which silica alters the CCSP expression in the lung, nor do they clarify the subsequent role that this altered CCSP expression plays in the pathogenesis of silicosis.

In this study, we provide evidence indicating that silica induces progressive inflammation of the small airways of the mouse lung, encasing the BADJ, where it compromises the proliferation of Club cells that harbor the putative capacity to regenerate both secretory and ciliated epithelial cell types. Because of the injury to Club cells, silica also decreased total lung CCSP mRNA, CCSP immunostaining BADJ cells, and increased CCSP protein detected in BAL. We are not able to determine whether reduced CCSP mRNA, observed in the total lung, is the result of excessive loss of in the number of CCSP positive cells or if it represents a change in the expression of CCSP mRNA by individual cells. Our current findings also indicate that silica compromises the ability

of CCSP expressing cells to proliferate. Our previous findings indicate exacerbated fibrotic and inflammatory response to silica in the lungs of CCSP-dnIκB transgenic mice, that experience increased epithelial apoptosis of CCSP expressing cells as they express, in Club cells, a mutant IκB that cannot be phosphorylated and therefore does not allow the nuclear translocation and activation of NF-κB [10]. Together, these findings favor a scenario in which silica is inducing cell death of CCSP expressing cells with the associated secretion of CCSP protein from Club cells into the luminal surface of the epithelium, thus explaining the increased levels of protein identifying in the BAL fluid of CCSP (figure 4) in silica exposed C57BL/6J mice at times when the mRNA coding for this protein is still down-regulated in the lung (figure 4).

Consistent with an anti-inflammatory role for CCSP in the pathogenesis of silicosis, we find that CCSP-/- mice exhibit an enhanced early TNF-α expression in BAL. This was somewhat unexpected in that untreated CCSP-/- mice exhibit a lower total number of inflammatory cells in BAL compared to their C57BL/6J counterpart (figure 7). However, when challenged with silica, CCSP-/- mice maintain a high total cell number compared to control throughout the 28 d tested, consisting of a high total amount of macrophages and neutrophils (as well as a higher percentage of PMN), and absent lymphocytes in their BAL. These data are in agreement with previous reports demonstrating exacerbated lung inflammation in the lungs of CCSP-/- mice to other environmental challenges such as ozone and LPS [74, 75]. Microarray analysis shows that compared to lungs from C57BL/6J mice, lungs from silica exposed CCSP-/- mice exhibit, in an exclusive manner, higher expression of a cluster of genes in the toll-like receptor family (including TLR6, 7, 8, 9) involved in the regulation of the innate immune response. Similar to these findings in mice, we also find statistically significant increases in TLR6, 7, and 8 in the lungs of 6 silica-exposed subjects when compared to the expression of these genes in 15 control subjects. Subsequently,

functional analysis reveals that silica induces expression of TLRs 7 and 9 protein and exacerbated production of TNF-α by primary macrophages from CCSP-/- mice but not C57BL/6J mice.

A role for TLRs was observed in CCSP-/- mice exposed to LPS in which an enhanced cell surface expression of TLR4 favors the release of a higher concentration of TNF-α by the alveolar macrophages of these mice [53]. However, silica exposure did not alter TLR4 expression (RNA or protein) in either human or mouse lung (Figure 11). In agreement with these data, Beamer et al. indicate that silica suppresses the ability of LPS to promote dendritic cell activation by modulating toll-like receptor ligand-induced activation of these cells [21]. Furthermore, the finding reported by Snyder et al. that the inflammatory phenotype of CCSP-/- macrophages could not be corrected in vitro with fractionated CCSP enriched BAL indicates that rather than exerting a direct role in regulating macrophage responsiveness CCSP deficiency causes an intrinsic alteration to the population of macrophages [53].

But what is the nature of this intrinsic alteration observed in CCSP-/- macrophages in response to silica? The group of TLRs that increased their expression in the lungs tissues of CCSP-/- mice and silica-exposed subjects are predominantly associated with the intra-cytoplasmic recognition and processing of pathogen-associated molecular patterns (PAMPs). Therefore, we reasoned that the intrinsic alteration responsible for the increased reactivity to silica could be related to the intracellular handling of silica by the macrophages rather than cell surface events. This hypothesis is consistent with the observations that stimulation of macrophages by silica requires the phagocytosis of silica particles [76, 77]. Thus, following phagocytosis of silica particles CCSP-/-, but not C57BL/6J-derived macrophages demonstrate increased expression of TLR7 and 9 moieties shortly after silica ingestion (Figure 11). This is followed by secretion

(observed as early as 1 h after stimulation with silica particles) of type Iα, but not type Iβ, interferon that preceded the release of interferon sensitive TNF-α [63].

In summary, the present work indicates that silica injures the airway epithelium of bronchoalveolar duct junctions, compromising the repairability of CCSP expressing cells and decreasing the expression of CCSP protein in the lung. Consistent with an anti-inflammatory function for CCSP, CCSP-/- mice demonstrate enhanced inflammatory responses, accompanied by enhanced expression of endoplasmic TLR proteins in macrophages that can promote the release of interferon I alpha and the production of TNF-α by these cells. These studies also suggest that prospective measurements of CCSP levels in serum and respiratory secretions may constitute a valid biomarker to determine enhanced susceptibility to inflammatory responses to silica. Further studies are needed to validate this concept and to comprehend better the interactions between the epithelium and the regulation of the innate immune responses in the lung during environmental injury.

3.0 Metabolic Adaptation of Macrophages as Mechanism of Defense Against Crystalline Silica

3.1 Introduction

Crystalline silica is one of the most abundant minerals on Earth. More than 230 million individuals around the world, and more than 2 million workers in the United States, predominantly in construction and mining occupations, are exposed to silica every year [2, 3]. Inhalation of crystalline silica leads to the development of silicosis, a progressive pneumoconiosis characterized by lung inflammation and fibrosis, for which no specific therapy is available. Silicosis is associated with increased risk of tuberculosis, lung cancer, chronic obstructive pulmonary disease (COPD), kidney disease, and autoimmune disease, and these health risks remain elevated even after silica exposure has ceased [3, 10, 11].

Macrophages are fundamental to the pathogenesis of silicosis. Similar to live bacteria, silica is phagocytosed by macrophages into phagosomes. Subsequently, macrophage activates pattern recognition receptors (PRRs) and the NLRP3 inflammasome, and release cytokines such as IL-1β, TNF-α, and Interferons, critical mediators of the pathogenesis of silicosis [19]. In contrast to bacteria, silica particles cannot be degraded, and the persistent activation results in an increased NADPH oxidase (Phox) activation, and mitochondrial ROS production that ultimately leads to macrophage cell death and release of silica particles that perpetuate inflammation [3, 44, 78, 79]. Activated macrophages exhibit altered immuno-metabolism, intracellular metabolic changes that govern immune effector mechanisms, such as cytokine secretion. For example, lipopolysaccharide (LPS)-stimulated macrophages demonstrate enhanced glycolysis and increased secretion of IL-1β

and TNF-α [46-48]. Inhibiting glycolysis or blocking succinate dehydrogenase (SDH), an enzyme that links glycolysis and the ETC, in LPS-stimulated macrophages inhibits IL-1β, but not TNF-α, production proving that the metabolic pathway is specifically involved in the cytokine production [47].

Despite decades of research, the nature of the macrophage metabolic response induced by silica, its contribution to cytokine specification, and the pathogenesis of silicosis are not well understood. In the current study, we applied state of the art techniques, such as high-resolution respirometry and liquid chromatography-high resolution mass spectrometry (LC-HRMS), to determine the effects of silica on mitochondrial respiration, and the changes in central carbon metabolism of silica-exposed macrophages. Specifically, we characterized the metabolic reprogramming of silica-stimulated macrophages, in terms of alteration in glycolysis, TCA cycle, mitochondrial respiration, and ETC activity, to correlate their contribution to cytokine specification. Using macrophage cell lines, we reported significant differences in metabolic responses of macrophages stimulated by silica and LPS. We found that similar to LPS exposure, silica increases glucose uptake and enhances glycolysis in macrophages.

In contrast to LPS, which induces accumulation of TCA intermediates such as citrate, succinate, and itaconate, silica reduces the absolute intracellular amount of TCA intermediates succinate and itaconate below control levels. Silica also induces specific ETC adaptations, enhanced mitochondrial complex II (CII) activity, and downregulation of mitochondrial complex I (CI) activity via reductions of the CI specific protein *Ecsit*, that are required for macrophage survival to silica-induced cytotoxicity.

These metabolic responses correlated with the observed differences in macrophage production of inflammatory cytokines in response to LPS and silica. Thus, although RAW 264.7

macrophages enhanced IL-1β and TNF-α production in response to LPS or silica, only LPS-stimulated RAW 264.7 macrophages exhibited HIF-1α stabilization under normoxic conditions, activation of the caspase 1, and malonylation of GAPDH in a time-related manner that preceded the release of IL-1β and TNF-α. Also, we observed differences in the RAW 264.7 macrophages accumulation of itaconate that correlate, inversely, with the transcription and release of interferon-beta (IFN-β) in response to LPS or silica

3.2 Materials and Methods

Cell culture

The mouse macrophage cell lines RAW 264.7 and IC-21 were purchased from the American Type Culture Collection (Rockville, MD) and were cultured in DMEM medium (Gibco BRL, Rockville, MD) or RPMI 1640 (ATCC, Rockville, MD) respectively, supplemented with 10% fetal bovine serum, 100Uml/1 of penicillin G and 100 mg/ml/1 streptomycin and grown at 37°C in 5% CO_2.

Silica particles, antibodies, and reagents

Crystalline silica was isolated from environmentally relevant sources and characterized at the National Institute of Occupational Safety and Health (NIOSH, Pittsburgh PA) using a Multi-Cyclone Sampling Array (MCSA) as previously described [79, 80]. α-quartz, average size of 1.7 μm, was also obtained from U.S. Silica (Berkeley Springs, WV). Particles were subjected to sedimentation, according to Stokes' law, acid hydrolyzed and baked overnight (200°C, 16 h) to inactivate endotoxin contamination.

Primary antibodies: Anti-HIF-1α (cat.# NB100-449), anti-GAPDH load control (cat# MA5-15738), were obtained from Thermo Fisher; Total OXPHOS Rodent WB Antibody cocktail (cat#ab110413), anti-*Ecsit* antibody (cat# ab21288), from Abcam; anti IL-1β/IL-1F2 Antibody (cat# AF-201-NA) from R&D System Inc, anti-caspase-1 p10 (M-20) (cat# SC-514) and A/G plus agarose beads (cat# sc-2003) and normal mouse IgG (cat# sc-2025) from Santa Cruz Biotechnology, anti b-actin (cat# 4967) from Cell Signaling Technology, anti malonyl lysine (cat# PTM-901) from PTM Biolabs, anti-GAPDH (cat# MAB374) from EMO Millipore Corp USA.

Secondary antibodies: anti-goat IgG (cat# ab6741) from Abcam, Anti-mouse IgG HRP-linked antibody (cat#7076) and anti-rabbit IgG HRP linked antibody (cat# 7074S) from Cell Signaling; ATP Synthase (cat# MA1-930) and anti-mouse Alexa 488 (cat# A11029) from Invitrogen, Anti-rabbit Cy3 (cat# 111-164-144) from Jackson Immuno.

Lipopolysaccharides from Escherichia coli 0111:B4 (cat# L4391-1MG), L-Lactate Dehydrogenase (L-LDH) from rabbit muscle (cat# 10127230001), and Sodium L-Lactate (cat# 71718) were purchased from Millipore-sigma (St Louis, MO, USA).

Pierce™ RIPA Buffer (cat# PI89900), Halt™ Protease and Phosphatase Inhibitor and Propidium Iodide-1.0 mg/mL Solution in Water (cat# P3566) were from Thermo Fisher. The D-glucose (U-13C6, 99%, cat# CLM-1396-0) was purchased from Cambridge Isotope Laboratories (Andover, MA, USA). Annexin V-FITC Apoptosis Kit Plus (cat # K201-100) was purchased from Biovision.

Detection of cell death

Cell death was analyzed by evaluating (flow cytometry) Annexin V binding and the exclusion of Propidium iodide by macrophages, as previously described [81].

Lactate Dehydrogenase assay

Lactate dehydrogenase (LDH) in the supernatant of exposed cells was measured using a commercial lactate dehydrogenase release assay (Sigma-Aldrich, TOX7) according to the manufacturer's instructions. The absorbance was measured spectrophotometrically at a wavelength of 490 nm, using Cytation 5 Cell Imaging Multi-Mode Reader Biotek.

Lactate Assay

Lactate concentration in the supernatant of exposed cells was assessed using a modification of the commercially available lactate assay (Sigma-Aldrich, TOX7). The reaction is based on the oxidation of lactate by lactate dehydrogenase (LDH). Cell supernatant was incubated with an equal volume of LDH (f.c. 1M), 1x LDH assay cofactor preparation, and LDH Assay Dye Solution (cat#L2277). Absorbance was acquired spectrophotometrically at a wavelength of 490 nm, using Cytation 5 Cell Imaging Multi-Mode Reader Biotek.

ETC Assays

Respirometric Experiments. An Oxygraph O2k Polarographic instrument (Oroboros Instruments, Innsbruck, Austria), equipped with a Clark-type electrode for high-resolution respirometry, was used to measure oxygen fluxes and concentrations. Dulbecco's Modified Eagle's medium (DMEM) without glucose (2.1 mL) was added to each chamber and equilibrated for 20 minutes before the addition of cell suspension (2.5×10^6cells/ml) (prepared as described above) into the Oxygraph chambers (sealed from the atmosphere) at 37°C. Oxygen turnover was examined by the addition of succinate (final concentration, f.c., 10 mM).

Substrate-uncoupler-inhibitor titration (SUIT) assay. SUIT protocol was used for the analysis of oxidative phosphorylation, to study respiratory control in a sequence of coupling and pathway control states induced by multiple titrations. After equilibration of the cells into the

chamber the substrates, inhibitors or uncoupler were added according to the following protocol: rotenone (f.c. 0.5 µM) to inhibit complex I, succinate (f.c., 10 mM) to stimulate complex II, ADP (f.c. 1mM) to measure the total respiratory capacity, Carbonyl cyanide m-chlorophenyl hydrazone CCCP (f.c. 0.05 µM) to determine the state of coupling of complex III, IV, V, antimycin A (f.c. 2.5 µM) to inhibit complex III (Sigma Aldrich). Hydrogen Peroxidase (H_2O_2) flux was assessed simultaneously using the H_2O_2-sensitive probe Amplex UltraRed, by the addition of Amplex Red (f.c. 10 µM) and Horseradish-Peroxidase (HRP) (f.c. 1U/ml) (Sigma Aldrich) following the variation of the resorufin concentration while performing the SUIT assay protocol. Additions by gas-tight syringe into the sealed Oxygraph chambers. Respirometric data analysis was carried out with DatLab 7 software provided by Oroboros.

Complex I Assay

Mitochondrial Complex I activity was measured spectrophotometrically (DU-530; Beckman Coulter). Mitochondrial pellets were lysed in 0.05mM potassium/phosphate buffer (0.05mM, pH 8) containing NADH (10.0 mM), $K_3Fe(CN)_6$ (25mM), a phospholipid supplement (0.005% n-Dodecyl-β-D-Maltopyranoside from Anatrace), Antimycin A (2.5mM) and 320 µg protein from the cell pellet by following the oxidation of NADH at 420 nm initiated by $K_3Fe(CN)_6$ at 30-38 C. Data were acquired for 100 seconds after initiation of the reaction.

Complex II Assay

Mitochondrial Complex II activity was measured spectrophotometrically (DU-530; Beckman Coulter), using a modification of the commercially available Complex II Enzyme Activity Microplate assay Kit (colorimetric) (Abcam, cat# ab109908). Proteins were extracted in PBS and detergent, then lysed in complex II activity buffer, lipid/phospholipid mix, 2,6-dichloroindophenol (DCIP), and Ubiquinone-2, and succinate as provided by the kit and 300 µg

protein from the cell pellet. The reaction was followed by measuring the decrease in absorbance at 600nm for 100 sec at room temperature. The activity of complex II was expressed as mAbs/min/μg protein.

Protein immunoprecipitation and western blotting

A total of $10x10^6$ cells/condition were lysed with 1 ml of ice-cold Pierce™ RIPA Buffer with protease inhibitors and disrupted by repeated aspiration through a 21 gauge needle. Protein concentration was measured using BCA protein assay (cat# 23225, Thermo Fisher) and normalized across samples prior to immunoprecipitation. 500 μl of lysate was pre-cleared with 1.0 μg of appropriate control IgG (normal mouse) and 20 μl A/G PLUS agarose, for 30 minutes at 4°C. For GAPDH immunoprecipitation, 100-500 μg of total cellular protein were incubated with 2 μg of primary antibody for 1 hour at 4°C, then added 20 μl A/G beads overnight and incubated overnight at 4°C on a rocker platform. Immunoprecipitates were collected by centrifugation at 1000xg for 5 minutes at 4°C, the liquid was removed and the pellets were washed 4 times with PBS. Immune complexes were eluted by adding 40 μl of 1x electrophoresis sample buffer, boiled for 5 minutes at 95°C and analyzed by SDS-PAGE.

Protein samples from cultured cells were prepared by lysis with RIPA buffer with protease inhibitors. Protein concentration was determined using the BCA protein assay (cat# 23225, Thermo Fisher). 20-50 μg protein samples were separated by SDS-PAGE and transferred onto a PVDF membrane via iBlot (Invitrogen) transfer. Membranes were blocked in 5% non-fat milk and incubated with primary antibodies and horseradish peroxidase (HRP)-conjugated secondary antibodies. Membranes were probed with the respective antibodies and visualized using SuperSignal West Femto Maximum sensitivity substrate (cat# 34095, Thermo Scientific) and Amersham Imager 600.

Immunofluorescence staining

RAW 264.7 macrophages were plated on coverslips, allowed to grow overnight and stimulated with LPS (1 ng/ml) or Silica (50 μg/cm^2) with or without priming with LPS (1 ng/ml) for 24h. Cells were fixed with 2% paraformaldehyde in PBS for 15 minutes at 4 degrees. Cells were permeabilized with 0.1% Triton X-100 in PBS with .5% BSA for 15 min. Cells were blocked with 2% normal goat serum for 45 minutes and stained overnight for primaries for ECSIT (ab21288, Abcam) with ATP Synthase(MA1-930, Invitrogen) and HIF-1 alpha (NB100-449, Novus) with ATP Synthase. Corresponding secondary antibodies anti-rabbit Cy3 (111-164-144, Jackson Immuno) and anti-mouse Alexa 488 (A11029, Invitrogen) were added for one hour. Nuclei were stained with Hoechst (B2883, Sigma) 1mg/100ml dH_20 for one minute, washed in PBS, and mounted in gelvatol. Large area scan images were obtained on Nikon A1 confocal microscope with NIS Elements v4.4 at 60x magnification.

Isolation of mitochondria

Mitochondria were isolated from control, silica, or silica plus LPS-stimulated RAW 264.7 macrophages using a mitochondria Isolation Kit for Cultured Cells (cat# 89874, Thermo Fisher) following manufacturer instructions.

Enzyme-Linked Immunosorbents Assay

Cytokines concentration in cell supernatants were measured using ELISA kits for mouse IL-1β, TNF-α and IFN-β, according to the manufacturer's instruction, Mouse IL-1β ELISA MAX™ Standard (cat# 432601) or Mouse TNF-α ELISA MAX™ Standard (cat#430902), both purchased by Biolegend. Mouse IFN-beta DuoSet ELISA (cat#DY8234-05) was purchased by Bio-Techne. Optical density values were measured at a wavelength of 450 nm, using Cytation 5 Cell Imaging Multi-Mode Reader Biotek.

RNA analysis

Total cellular RNA was isolated from cells using TRIZOL reagent (Invitrogen) following the manufacturer's instructions. The concentration of total RNA was quantified at an absorbance of 260nm. Real-time qPCR was performed on RNA by an RT-PCR using TaqMan RNA-to Ct 1-Step Kit (Applied Biosystems), according to the manufacturer's instructions, using 500 ng of RNA as a starting material, in a total reaction volume of 10 µL PCR conditions were following: 15 min 48°C, 10 min 95°C, followed by 40 cycles with 15 sec at 95°C and 1 min at 60°C in the ABI 7300 real-time PCR system. The qRT-PCR was performed on RNA using probes specific for TNF-α (IDMm00443258_m1), IL-1β (ID Mm00434228_m1) and IFN-β (Mm00439552_s1) (Thermo Fisher). The GUSB (ID Mm01197698_m1) or GAPDH (Mm9999915_g1) (Thermo Fisher) was used for normalization; fold change was calculated using the equation described in the last. The ΔCt was calculated subtracted the Ct of GUSB or GAPDH from the Ct of the gene of interest. ΔΔCt was calculated by subtracting the ΔCt of the reference sample from ΔCt of Control sample. Fold change was generated using the equation $2^{-\Delta\Delta}$.

Metabolic assay

Stable isotope labeling. ^{13}C tracer analysis and high-resolution mass spectrometry were used to discern subtle shifts in energy substrate metabolism in specific reactions through the detection and quantification of metabolite isotopologues. RAW 264.7 macrophages ($1x10^6$/well 6-wells plate) were activated with LPS (10 ng/ml) or silica (50 µg/cm^2) dissolved in DMEM without glucose, supplemented with ^{12}C- or U^{13}C-labeled glucose (4.5 mg/l), 5% Fetal Bovine Serum dialyzed. Experiments were conducted n = 6/condition. Controls included vehicle control and the ^{12}C glucose control for each treatment condition.

Untargeted liquid chromatography-high resolution mass spectrometry (LC-HRMS). **Sample preparation.** Metabolic quenching and polar metabolite extraction were performed using ice-cold 80% methanol/0.1% formic acid at a ratio of 500 µL per $1x10^6$ adherent cells. An internal standard mix containing (D3)-creatinine and (D3)-alanine, (D4)-taurine, and (D3)-lactate (Sigma-Aldrich) was added to the sample lysates at a final concentration of 100 µM. After 3 minutes of vortexing, the supernatant was cleared of protein by centrifugation at 16,000 x g. Cleared supernatant (3 µL) was subjected to online separation and analysis. **LC-HRMS Method.** Analyses were performed by untargeted LC-HRMS. Briefly, samples were injected via a Thermo Vanquish UHPLC and separated over a reversed-phase Thermo HyperCarb porous graphite column (2.1×100mm, 3µm particle size) maintained at 55°C. For the 20 minute LC gradient, the mobile phase consisted of the following: solvent A (water/0.1% FA) and solvent B (ACN/0.1% FA). The gradient was the following: 0-1min 1% B, increase to 15%B over 5 minutes, increasing to 98%B over 5 minutes, and held at 98%B for five minutes before equilibration to starting conditions. The Thermo ID-X tribrid mass spectrometer was operated in positive and negative ion mode, scanning in Full MS mode (2 µscans) from 100 to 800 *m/z* at 70,000 resolution with an AGC target of 2 x 10^5. Source ionization setting was 3.0 kV/2.4kV spray voltage for positive and negative mode, respectively. Source gas parameters were 45 sheath gas, 12 auxiliary gas at 320°C, and 8 sweep gas. Calibration was performed prior to analysis using the PierceTM FlexMix Ion Calibration Solution (Thermo Fisher Scientific). Alignment and peak area integration were then extracted manually using Quan Browser (Thermo Fisher Xcalibur ver. 2.7). Atomic percent enrichment was calculated using the established Mass isotopomer multi-ordinate spectral analysis (MIMOSA) method to remove the natural ^{13}C abundance background [82].

Transmission electron microscopy (TEM) analysis

At one, two, and four hours after exposure, cells were fixed in 2.5% glutaraldehyde in phosphate-buffered saline (PBS) and post-fixed in 1% osmium tetroxide in PBS, dehydrated through a graded series of alcohols and embedded in Epon (Energy Beam Sciences, Agawam, MA). Thin (70-nm) sections were cut using a Reichert Ultracut S (Leica, Deerborn, MI), mounted on 200-mesh copper grids and counterstained with 2% aqueous uranyl acetate for seven minutes and 1% aqueous lead citrate for two minutes. Observation was with a JEOL 1011 transmission electron microscope (Peabody, MA). After TEM images were collected, they were formatted using Adobe Photoshop for brightness and contrast. In addition, during slide preparation, a silica particle could create stretching in the epon resin during the slicing sequence, and when stretching was severe, the silica particle could fall out of the resin. During TEM imaging, any areas where the silica particles fell out will show as bright white, causing difficulty in image focusing. These images were corrected by recoloring the white areas back to the color of the silica particles. Importantly, this may result in a slight increase in the silica particle size for the areas that were recolored. In the images at higher magnification, these areas are labeled.

Statistics

The results are presented as mean $\pm$ SD from at least three experiments, and statistical analyses were performed using the Student *t*-test or one-way ANOVA corrected for multiple comparisons using Prism software (version 7, GraphPad Software Inc). The statistical significance of differences was set at $p<0.05$.

3.3 Results

3.3.1 Crystalline silica and low dose LPS enhance glycolysis without affecting macrophage viability

To study the effect of silica on glycolysis, we utilized RAW 264.7 macrophages cell, which we have previously shown to release high concentrations of TNF-α and IL-1β in response to silica while experiencing low cytotoxicity to a wide range of concentrations of silica particles [78]. Using these macrophages, we show that both low dose LPS (1 ng/ml), that did not alter macrophage viability, as well as high dose concentrations (10 ng/ml), that induced a significant amount of cell necrosis with associated release of lactate dehydrogenase (LDH), were as effective as non-amounts of lactate in RAW 264.7 macrophages, over a period of 24h **(Figure 20A).** Addition of silica to low dose LPS-primed RAW 264.7 macrophages induced a significantly greater increase in the release of lactate compared to cells treated with LPS alone **(Figures 20B).**

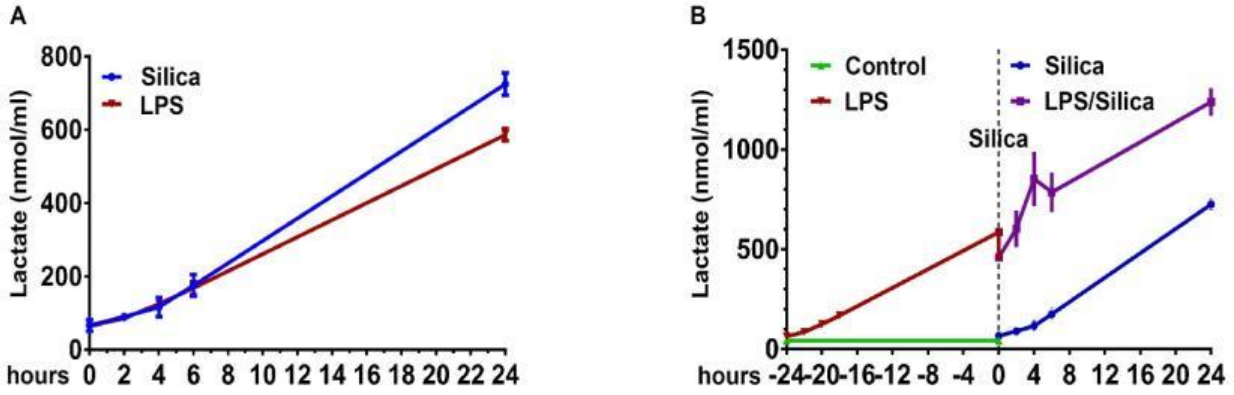

Figure 17 Lactate release from cells exposed to LPS or silica with or without priming with LPS

Under these experimental conditions, RAW 264.7 macrophages exposed to silica or LPS alone experienced low levels of necrosis, and less than 30% of the cells exhibited propidium iodide

uptake 24h after exposure **(Figure 21A-C**). In contrast, the combination of silica and LPS induced significant necrosis, with 70% of the cells up taking propidium iodine 24h after exposure **(Figure 21A-C)**. In **Figure 21C,** it is illustrated the gating strategy to differentiate cells death by early apoptosis (Annexin V^+PI^-), late apoptosis (Annexin V^+PI^+) or necrosis (Annexin V^-/PI^+). Primed cells treated with silica showed a larger number of necrotic cells (Annexin V^-/PI^+), while in response to silica or LPS alone, the number of necrotic cell death was lower. Cell death due to apoptosis was very little or absent. **** $p<0.0001$

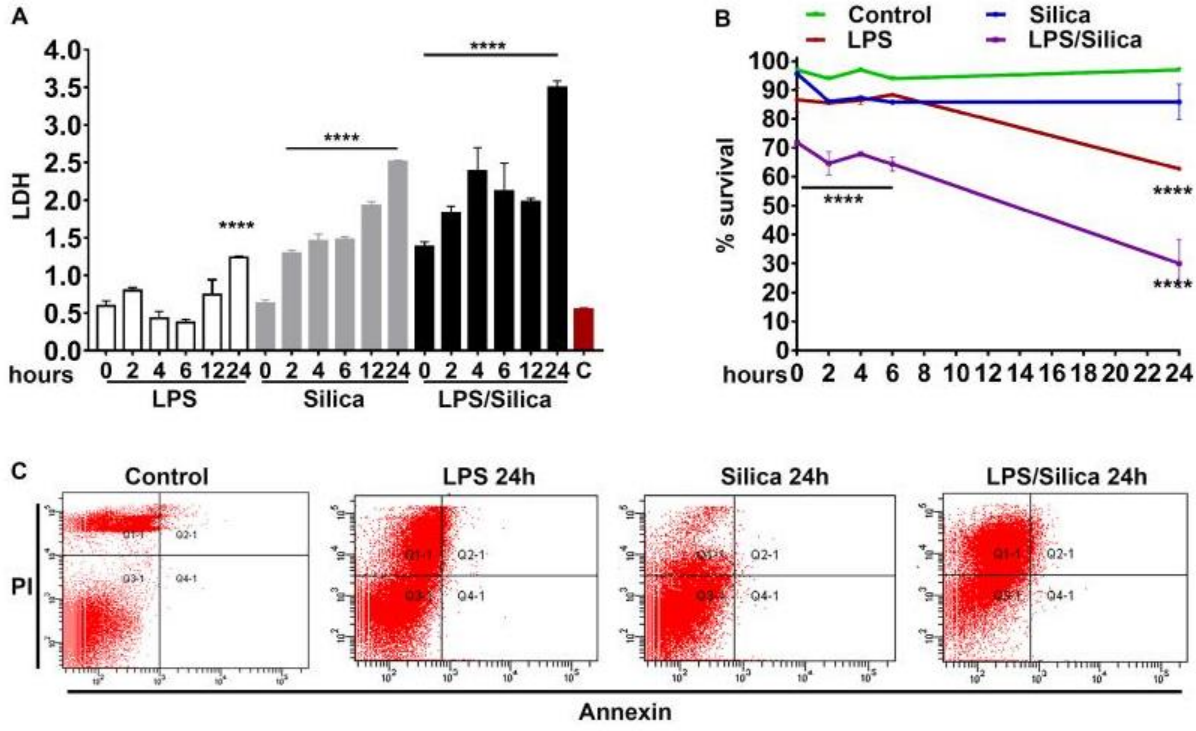

Figure 18 Assessment of cell damage and cell death

(A) LDH released from cells exposed to LPS or silica with or without priming. (B) Annexin V and Propidium iodide used to analyze cell survival by flow cytometry. (C) graph summarizing the survival of cells.

3.3.2 Silica remodels ETC-complexes activity

In response to live bacteria, but not LPS, macrophages experience mitochondrial respiratory change adaptations that contribute to their antibacterial response [48]. These effects require the phagocytosis of bacteria into a phagosome are metabolically demanding and contribute to cytokine production [48]. Similar to bacteria, macrophages phagocytose silica particles into phagosomes and attract mitochondria to these organelles **(Figure 22)** [79]. Figure 22 displays transmission electron microscopy (TEM) images obtained from a RAW 264.7 macrophages, as a function of time, following silica (20 $\mu g/cm^2$) exposure. Images illustrate the incorporation of silica particles into phagosomes, 1h after exposure (A), and the subsequent recruitment of mitochondria to the silica-containing phagosomes 2h (B), 4h (C), and 6h (D) after silica exposures.

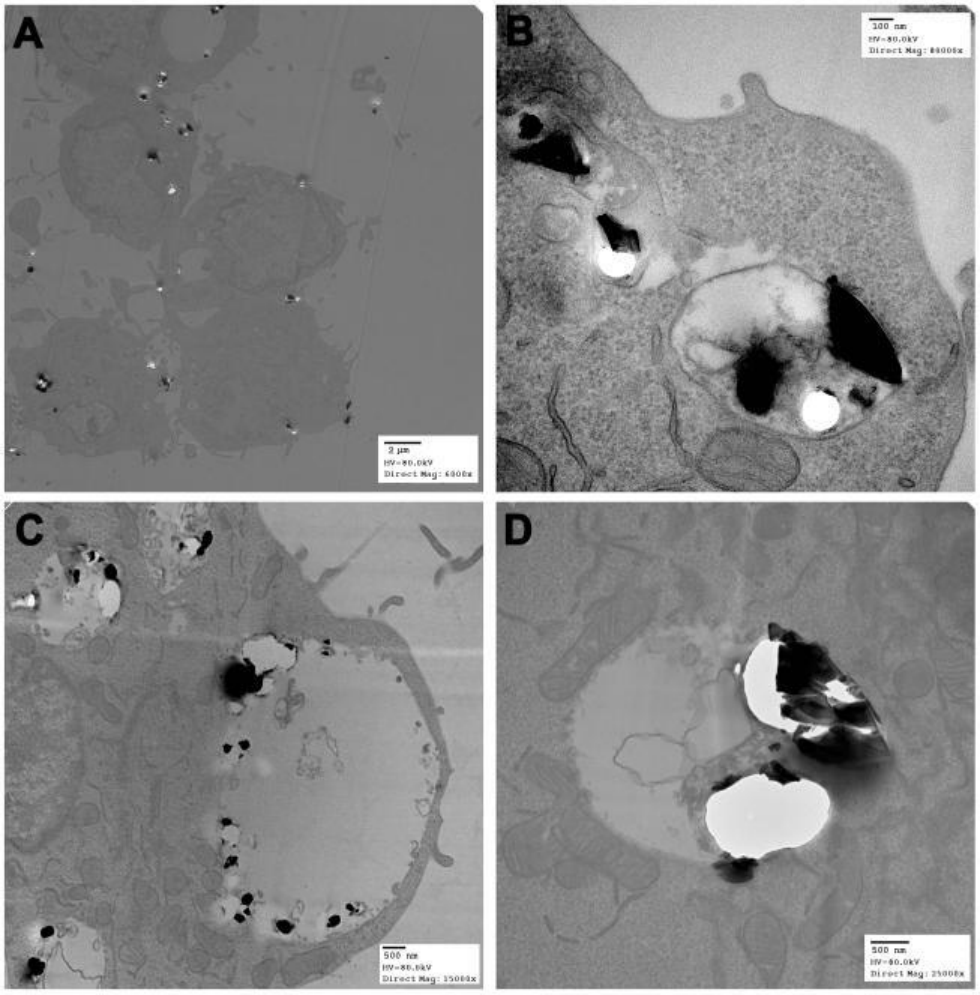

Figure 19 Macrophages recruit mitochondria to silica-containing phagosomes

Using a high-resolution respirometer, we evaluated the effects of silica on mitochondrial respiration as well as the activity and integrity of the ETC in RAW 264.7 macrophages. To evaluate the contribution of CII in the respiration of silica-activated macrophages, LPS or silica-exposed RAW 264.7 macrophages were stimulated with succinate, the CII substrate, and the oxygen flux was subsequently recorded. RAW 264.7 macrophages ($5x10^6$/chamber) were allowed to equilibrate in the chamber for about 10 minutes prior to measuring oxygen flow. Default

respirometric settings of block temperature 37°C; stir bar speed 400 rpm, and data recording every 2s were used.

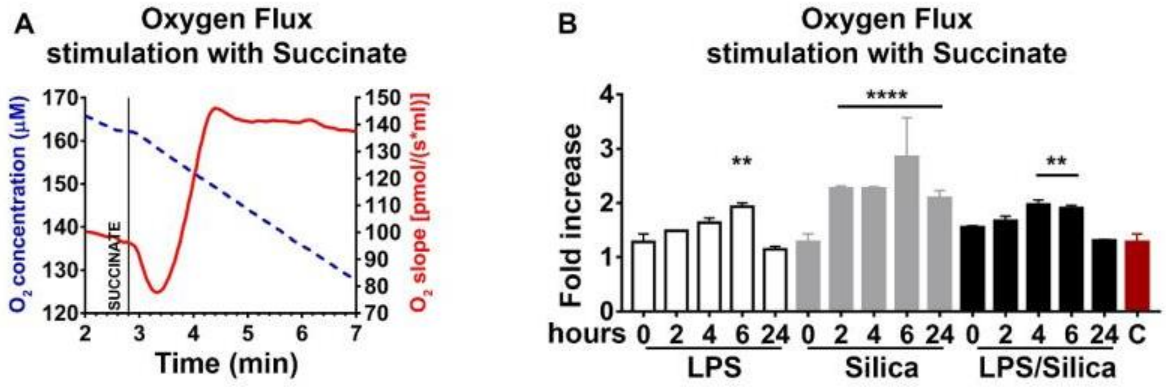

Figure 20 Assessment of Oxygen flux after stimulation of RAW 264.7 macrophages with succinate (A) Graph of oxygen flux. (B) Oxygen flux fold of increase.

Figure 23A shows the oxygen turnover (oxygen concentration, left *y*-axis, oxygen flux, right *y*-axis) by treated RAW 264.7 macrophages cells followed at the equilibrium after the addition of succinate (final concentration 10 mM). Since the variation in oxygen concentration (broken traces) are difficult to appreciate because it is very little, the slope of the oxygen concentration is also shown (solid trace), which represents the negative derivative of the oxygen concentration. Variations in oxygen flux as fold increase were measured as a ratio between the value of the O_2 slope at the equilibrium after treatment with succinate, and the value of O_2 slope at the baseline.

When healthy untreated cells were stimulated with succinate, the oxygen flux through the ETC physiologically increased **(Figure 23A)**. This physiologic response, identified 2h after exposure, was significantly augmented in cells treated with silica and, although it peaked 6h after exposure when the oxygen flux increased threefold, it lasted for the 24 h experiment. In contrast,

RAW 264.7 macrophages exposed to LPS only showed a modest, although significant, and transitory, achieving maximal response by 6h, increase in mitochondrial respiration in response to succinate, even in the presence of silica **(Figure 23B)**

To assess the production of ROS and oxygen consumption by CII in the forward direction (toward complex V, ATPase enzyme), we performed a substrate-uncoupler-inhibitor titration (SUIT) assay, wherein pre-treated RAW 264.7 macrophages were incubated with CI inhibitor (rotenone), before stimulation with CII substrate (succinate). (see Experimental section).

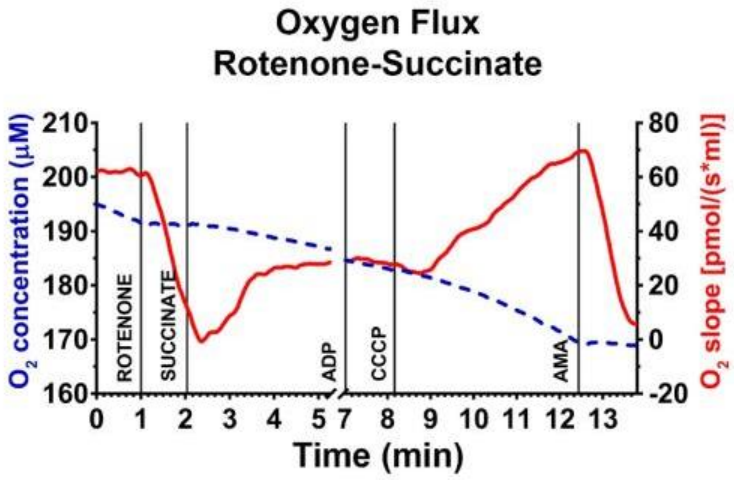

Figure 21 Graph of oxygen flux in RAW 264.7 macrophages cells following a SUIT assay protocol

Figure 24 shows the oxygen turnover (oxygen concentration, left *y*-axis, oxygen flux, right *y*-axis) by treated RAW 264.7 macrophages followed after addition of rotenone (final concentration, f.c. 0.5 µM), succinate (f.c. 10 mM), ADP (f.c. 2.5 mM), CCCP (f.c. 0.05 µM) and antimycin A (f.c. 2.5 µM). Variations in oxygen flux for each condition were measured as a ratio between the value of the O_2 slope at the equilibrium after inhibition of complex I with rotenone and stimulation of complex II with succinate, and the value of O_2 slope at the baseline.

SUIT assay performed on resting cells showed a decrease in O_2 flux after inhibition of CI, followed by a slight recovery of the O_2 consumption and flux resulting from stimulation of CII

with succinate. Subsequently, the uncoupler increased the O_2 slope above the baseline, while antimycin A, blocking CIII, cytochrome *c* reductase, suppressed the mitochondrial respiration **(Figure 24)**.

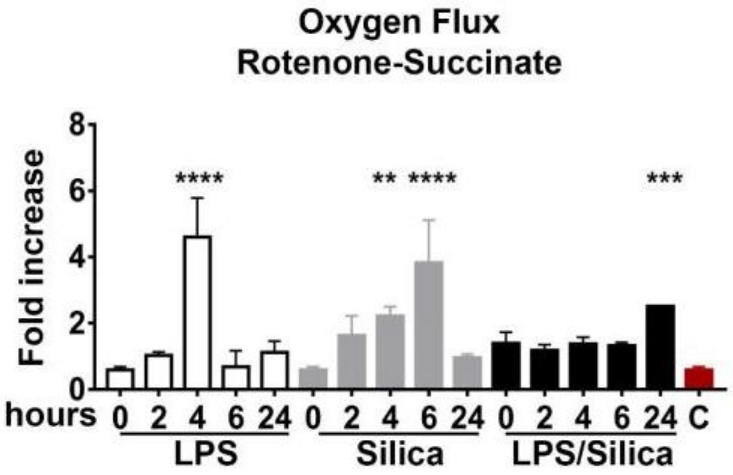

Figure 22 Oxygen flux after the inhibition of CI with rotenone and stimulation of CII with succinate

The sequential treatment of silica exposed RAW 264.7 macrophages with CI inhibitor and CII substrate confirmed the aforementioned synergistic effect of silica on the enzymatic effect of CII as these cells exhibited a significant time-dependent increase of O_2 consumption, that, although identified at 2h, it peaked at 6h exposure, proving a substantial rise in respiration only through complex II (**Figure 25**). In contrast, cells exposed to LPS showed transitory enhancement on mitochondrial respiration and was only identified 4h after treatment (**Figure 25**). Similarly, priming with LPS before silica did not alter the O_2 flux over 24h (**Figure 25)**.

The integrity of the mitochondrial membrane was also assessed by the addition of the uncoupler **(Figure 26A)**. Silica itself did not uncouple the ETC even in the presence of priming, as shown by the increase of O_2 flux after the addition of CCCP **(Figure 26C, D).** In contrast, LPS markedly damaged the mitochondrial membrane, as shown by the absence of alteration in the O_2 curve after the addition of CCCP **(Figure 26B).**

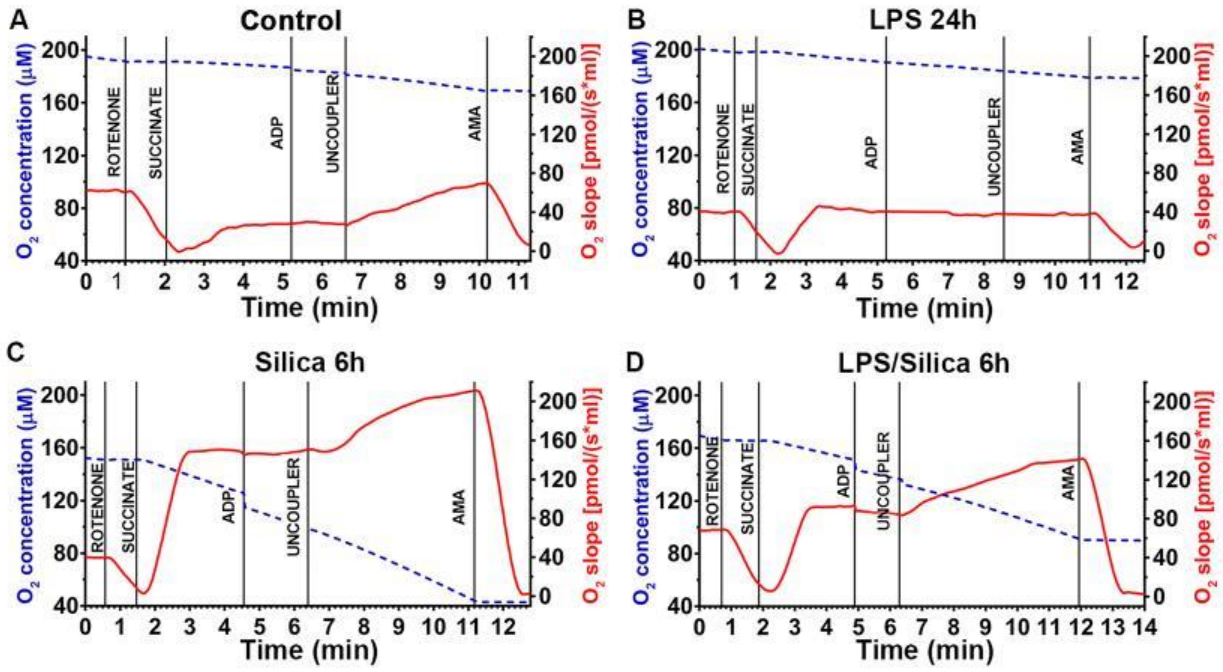

Figure 23. Graph of Oxygen flux following SUIT assay in different condition

Subsequently, we then examined the CII-mediated production of hydrogen peroxide (H_2O_2) by Amplex Red while subjecting the RAW 264.7 macrophages to the SUIT assay protocol.

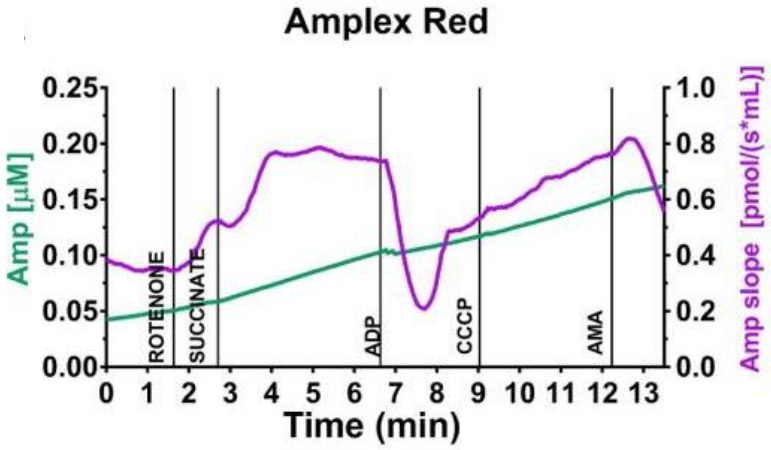

Figure 24 Graph of Amplex Red flux following a SUIT assay protocol

Figure 27 shows the production of H_2O_2 assessed following the slope (purple trace) of the concentration of the fluorescent Amplex Red assay product resorufin (green trace) while

performing a SUIT assay protocol (see Experimental section). Variations in H_2O_2 for each condition were measured as the ratio between the value of the slope at the equilibrium after the inhibition of CI with rotenone and the stimulation of CII with succinate, and the slope at the equilibrium at the baseline.

CI inhibition, followed by CII stimulation in resting RAW 264.7 macrophages, caused an immediate increment of H_2O_2 generation, similar to the one observed above during the proton leak state. Addition of ADP, inducing CII-linked oxidative phosphorylation (OXPHOS), reduced H_2O_2 production. Furthermore, the uncoupling of the system rebooted the production of H_2O_2 that was ultimately suppressed by CIII inhibition **(Figure 27).**

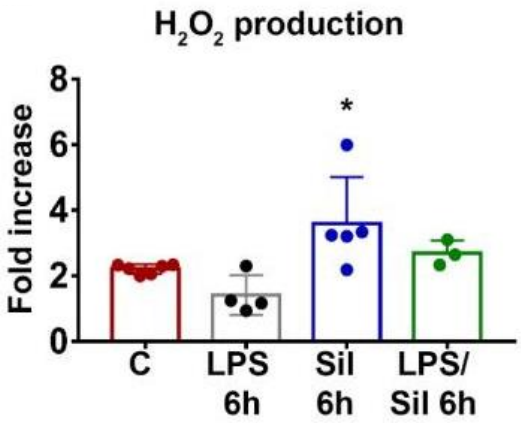

Figure 25 Fold increases H_2O_2 production after the addition of rotenone and succinate

Compared to LPS treated cells, silica exposed RAW 264.7 macrophages showed significantly higher production of H_2O_2 6h after silica exposure, confirming the increased O_2 consumption through CII **(Figure 28).** These findings suggest that silica itself acts within the cells to enhance the activity of mitochondria complex II.

3.3.3 Silica inhibits CI activity in part by reducing ECSIT expression

In addition to the high-resolution respirometry, we measured, via the enzymatic assays, the individual activity of CI and CII of silica exposed RAW 264.7 macrophages. Previously, we have shown that in RAW 264.7 macrophages, silica induces a time-dependent decrease in the expression of 39-kDa CI subunit, and subsequently, CI enzymatic activity was downregulated [78].

Mitochondria pellets were isolated from RAW 264.7 macrophages, and complex I and complex II enzymatic activity were measured spectrophotometrically and measured as mAbs/min/μg proteins**.** In agreement with our previous data, we found that silica downregulates CI activity significantly in a time-dependent fashion with a lower activity after 6h exposure, while the non-toxic concentration of LPS (1ng/ml) did not interfere with the enzyme function of this mitochondrial complex **(Figure 29)**.

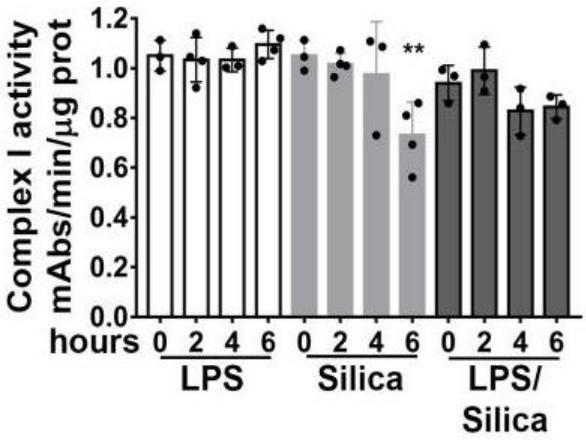

Figure 26 Measurement of Complex I activity

Conversely, CII activity was significantly enhanced by silica alone in a time-dependent manner, with the most significant increase in enzymatic activity observed 6h after exposure **(Figure 30)**. In contrast, LPS weakly stimulated the enzyme's activity at 4-6h exposure. **(Figure**

30). These findings reproduced the results of the respirometric assay, confirming a crucial role of CII in the mitochondrial response of macrophages to silica.

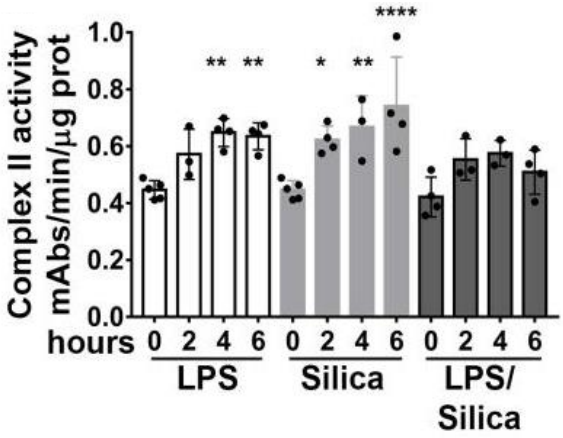

Figure 27 Measurement of Complex II activity

CI is the largest of the five ETC complexes in the mitochondrial membrane; it consists of 44 core and accessory subunits [83-85]. Among the 14 factors involved in this assembly process, Evolutionarily Conserved Signaling Intermediate In Toll Pathway (*Ecsit*) has a crucial role in the regulation of the stability and activity of the CI and subsequently the mitochondrial function [86]. To understand the mechanism that drives the decreased enzymatic activity of CI in silica-exposed RAW 264.7 macrophages, we studied the expression of *Ecsit* in the mitochondria of silica-exposed cells. *Ecsit* (37 kDa subunit) abundance was determined by western blot while using Complex IV subunit MTCO1 as markers for mitochondria and GAPDH expression as a loading control. Mitochondrial protein derived from silica-exposed cells showed a time-dependent decreased abundance of *Ecsit* 6h after silica exposure **(Figure 31).**

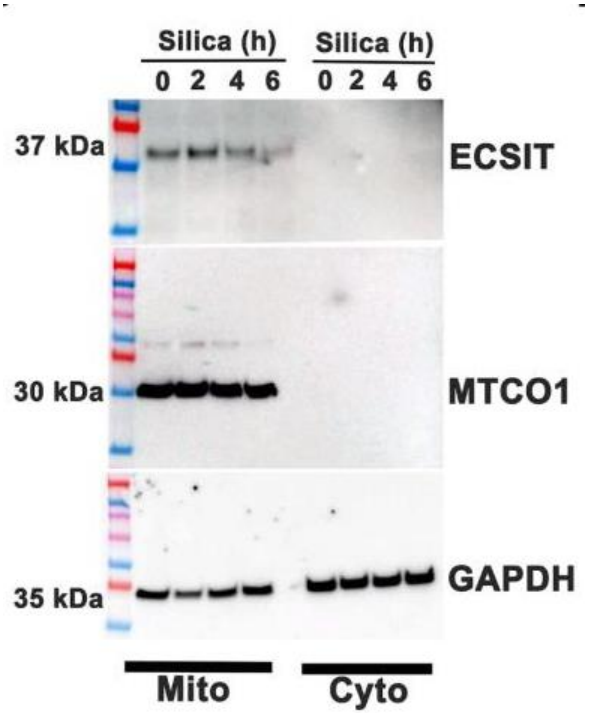

Figure 28 ECSIT abundance determined by Western Blot

This finding was confirmed by direct visualization of the protein using immunofluorescence, wherein cells treated with silica with or without LPS priming exhibit a significantly decreased content of *Ecsit* overtime with a peak after 4 hours exposure **(Figure 32)**. In contrast, cells treated with LPS did not show a substantial decrease in *Ecsit* protein and demonstrated persistent expression of *Ecsit* **(Figure 32).** In figure 32, mitochondria are visualized by staining with ATPase (red), DNA into the nuclei of cells with DAPI (4′,6-diamidino-2-phenylindole), followed by the analysis of *Ecsit* (green). Scale bar 10 microns.

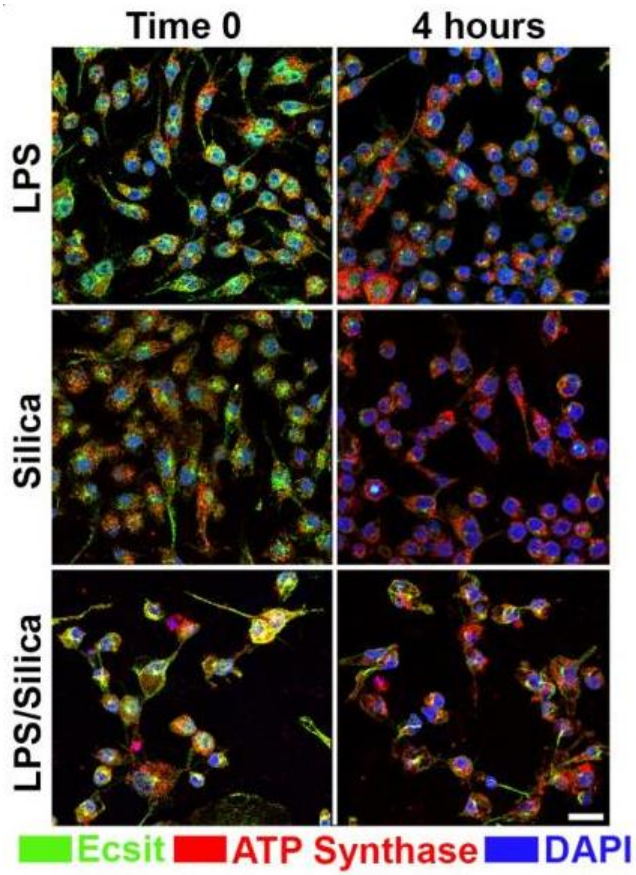

Figure 29 Ecsit protein visualized at confocal microscopy in RAW 264.7 macrophages

3.3.4 The importance of mitochondrial Complex II activity on macrophage survival to silica

Macrophages differ significantly in their response to silica, and previously we reported that the RAW 264.7 and IC-21 macrophages cell lines, which reproduce the effects of silica on primary mouse macrophages derived from BALB/c and C57BL/6J mice respectively [81, 87], differ significantly in their viability and cytokine response to silica [78]. Thus, while RAW 264.7 macrophages release TNF-α and exhibit a low rate of cell cytotoxicity in response to silica, S macrophages do not release TNF-α and experience universal cell death, even at low concentrations

of silica particles [78]. Therefore, to better understand the role of mitochondrial complex II on macrophage survival, we compared the effect of silica particles on the enzymatic activity of complex II on RAW 264.7 and IC-21 macrophages.

Our studies on cell viability demonstrated that while silica-induced significant cell cytotoxicity and LDH release in IC-21 macrophages, LPS does not impact these parameters 6-24 hours after exposure **(Figure 33A, B)**. Importantly, the addition of silica to IC-21 macrophages primed with a non-toxic concentration of LPS resulted in a synergistic effect that reduced the cell survival to 5% at 24h post-exposure **(Figure 33A, B)**.

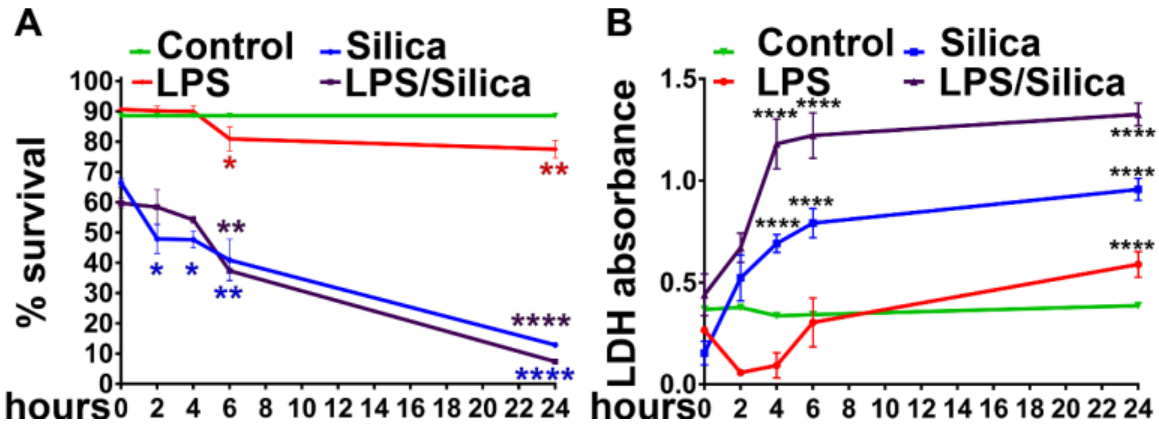

Figure 30 Graph summarizing the survival of IC-21 macrophages treated as above

(A) Annexin and PI staining, (B) LDH release.

Under these experimental conditions, LPS-stimulated IC-21 macrophages enhanced the release of lactate to a greater extent than IC-21 macrophages exposed to silica **(Figure 34)**.

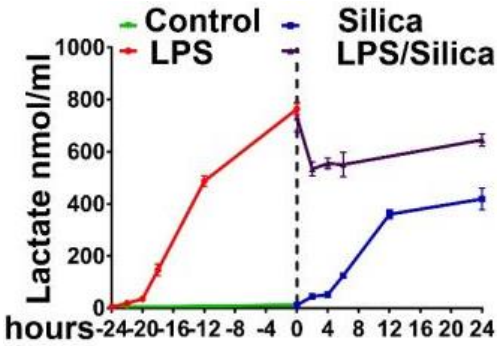

Figure 31 Lactate released in the supernatant from IC-21 macrophages

Figure 35 shows the respirometric analysis on IC-21 macrophages, illustrated as fold increase of oxygen flux after stimulation with succinate (**A**), or after the inhibition of CI with rotenone and stimulation of CII with succinate (**B**), and fold increase of the production of H_2O_2 after rotenone-succinate (**C**).

In contrast to the data described above for RAW 264.7 macrophages, stimulation of CII with succinate, in the presence or absence of rotenone-inhibition of CI, does not affect the oxygen flux, nor the ROS production in LPS treated IC-21 macrophages **(Figure 35A-C)**. In contrast to LPS, silica particles induced significant increases in the oxygen flux and ROS production in IC-21 macrophages **(Figure 35A-C),** suggesting that the enzymatic activity of CI was not affected by silica exposure on IC-21 macrophages **(Figure 36A)**. Conversely, CII activity was significantly inhibited in IC-21 by silica alone as early as 2 hours post-exposure, even after LPS priming **(Figure 36B)**

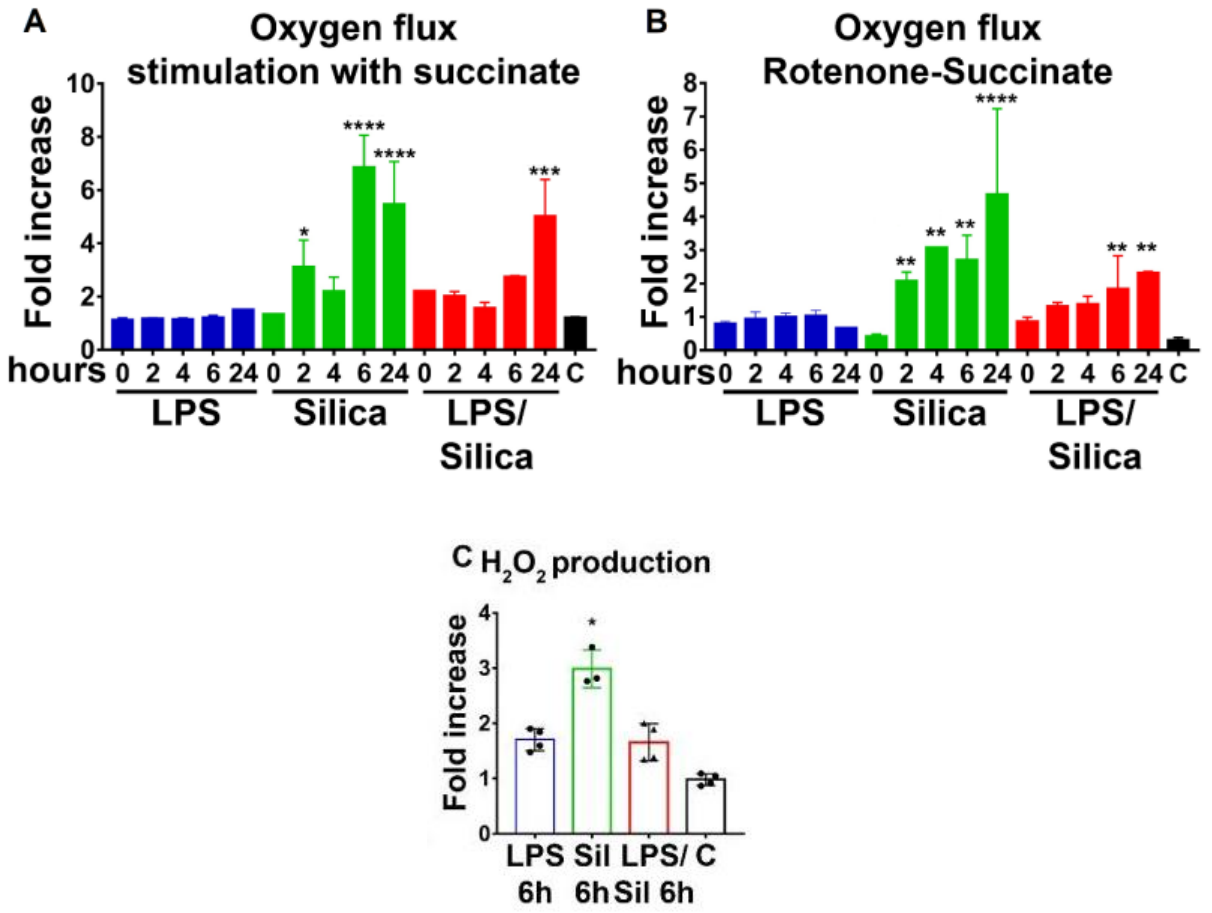

Figure 32 Respirometric analysis in IC-21 macrophages

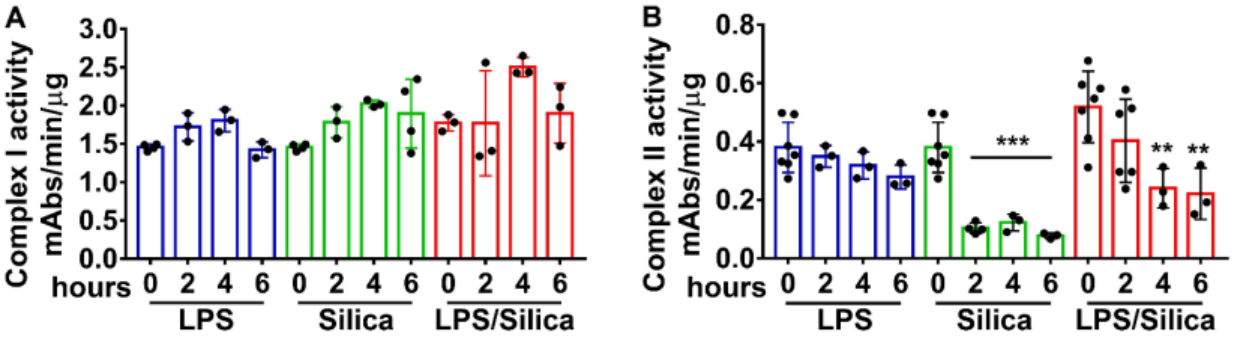

Figure 33 Measurement of CI and CII enzymatic activity in IC-21 macrophages

3.3.5 Silica and LPS exert similar effects on glucose uptake and glycolysis but differ on the effects on the TCA cycle in macrophages

LPS-stimulation of macrophages leads to perturbations of glycolysis and TCA cycle that contribute to cytokine specification [47, 88-92]. To investigate the effects of silica on glucose metabolism and the TCA cycle activity of RAW 264.7 macrophages, we fed cells with $^{13}C_6$-glucose, and conducted a stable isotope tracer analysis using high-resolution mass spectrometry to discern subtle shifts in energy substrate metabolism, through the detection and quantification of metabolite isotopologues from control, non-cytotoxic dose of silica (50 μg/cm^2), or LPS (10 ng/ml) exposed macrophages **(Figure 37 and Appendix B)**.

In figure 37 is represented a summary of metabolic changes in RAW 264.7 macrophages exposed to silica. The arrows indicate increases or decreases of metabolite normalized on control. (IDH, isocitrate dehydrogenase. SDH, succinate dehydrogenase)

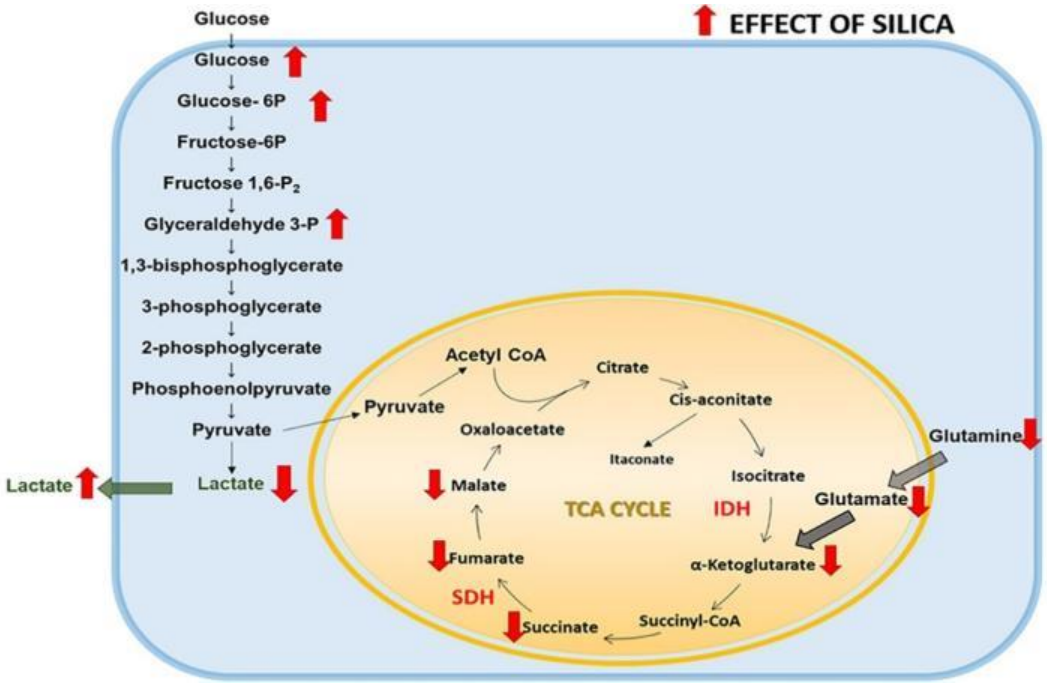

Figure 34 Schematic of metabolic changes in RAW 264.7 macrophages exposed to silica

Our LC-MS analysis revealed that when compared to control cells, both LPS, as well as silica, induce an increase in the uptake and phosphorylation of glucose, as illustrated by intracellular enrichment in glucose-6-phosphate and glyceraldehyde-3-phosphate **(Figure 38 A-C)**.

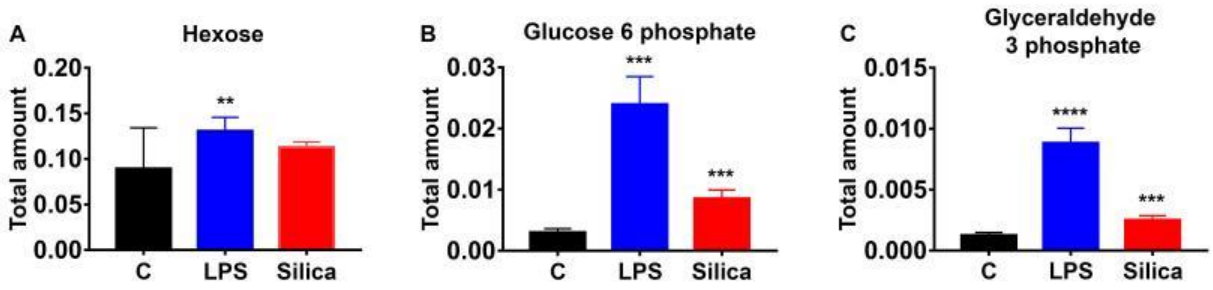

Figure 35 Intracellular total amount of hexose uptake and glycolytic metabolites glucose-6-phosphate and glyceraldehyde-3-phosphate

Isotopologues analysis shows that compared to control cells, both silica-, as well as LPS-exposed RAW 264.7 macrophages exhibit higher, but comparable, enrichment in intracellular levels of pyruvate and lactate **(Figure 39A-C)**. [Atomic percent enrichment calculated using the Mass isotopomer multi-ordinate spectral analysis (MIMOSA) method.]

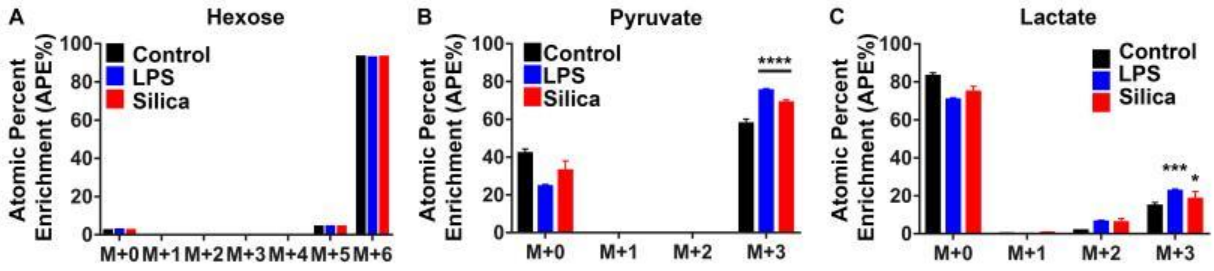

Figure 36 $^{13}C_6$ uptake and intracellular pyruvate and lactate enrichment determined by LC-HRMS

However, LPS treated RAW 264.7 macrophages demonstrate a higher ratio (0.38) of conversion of pyruvate into lactate when compared to control (0.29) or silica exposed (0.33)

macrophages **(Figure 20A and Table 1)** leading to a greater intracellular and extracellular enrichment in lactate **(Figure 40)**.

Table 1 Rate of conversion measured as a ratio between the sum of enrichment(M+1 to M+6) of 2 metabolites

	CONVERSION RATE		
	CONTROL	LPS	SILICA
PYRUVATE/HEXOSE	0.593519	0.775263	0.686769
LACTATE/PYRUVATE	0.290996	0.387615	0.330857
LACTATE/HEXOSE	0.172712	0.300503	0.227222
SUCCINATE/GLUTAMMATE	0	0.594009	0

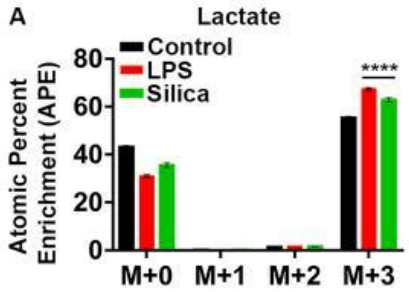

Figure 37 Changes in lactate intracellular atomic percent enrichment

Compared to control or silica-treated RAW 264.7 macrophages, LPS induces intracellular enrichment of the TCA cycle intermediates glutamine, succinate, fumarate, malate, and itaconate while maintaining the levels of citrate, alpha-ketoglutarate, and glutamate **(Figure 41A-H)**. In addition, LPS-stimulated cells show enrichment on amino acids, glutamine, proline, arginine, derived from these intermediates **(Figure 41G, I, L)**. In contrast to control or LPS-exposed macrophages, intracellular levels of citrate are not detectable in silica-exposed macrophages **(Figure 41A)**, and these silica-exposed macrophages exhibit significant reduction, compared to control or LPS-stimulated cells, in the intracellular enrichment of alpha-ketoglutarate, itaconate, succinate, fumarate, malate, glutamine, and glutamate **(Figure 41A-H)**.

Our data show that both LPS, as well as silica, influence the enzymatic activity of SDH, an enzyme that plays a fundamental role in both glycolysis and ETC **(Figure 25 and 30)**. Glutamine-dependent anaplerosis is the principal source of succinate, although the 'GABA (γ-aminobutyric acid) shunt' pathway also has a role in LPS-stimulated macrophages. Therefore, we measured the rate of conversion of glutamate into succinate **(Table 1)**. LPS treated macrophages show increased rates (0.59) of glutamate conversion to succinate. This conversion rate was not significantly altered by silica, and isotopologues analysis showed that while the baseline glutamate enrichment was comparable among control, LPS-, or silica- treated cells (M+0 to M+4); a higher enrichment of succinate was detected at M+2 only in LPS-exposed macrophages **(Figure 6M, N)**.

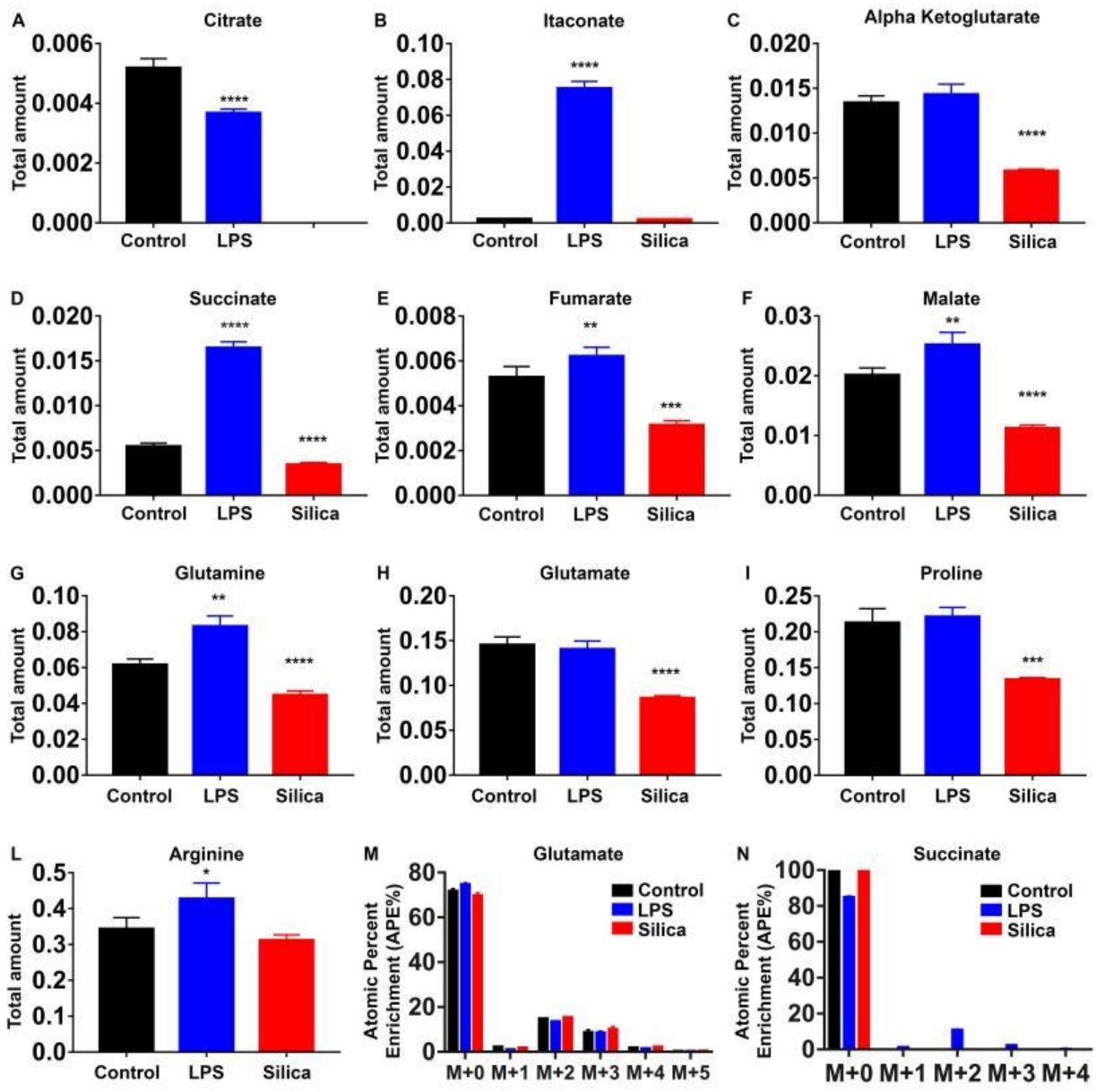

Figure 38 (A-L) Intracellular total amount of TCA cycle

(A-F) metabolites and (G-L) aminoacids. (M, N) Changes in succinate and glutamate atomic percent enrichment.

3.3.6 LPS, but not silica exposure, induces stabilization of HIF-1α, activation of caspase 1, and release of IL-1β

As we described in the introduction, LPS-stimulated macrophages exhibit altered intracellular metabolic changes that specify immune effector mechanisms such as cytokine secretion. To determine whether these changes also take place in silica exposed macrophages we correlated the metabolic changes observed in RAW 264.7 macrophages in response to silica with the production of IL-1β, TNF-α, and INF-β, three cytokines that have been implicated on the pathogenesis of silicosis [23]. In bone marrow-derived macrophages LPS enhances succinate levels, leading to succinate-mediated stabilization of HIF-1α, activation of NLRP3 inflammasome, and IL-1β production [46, 47, 93, 94]. In this work, we find that in contrast to LPS, silica reduced the intracellular levels of succinate below the baseline levels observed in unstimulated RAW 264.7 macrophages **(Figure 41D)**. To assess the correlation between the SDH activity, the level of succinate, and expression of HIF-1α, we stimulated RAW 264.7 macrophages with silica for 6 hours, with or without priming with LPS (1 ng/ml for 24h). Giving the well-known sensitivity of HIF-1α gene to oxygen tension, we documented the ability of silica or LPS to stabilize HIF-1α expression under either normoxic (O_2=20%) or hypoxic (O_2 less than 5%) conditions. Silica, as well as LPS, promoted the time related, stabilization of HIF-1α protein under normoxic conditions as demonstrated via immunoblotting **(Figure 42A upper panel)**, and confirmed by immunofluorescence. **(Figure 42B)**.

However, these changes on HIF-1α protein expression, that were accentuated by hypoxia, were associated with activation of the NLRP3 inflammasome, documented by the cleavage of the pro-caspase 1 into low molecular weight (p10) mature caspase 1, and the fragmentation and release of IL-1β only in LPS-stimulated RAW 264.7 macrophages **(Figure 42A middle panel)**.

Figure 41 A illustrates HIF-1α (110 kDa subunit) abundance, Pro-Caspase 1, Caspase 1 (10 kDa), and IL-1β (37 kDa) determined by western blot while using β-actin expression as a loading control, from proteins isolated from RAW 264.7 macrophages and exposed as described. Figure 41B represents confocal microscopy of RAW 264.7 macrophages stimulated for 6 hours with LPS (1 ng/ml) or Silica (50 μg/cm^2) in the presence or absence of priming. DNA into the nuclei of cells is visualized with DAPI (4′,6-diamidino-2-phenylindole), followed by the analysis of HIF-1α (red). Scale bar 10 microns.

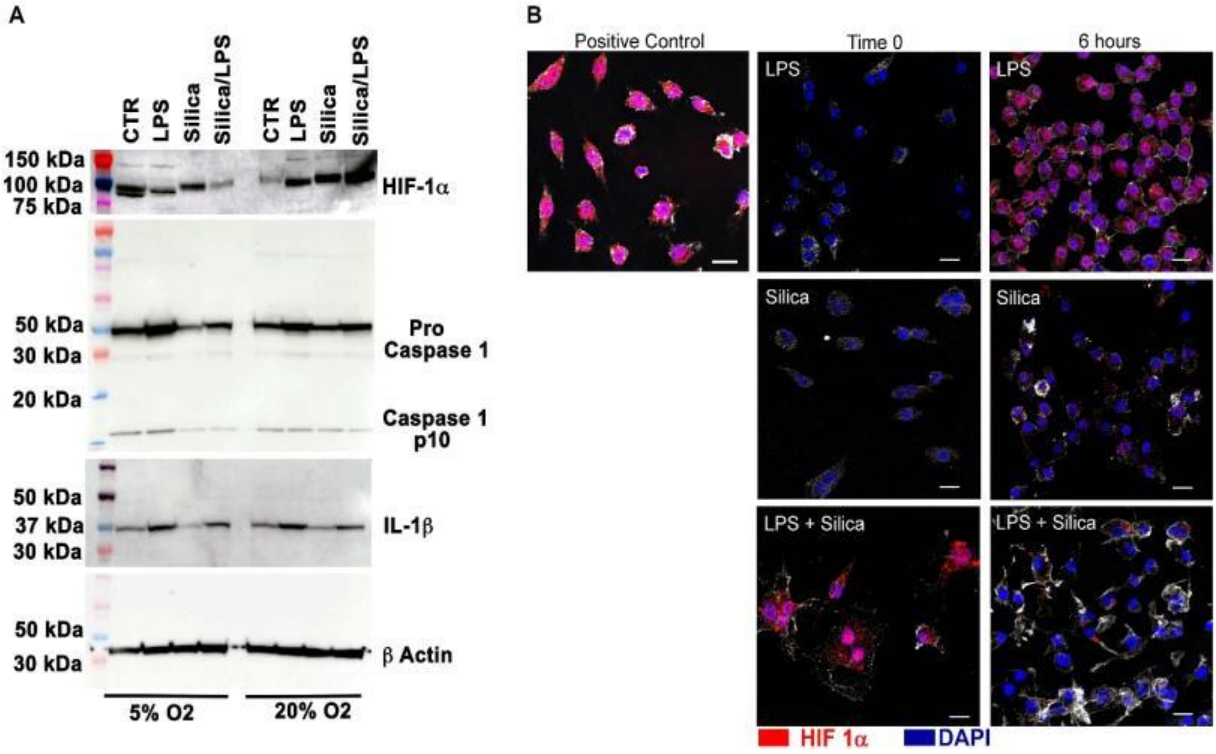

Figure 39 HIF-1α (110 kDa subunit), Pro-Caspase 1, Caspase 1 (10 kDa), and IL-1β (37 kDa) abundance determined by western blot and immunofluorescence

Yet, silica-stimulated RAW 264.7 macrophages demonstrated enhanced IL-1β mRNA and release of IL-1β peptide in culture in the absence of pro-caspase 1 activation **(Figure 43A, B)**

suggesting that silica-induced IL-1β production could take place independent of succinate associated-HIF-1α mediated NLRP3 inflammasome activation.

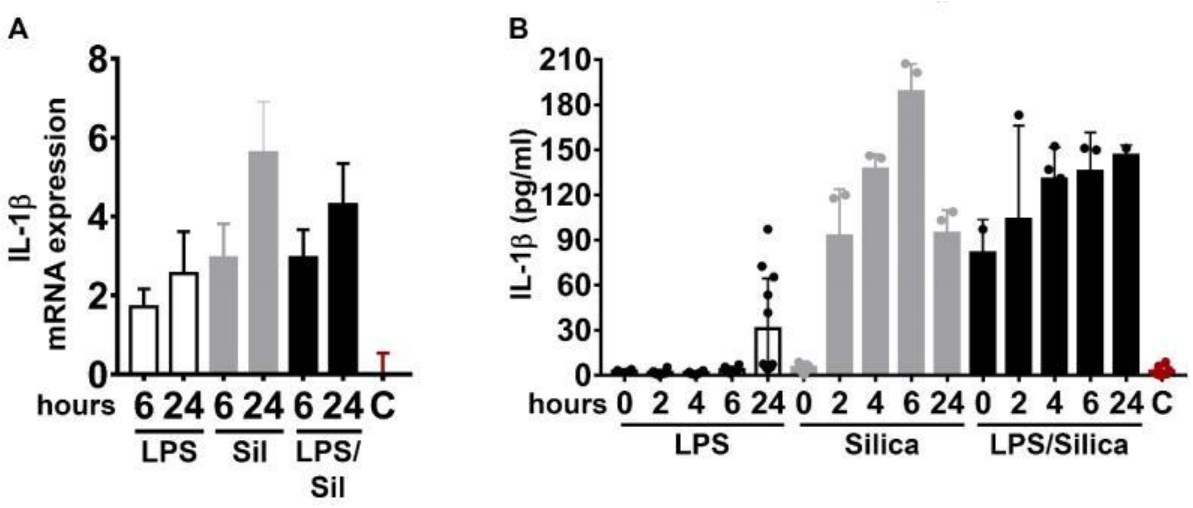

Figure 40 Measurement of IL-1 β expression and release

(A) IL-1β mRNA expression quantified by RT–PCR. (B) ELISA of IL-1β released in the supernatant.

3.3.7 Malonylation of GAPDH correlates with TNF-α production in LPS, but not in silica exposed macrophages

The citrate-derived metabolite malonyl CoA induces the malonylation of multiples proteins, including glyceraldehyde-3-phosphate dehydrogenase (GAPDH), specifically on Lysine 213. In resting cells, GAPDH sequesters the TNF-α mRNA, blocking its translation. Upon LPS stimulation, GAPDH undergoes malonylation, a reaction that facilitates the release of TNF-α mRNA for transcription and subsequent secretion [95]. In our study, we find that LPS, as well as silica, stimulated macrophages release TNF-α in a dose-dependent manner **(Figure 44A)** Compared to non-stimulated RAW 264.7 macrophages, silica, as well as LPS, enhanced GAPDH and TNF-α mRNA expression **(Figure 44B**).

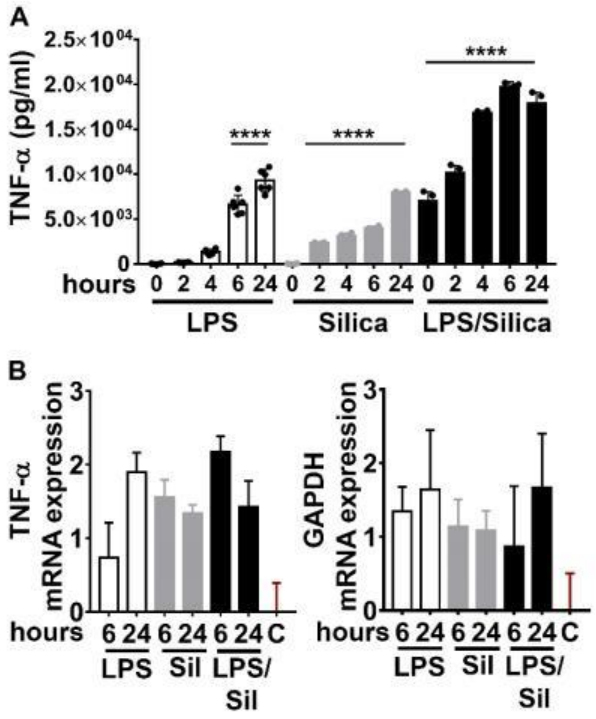

Figure 41 Assessment of TNF-α expression and release

(A) Cell supernatants examined for TNF-α secretion using ELISA. (B) TNF-α and GAPDH mRNA expression levels quantified by RT–PCR.

However, immunoprecipitation of GAPDH from protein lysates obtained from silica or LPS-stimulated RAW 264.7 macrophages identified GAPDH malonylation, in a manner that proceeded TNF-α release, exclusively in LPS exposed macrophages **(Figure 45)**.

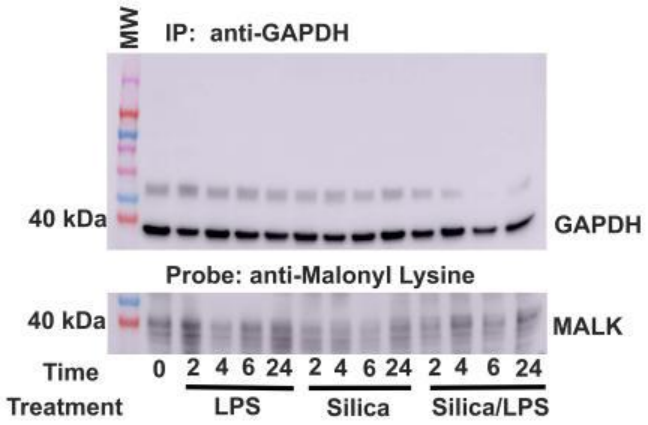

Figure 42. Samples probed with an anti-malonyl lysine (anti malk) and GAPDH expression in the immunoprecipitated (upper panel) samples

3.3.8 Decreased itaconate levels correlate with decreased IFN-β in silica-exposed macrophages

The anti-inflammatory features of the TCA metabolite itaconate have been described in LPS treated macrophages. Endogenous itaconate regulates succinate levels and limits IL-1β production in LPS-activated macrophages [96, 97]. Our data show that LPS-activated RAW 264.7 macrophages increase the intracellular amount of itaconate, while silica-activated macrophages reduce the concentrations of this TCA intermediate below control levels **(Figure 41B)**. Thus, LPS (10 ng/ml) stimulates the transcription of IFN-β in macrophages, while silica reduces the transcription and release of this mediator over a 24 h period **(Figure 46A)**. Addition of silica to LPS-primed RAW 264.7 macrophages restores the ability of RAW 264.7 macrophages to release IFN-β in a synergistic manner **(Figure 46B).**

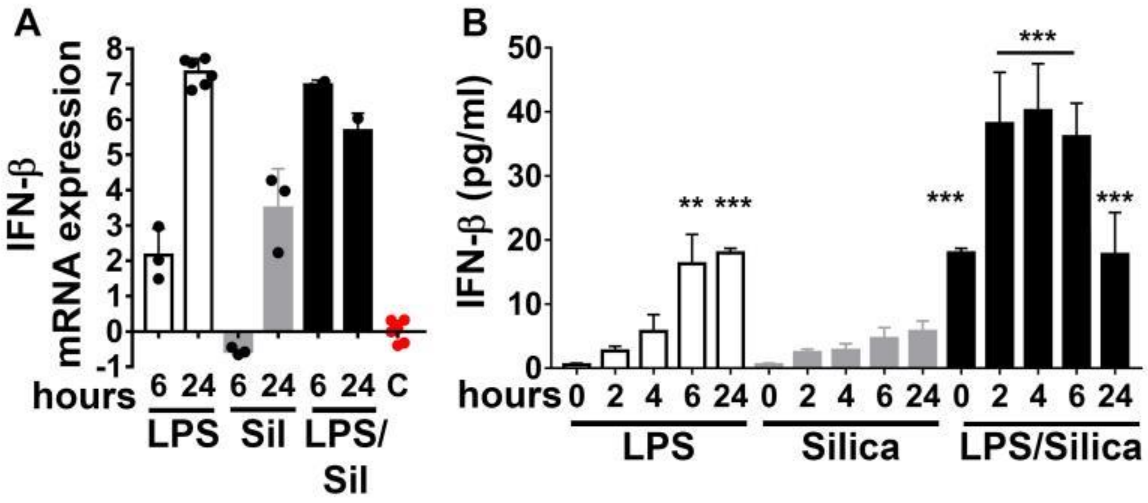

Figure 43 Assessment of IFN--β expression and release

(A) IFN--β mRNA expression levels quantified by RT–PCR. (B) Cell supernatants examined for IFN-β secretion using ELISA.

4.0 Discussion

The main finding of the current work is that in contrast to the prevalent view, respirable, sterile, crystalline silica alone is capable of inducing an innate immune response without requiring previous macrophage activation by LPS. This silica-induced activation of macrophages is different from the LPS-induced since they affect differently the CII of ETC, which plays a crucial role in macrophages survival and silica-induced inflammatory response.

In contrast to LPS, very little data are available regarding the metabolic reprogramming of macrophages in the silica-induced inflammation and subsequent development of silicosis. The purpose of our study is to elucidate critical aspects of silica-induced fibrotic inflammation, comparing the metabolic effect of low dose LPS, to silica with or without priming with LPS.

LPS-activated macrophages switch their metabolism from OXPHOS to aerobic glycolysis, "Warburg effect" [45], which consists of increased uptake of glucose, glycolysis rate and subsequent secretion of lactate, in conjunction with a reduced level of OXPHOS via the TCA cycle [47]. In our study, we found that non-toxic concentration of LPS, as well as silica, induce increased uptake of hexoses, increased concentration of intracellular glycolytic metabolites, and augmented absolute amount of intra- and extracellular lactate. Moreover, priming of macrophages with LPS before silica exposure enhanced cytotoxicity and the observed effect of LPS alone.

In a recent study, Garaude et al. reported that following phagocytosis of live bacteria by bone marrow-derived macrophages (BMDM) showed alterations in the assembly of the ETC super-complexes, consisting of reduced CI activity, and enhanced CII abundance and activity [48]. These findings were not observed when BMDM were stimulated with LPS [48]. Consistent with this work, our study demonstrates that shortly after macrophage engulfs silica particles,

phagosomes are formed and recruit mitochondria (Supplemental Figure 1). Concomitant to these ultrastructural findings, silica exposed macrophages remodel the activity of ETC and increase mitochondrial oxygen flux through CII, 2 h post-exposure, even after the inhibition of CI with rotenone (Figure 2). In contrast to silica, LPS only induces a transitory enhancement on mitochondrial respiration in the absence of mitochondrial CI inhibition by rotenone (Figure 2). The measurement of mitochondrial ROS production also revealed that silica engulfment is more efficient than LPS in the induction of mitochondrial H_2O_2 release from the activated macrophages. Priming of macrophages with LPS before silica treatment did not enhance the effect of silica on CII, nor the production of mitochondrial ROS (Figure 2). The analysis of the kinetic enzymatic activity of CI and CII also confirmed that while LPS did not alter CI activity, it only slightly enhanced CII activity, 4-6 h post-exposure, in contrast to silica that significantly decreased CI activity while simultaneously enhancing CII activity (Figure 3).

The most commonly observed CI dysfunctions are explained by alterations in CI subunits critical for its assembly. *Ecsit* is a CI subunit that plays a critical role in both the CI assembly stability and the metabolic activity of the complex in macrophages [84, 86, 98]. This confers an essential role for *Ecsit* in the antibacterial response of macrophages, due to its involvement in the recruitment of mitochondria around the site of intracellular bacteria [99], and its regulation of mitochondrial ROS production from the ETC [86]. In our study, the downregulation of *Ecsit* occurs in silica-, but not in LPS, exposed macrophages in a time-dependent manner, supporting the notion that this protein plays an essential role in the modulation of CI activity in response to silica.

IC21 macrophages, that we previously demonstrated generate more significant amounts of mitochondrial ROS, experience higher levels of cell death, and secrete lower amounts of TNF-α

than RAW 264.7 macrophages in response to silica [78], we further show evidence supporting the notion that in the absence of a functional CI, the enhanced activity of mitochondrial CII is fundamental to preserve mitochondrial respiration and the survival of macrophages in response to silica. Thus, in IC21 macrophages CI activity is preserved (Figure 4), and in contrast to RAW 264.7 macrophages, silica exposure rapidly diminishes, as early as 2h, the enzymatic activity of mitochondrial CII (Figure 4) and oxygen flux proceeds via mitochondrial CI activity leading to higher amounts of mitochondrial ROS generation that we previously show contributes to cardiolipin oxidation and cell death [78]

Our data also support the concept that although both LPS, as well as silica, stimulates aerobic glycolysis, they affect the TCA cycle in a different manner. An important difference observed between LPS- and silica-stimulated macrophages in the activity of the TCA cycle is the accumulation of succinate, which acts as a potent pro-inflammatory signal [46, 47]. LPS-induced increases in succinate can be explained by several mechanisms, including the inhibition of SDH by itaconate, as well as replenishment of succinate from glutamine through the anaplerosis by alpha-ketoglutarate, or through the GABA shunt [47]. In contrast, silica induces an overall intracellular depletion of TCA metabolites and amino acids, including succinate, alpha-ketoglutarate, fumarate, glutamine, glutamate (Figures 5 and 6). These data suggest that in contrast to LPS, silica enhances the enzymatic activity of mitochondrial CII, demonstrated here as enhanced CII-mediated mitochondrial respiratory, in the absence of a functional CI (Figure 2). This CII activity enhances TCA dynamics with consumption, rather than accumulation, of succinate. Similarly, our data show that silica does not enhance the conversion of glutamate into succinate observed in LPS exposed macrophages (Figure 5).

Activated macrophages exhibit altered metabolism that governs immune effector mechanisms such as cytokine secretion. Similar to LPS, silica treated RAW 264.7 macrophages release TNF-α and IL-1β in a dose-dependent manner (Figures 7 & 8). However, studies in LPS-stimulated macrophages show that these metabolic changes contribute to the production of TNF-α and IL-1β by different mechanisms leading to cytokine specification [47]. Thus, inhibiting glycolysis or blocking SDH in LPS-stimulated macrophages inhibits IL-1β, but not TNF-α, production [47]. In macrophages, succinate is an inflammatory signal that contributes to the activation of NLRP3 inflammasome [46, 94]. These effects, described in LPS-stimulated macrophages, are mediated via the stabilization of HIF-1α that subsequently induces transcription of HIF-1α target genes such as IL-1β [46, 47, 93, 94]. In the current work, we find that silica-stimulated RAW 264.7 macrophages demonstrate stabilization of HIF-1α, and enhanced transcription and release of IL-1β (Figure 7). However, in contrast to LPS, these silica-induced changes occur in the presence of decreased levels of intracellular succinate (figure 6) and are unrelated to NLRP3 inflammasome activation as these RAW 264.7 macrophages do not show caspase1 activation in response to silica particles alone (Figure 7). Importantly, previous reports demonstrating the ability of silica to activate the NLRP3 inflammasome were conducted in LPS-primed macrophages [19, 20, 23].

The role of TNF-α in the pathogenesis of silicosis is well recognized [24]. However, the mechanisms specifying TNF-α production by silica exposed macrophages are not entirely understood. Recent information shows that macrophages secretion of TNF-α and interferons in response to LPS is mediated, in part, via malonylation of glyceraldehyde-3-phosphate dehydrogenase (GAPDH) [95, 100, 101]. White et al. identified a role for GAPDH as a noncanonical RNA-binding protein [102]. In resting macrophages, GAPDH binds to and

suppresses the translation of inflammatory mRNAs, including IFN and TNF-α [102]. GAPDH binds NAD+ to retain mRNAs silent. LPS-induced malonylation of GAPDH requires the separation of NAD+ from the enzymatic domain to facilitate protein malonylation on lysine 213 [95]. However, in this work, we only documented lysine 213 malonylation on protein precipitates from LPS exposed RAW 264.7 macrophages, in a manner that precedes the transcription and release of TNF-α (figure 8). These data agree with previous observations linking the silica-induced TNF-α generation to NADPH- and mitochondrial ROS mediated NF-κB activation and TNF-α mRNA transcription [99, 103, 104].

The anti-inflammatory properties of itaconate, a TCA cycle metabolite generated through the decarboxylation of cis-aconitate, a product of citrate, have also been described in LPS-activated macrophages [105]. LPS-induced accumulation of itaconate, mainly due to the isocitrate dehydrogenase impairment, inhibits SDH, thereby decreasing the inflammatory response, and also regulate the IFN-β secretion [97, 106]. In this study, we observed that, while the intracellular level of itaconate is significantly augmented in LPS-activated macrophages, the same does not occur after silica engulfment, and consequently this directly correlates with the transcription and release of interferon-beta (IFN-β) in response to either LPS or silica (figure 8).

In summary, the present work indicates that upon internalization into phagolysosomes, respirable crystalline silica drives a metabolic adaptation of macrophages consisting of increased uptake of glucose, increased glycolysis rate, accompanied by an increased lactate secretion, at the expense of the OXPHOS, which becomes sustained only by an increased CII activity, while CI activity is reduced **(Figure 44)**. Given the role of CII as a component of both the TCA cycle and the ETC, its activity becomes a key regulator of macrophages' survival. Silica also modulates the TCA cycle, where not only the succinate level is measured below baseline, but also the total

intracellular level of all key TCA cycle intermediates and amino acids examined are decreased probably as a result of high demand and consumption. In contrast to LPS, these silica-induced metabolic adaptations do not correlate with IL-1β, TNF-α, production but with the suppressed release of IFN-β. Further studies are needed to validate this concept and to understand better the mechanisms that induce the release of inflammatory cytokines after the phagocytosis of silica into macrophages.

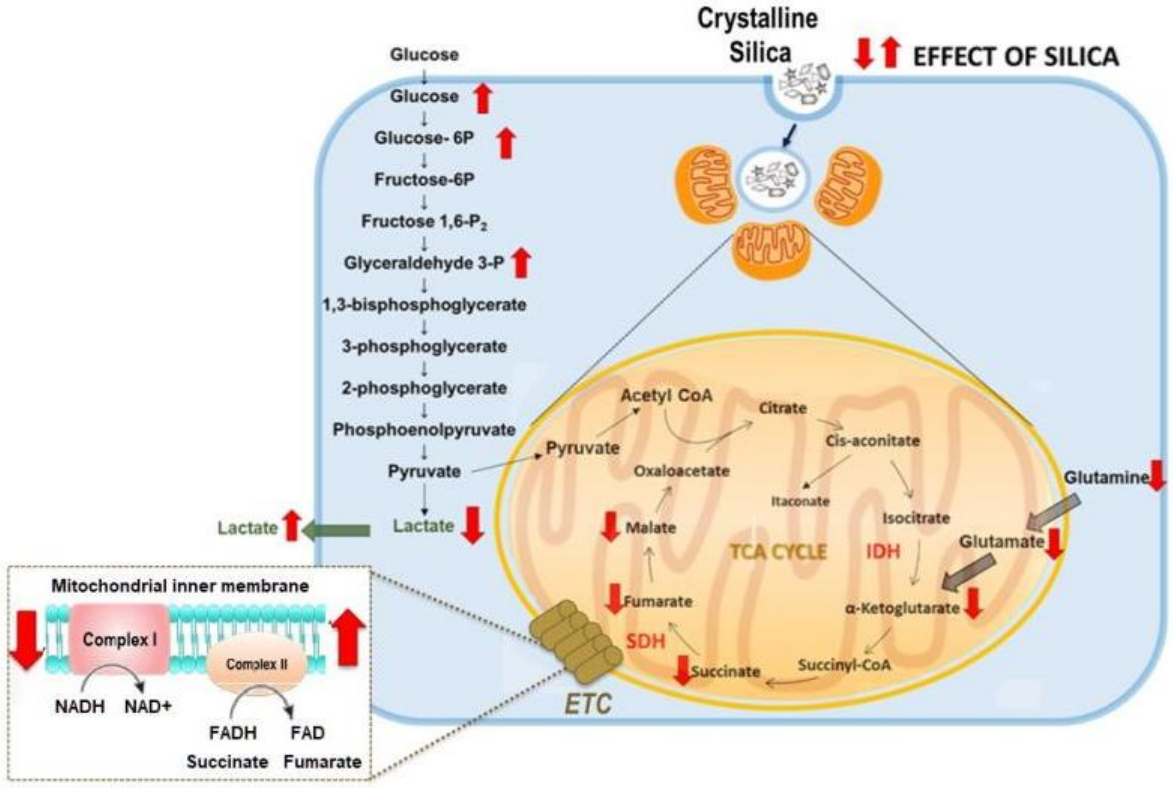

Figure 44 Graphical summary

5.0 Conclusions

Exposure of workers to crystalline silica in the US and worldwide has resulted in extensive disease and continues to be an occupational hazard for millions of workers [107, 108]. Although preventive measures have decreased the mortality attributable to silica-related lung disease, a large number of silica-exposed patients are still dying [68, 109]. Moreover, the public health concern is also raised due to the evidence that silica is a potent risk factor (4 times) for the development of tuberculosis among exposed miners and stone crushers [4, 13, 14]. Thus, even if preventable, silicosis remains a disease without specific and effective treatment available, including lung transplant [66, 70]. Therefore, understanding the pathogenic mechanisms of silicosis is essential to identify targets that predict individual susceptibility or provide a window of opportunity for therapeutic intervention.

Gulumian et al. identified CCSP, the main secreted product of Club cells, as a possible biomarker of silica-induced lung disease [71]: in healthy subjects, CCSP concentration in the BAL is between 1-2 mg/l [49], at the surface of the airways has been estimated at 100 mg/l [49], while serum CCSP levels are in the range of 10-15 μg/l [73]. Interestingly, a significant reduction of serum CCSP and lung CCSP mRNA was found in asymptomatic silica-exposed workers [43], as well as in patients suffering for sarcoidosis, asthma, and pulmonary fibrosis [49].

Nonetheless, it is still unclear the mechanisms by which silica alters the CCSP expression in the lung and the subsequent role that this altered CCSP expression plays in the pathogenesis of silicosis. Club cells might be directly damaged by silica or indirectly, secondary to lesions of other cell types within the respiratory epithelium, which are sensitive to lung irritants, or by cytotoxic mediators released from activated macrophages that have engulfed silica particles [43].

Macrophages are indeed the only immune cells involved in the removal of silica particles from the lung, and on their ability depends the development of the disease. Following the deposition of silica particles in the distal lung, resident macrophages mobilize to the site of particles and phagocytose them. The activation of the NLRP3 inflammasome is recognized as the principal mediator of the silica-induced inflammation [19, 20, 23, 44]. In LPS-activated macrophages, the metabolic switch from mitochondrial respiration to glycolysis ("Warburg effect" of aerobic glycolysis), and accumulation of succinate [45, 47] lead to the activation of NLRP3 and subsequent transcription and release of many inflammatory cytokines [46, 47, 89, 90, 92-95, 100]. In contrast, very little data are available regarding the metabolic reprogramming of macrophages in the silica-induced inflammation and subsequent development of silicosis.

In the absence of consistent data on the cellular and molecular mechanisms that regulate the innate immune response and its relevance to the regenerative program of the conductive lung epithelium, it is complicated to find a therapeutic strategy for this disease. In an attempt to fill the gaps in the literature, this dissertation describes:

1) the silica-related damage of conducting epithelium at the BADJ, represented by disorganization of Club cells, decreased proliferation of Club cells progenitor cells, and reduced CCSP content, which leads to increased TLR responses and of TNF-α release from alveolar macrophage activated in response to silica;

3) The nature of the metabolic response induced by silica in macrophages, and its contribution to cytokine specification, and the pathogenesis of silicosis. Internalization into phagolysosomes of respirable crystalline silica, in the absence of LPS, drives a metabolic adaptation of macrophage consisting of increased glycolysis, decreased mitochondrial respiration,

sustained only by CII, which becomes critical for cell survival, and it's associated to the release of inflammatory cytokines IL-1β, TNF-α, IFN-β.

5.1.1 Silica-induced damage of Club Cells alters the BADJ, compromising the regenerative capacity while eliciting macrophage activation

In this study, we provide evidence that silica causes progressive inflammation and remodeling of the small airways of the mouse lung, due to recruitment and accumulation of inflammatory cells and promotion of fibrosis (deposition of collagen and hydroxyproline) in the peribronchiolar and perivascular regions substantially at the terminal bronchial region (BADJ). This process compromises the proliferation of Club cells, which retain the capacity to regenerate both secretory and ciliated epithelial cell types during a fibrotic injury in mice.

These effect of silica are associated with noticeable disorganization of CCSP immunoreactive cells and reduced CCSP content: because of the direct cell damage and death, Club cells enhances the release of CCSP protein into the luminal surface of the epithelium, resulting in higher CCSP protein levels into BAL concomitantly to a persistent inhibition in the total lung CCSP mRNA expression, already 3 d after silica exposure.

Our findings also indicate that silica compromises the ability of CCSP expressing cells to proliferate: exposure of mice to silica results in epithelial disorganization in the absence of epithelial proliferation, as opposed to naphthalene, which resulted in depletion of CCSP cells in the presence of naphthalene-resistant stem cell proliferation. That signifies an impairment of the reparative capacity of epithelial cells within terminal bronchioles due to the silica damage.

These processes take place alongside with the establishment of adaptation in lung immune responses that include significant changes in the number of silica-laden macrophages recovered by BAL from these mice.

Previous reports indicate that Club cells function in an anti-inflammatory capacity, and CCSP-/- mice mount an exacerbated inflammatory response to infectious or environmental agents [53, 60]. Consistent with an anti-inflammatory role for CCSP in the pathogenesis of silicosis, this study provides evidence that CCSP-/- mice exposed to silica, exhibit early recruitment of PMN and macrophages in the BAL, and enhanced early TNF-α expression in BAL, correlated with prominent expression of genes of TLR7 and 9 specifically in CCSP-/- macrophages located in areas of inflammation surrounding the terminal bronchioles. Shortly after phagocytosis of silica particles, CCSP-/- macrophages exhibit increased expression of TLR7 and 9, followed by rapid secretion of type Iα, but not type Iβ, interferon, and TNF-α.

Altogether, these data support the possibility that CCSP levels in serum and respiratory secretions may constitute a valid biomarker to determine enhanced susceptibility to inflammatory responses to silica. Secondarily, the initial alteration responsible for the increased reactivity to silica could be related to the intracellular handling of silica by the macrophages rather than cell surface events.

5.1.2 Immune metabolic response of macrophages to silica

In this study, we demonstrate that in contrast to the prevalent view, respirable crystalline silica alone is capable of stimulating an innate immune response without requiring previous macrophage activation with LPS, and yet different from the one LPS-induced, since they affect

differently the CII of ETC, which plays a crucial role in macrophage survival and silica-induced inflammatory response.

Using RAW 264.7 macrophages cell lines, we demonstrate that upon internalization into phagolysosomes, respirable crystalline silica drives a metabolic adaptation of macrophage consisting of increased uptake of glucose, increased glycolysis, accompanied by an increased lactate secretion, at the expense of the mitochondrial respiration. This process is also known as the "Warburg effect" of aerobic glycolysis in LPS-activated macrophages. [45, 110].

The study of the mitochondria respiration and kinetic enzymatic activity of CI and CII demonstrate that in silica-activated macrophages, the ETC becomes sustained only by an increased CII activity, while CI activity is reduced, due to the direct impact of silica on *Ecsit* protein. Given the role of CII (succinate dehydrogenase) as a component of both the TCA cycle and the ETC, its activity becomes a key regulator of macrophages' survival.

The use of IC-21 macrophages has generated more evidence on the crucial role played by CII in the immune response and macrophages survival in response to silica. Previously we reported that IC-21 macrophages treated with silica do not release IL-1β, nor TNF-α, while LPS priming enhanced the release of inflammatory cytokines [72]. Through the study of viability and mitochondrial respiration, we proved that in the absence of a functional CI, the enhanced activity of CII is fundamental to preserve mitochondrial respiration and the survival of macrophages in response to silica.

Affecting CII, silica also modulates the TCA cycle, where not only the succinate level is decreased at 6h compared to control-treated cells, but also the total intracellular level of all key TCA cycle intermediates and amino acids examined (i.e., itaconate, glutamine, glutamate) are decreased at the same timepoint, probably as a result of high demand and consumption. In contrast

to LPS, these silica-induced metabolic adaptations do not correlate with IL-1β, TNF-α, production but with the suppressed release of IFN-β.

5.1.3 Future directions

The first line of defense against crystalline silica in the human lungs is represented by alveolar macrophages, whose unique function is to clear the lung of inhaled debris. According to the current literature, after the internalization of silica particles into macrophages, they become activated, following a process that requires the interaction between LPS and TLR4 initially. [19, 23, 44]TLRs are a class of pattern recognition receptors (PRRs) that play a fundamental role in the innate immune response because they recognize bacterial or viral pathogen-associated molecular patterns (PAMPs) and activate a cascade of event that leads to the secretion of inflammatory cytokines [111-113]. TLR, however, are classified as plasma membrane receptors, including TLR1, TLR2, TLR4, TLR5, TLR6, and TLR10 [112, 114], and endosomal receptor, including TLR3, TLR7, TLR8, and TLR9 [113, 115]. Based on this evidence, in our study, we have analyzed 10 TLR transcripts in mice and humans, and in contrast with the current literature, we found that CCSP-/- mice reported higher expression of TLR7 and TLR9 immunoreactivity was in macrophages located in areas of inflammation surrounding the terminal bronchioles.

While TLR9 is essential for recognition of bacterial DNA through the presence of unmethylated CpG motifs [116], TLR 7 recognizes purine-rich single-stranded ribonucleic acid (ssRNA) [113]. Previous studies reported that TLR9 could recognize mitochondrial DNA, which is also unmethylated at CpG motifs [117], and TLR7 and 9 have been implicated in the pathogenesis of autoimmune diseases, such as systemic lupus erythematosus, which is also correlated with a high level of Type I Interferon (IFN) [118].

Our data suggest the necessity to study the mechanism that leads to increased expression of in TLR7/9 in murine and human alveolar macrophages. Performing a microarray analysis on RAW 264.7 macrophages exposed to LPS or silica, with or without priming, help to elucidate which specific TLR is enhanced by silica alone and the contribution of LPS in the development of inflammation.

Previous studies have also found a correlation between TLR7/9 signaling and macrophage metabolic alteration. Wu et al. reported that that TLR7/9 were associated with increased glycolysis and lipid metabolism in plasmacytoid dendritic cells [119]. Specifically, TLR7 signaling induces early glycolysis and extracellular acidification rate, through HIF-1α-mediated enhanced expression [119]. Consequently, it is essential to perform the metabolomic analysis in macrophages in the presence of TLR7/9 inhibitor, to study the correlation between TRL7/9 expression and the metabolic reprogramming of alveolar macrophages.

Previous studies reported that in contrast to silicosis, BAL, and serum concentrations of CCSP are markedly increased in IPF, although most of the studied IPF patients were smokers [37], and the serum concentration of CCSP is also grown in other fibrotic lung diseases like hypersensitivity pneumonitis and those associated with some connective tissue diseases [37-39]. Based on this evidence, we have analyzed samples of lungs explants from healthy control and IPF patients, and we found classical fibrotic changes, including honeycomb and fibroblastic foci, mainly in the lower lung lobe. The flow sorting of cells from lung tissue instead revealed that fibrosis altered the proportion of cell types, but in particular, the club cells and macrophages were highly increased in IPF. In sharp contrast, the CCSP expression was reduced in the lung of silica-exposed subjects, which was associated with caspase activation and increased expression of TNF-α in silica loaded alveolar macrophages. These preliminary data suggest the necessity to study the

mechanism that regulates the different expression of CCSP in silica and IPF. Performing a single-cell RNA sequencing in these lungs helps to understand the changes in epithelial or macrophages hierarchy. Moreover, it would be essential to perform metabolic and respiratory analysis on human alveolar macrophages to determine the effects of silica on glycolysis, ETC complexes and TCA intermediates, and the correlation to the secretion of pro-inflammatory cytokines.

Macrophages are the only cells capable of removing silica particles from the lung, and the development of chronic inflammation and the progression of interstitial fibrosis is based on their survival and ability of clear silica particles. Therefore, it is possible that improving macrophages viability could reduce the burden of silica particles from the lungs of silica-exposed mice. Studies on Nitrated derivatives of fatty acids (NO_2-FA) have shown that they can modulate nuclear factor (erythroid-derived 2)-like 2 (Nrf2)-regulated antioxidant gene expression and NF-κB-dependent signaling, inhibiting DNA binding and downstream pro-inflammatory gene expression. Specifically, NO_2-FAs can induce stabilization of Nrf2 by forming a covalent adduct with determinant cysteine residues (Cys273 and 288) of Kelch-like ECH-associated protein (Keap)-1 in the cytoplasm, and inhibition of the pro-inflammatory transcriptional activity of NF-κB via alkylation of essential cysteines of the p65 (Cys 38) and p50 (Cys 62) subunits of NF- κB[120] [121], which is fundamental for the resolution of silica-induced injury [10]. In support of the anti-inflammatory role of NO_2-FAs, Ambrozova et al. reported that nitro-oleic acid (OA-NO_2) inhibits the production of reactive inflammatory mediators (ROS) and pro-inflammatory cytokines (TNF-α, and IL-1β) through downregulation of MAPKs and NF-κB, in LPS-activated RAW 264.7 and BMD macrophages [122].

Based on this evidence, we speculate that electrophilic NO_2-FA can block NF-κB activation in silica exposed macrophages, decrease the release of pro-inflammatory cytokines IL-

1β, TNF-α and interferon, improving macrophages survival, and ultimately stimulating the resolution of silica-induced pulmonary inflammation and fibrosis, resulting in a possible therapeutic intervention on the progression and resolution of lung fibrosis, and the risk of mycobacterial infections.

Appendix A Microarray Analysis Transcripts

Appendix Table 1 List of Genes

Gene bank	Symbol	Description	Gene name
NM_009652	Akt1	Thymoma viral proto-oncogene 1	Akt, PKB, PKB, Akt, PKBalpha
NM_007497	Atf1	Activating transcription factor 1	-
NM_009715	Atf2	Activating transcription factor 2	Atf-2, CRE-BP, Creb2, D130078H02Rik, D18875, MGC105211, MGC105222, Tg(Gzma-Klra1)7Wum, mXBP
NM_009740	Bcl10	B-cell leukemia/lymphoma 10	AI132454, BCL-10, C81403, CARMEN, CIPER, CLAP, ME10, cE10
NM_033601	Bcl3	B-cell leukemia/lymphoma 3	AI528691, Bcl-3
NM_009778	C3	Complement component 3	AI255234, ASP, Plp
NM_130859	Card10	Caspase recruitment domain family, member 10	AI449026, Bimp1, CARMA3
NM_172729	Nod1	Nucleotide-binding oligomerization domain containing 1	C230079P11, Card4, F830007N14Rik, Nlrc1
NM_009807	Casp1	Caspase 1	ICE, Il1bc
NM_009812	Casp8	Caspase 8	Caspase-8, FLICE, MACH, Mch5
NM_011333	Ccl2	Chemokine (C-C motif) ligand 2	AI323594, HC11, JE, MCAF, MCP-1, MCP1, SMC-CF, Scya2, Sigje
NM_009805	Cflar	CASP8 and FADD-like apoptosis regulator	2310024N18Rik, A430105C05Rik, AI646576, AU021929, CLARP, Cash, Casper, ENSMUSG00000072980, FLAME, Flip, I-FLICE, MGC103395, MRIT, c-Flip
NM_007700	Chuk	Conserved helix-loop-helix ubiquitous kinase	AI256658, Chuk1, Fbx24, Fbxo24, IKK-1, IKK-alpha, IKK1, IKK[a], IKKalpha
NM_001025432	Crebbp	CREB binding protein	AW558298, CBP, CBP, p300, KAT3A, p300, CBP
NM_009969	Csf2	Colony stimulating factor 2 (granulocyte-macrophage)	Csfgm, Gm-CSf, MGC151255, MGC151257, MGI-IGM
NM_009971	Csf3	Colony stimulating factor 3 (granulocyte)	Csfg, G-CSF, MGI-IG
NM_010336	Lpar1	Lysophosphatidic acid receptor 1	5031439C20, AI326300, Edg2, Gpcr26, Kdt2, MGC29102, lpA1, vzg-1
NM_007913	Egr1	Early growth response 1	A530045N19Rik, ETR103, Egr-1, Krox-1, Krox-24, Krox24, NGF1-A, NGFI-A, NGFIA, TIS8, Zenk, Zfp-6, Zif268, egr

Appendix Table 1 Continued

NM_007922	Elk1	ELK1, member of ETS oncogene family	Elk-1
NM_010169	F2r	Coagulation factor II (thrombin) receptor	AI482343, Cf2r, MGC28086, Par1, ThrR
NM_010175	Fadd	Fas (TNFRSF6)-associated via death domain	Mort1, FADD
NM_010177	Fasl	Fas ligand (TNF superfamily, member 6)	APT1LG1, CD178, CD95L, Fas-L, Fas-Ligand, Faslg, Tnfsf6, gld
NM_010234	Fos	FBJ osteosarcoma oncogene	D12Rfj1, c-fos
NM_010288	Gja1	Gap junction protein, alpha 1	AU042049, AW546267, Cnx43, Cx43, Cx43alpha1, Gja-1, Npm1, connexin43
NM_008311	Htr2b	5-hydroxytryptamine (serotonin) receptor 2B	5-HT2B, AJ012488, AV377389
NM_010493	Icam1	Intercellular adhesion molecule 1	CD54, Icam-1, Ly-47, MALA-2, MGC6195
NM_008337	Ifng	Interferon gamma	IFN-g, IFN-gamma, Ifg
NM_010546	Ikbkb	Inhibitor of kappaB kinase beta	AI132552, IKK-2, IKK-beta, IKK2, IKK[b], IKKbeta
NM_019777	Ikbke	Inhibitor of kappaB kinase epsilon	AW558201, IKK-i, IKKepsilon, Ikki
NM_010547	Ikbkg	Inhibitor of kappaB kinase gamma	1110037D23Rik, AI848108, AI851264, AW124339, IKK[g], NEMO
NM_010548	Il10	Interleukin 10	CSIF, Il-10
NM_010554	Il1a	Interleukin 1 alpha	Il-1a
NM_008361	Il1b	Interleukin 1 beta	IL-1beta, Il-1b
NM_008362	Il1r1	Interleukin 1 receptor, type I	CD121a, CD121b, IL-iR, Il1r-1, MGC129154
NM_031168	Il6	Interleukin 6	Il-6
NM_008363	Irak1	Interleukin-1 receptor-associated kinase 1	AA408924, IRAK, IRAK-1, IRAK1-S, Il1rak, Plpk, mPLK
NM_172161	Irak2	Interleukin-1 receptor-associated kinase 2	6330415L08Rik, AI649099, IRAK-2, MGC102586
NM_008390	Irf1	Interferon regulatory factor 1	AU020929, Irf-1
NM_010591	Jun	Jun oncogene	AP-1, Junc, c-jun
NM_010735	Lta	Lymphotoxin A	LT, LT-[a], LT-alpha, LT[a], LTalpha, Ltx, MGC117668, TNF-beta, TNFSF1, Tnfb, Tnfsf1b, hlb382
NM_010736	Ltbr	Lymphotoxin B receptor	AI256028, CD18, LTbetaR, Ltar, TNF-R-III, TNFCR, TNFR-RP, TNFR2-RP, TNFRrp, Tnfbr, Tnfrsf3
NM_011945	Map3k1	Mitogen-activated protein kinase kinase kinase 1	MAPKKK1, MEKK1, Mekk
NM_011952	Mapk3	Mitogen-activated protein kinase 3	Erk-1, Erk1, Esrk1, Prkm3, p44, p44erk1, p44mapk

Appendix Table 1 Continued

NM_010851	Myd88	Myeloid differentiation primary response gene 88	-
XM_904112	Nlrp12	NLR family, pyrin domain containing 12	Nalp12
NM_008689	Nfkb1	Nuclear factor of kappa light polypeptide gene enhancer in B-cells 1, p105	NF-KB1, NF-kappaB, NF-kappaB1, p105, p50, p50, p105
NM_019408	Nfkb2	Nuclear factor of kappa light polypeptide gene enhancer in B-cells 2, p49/p100	NF-kappaB2, lyt, p49, p49, p100, p50B, p52
NM_010907	Nfkbia	Nuclear factor of kappa light polypeptide gene enhancer in B-cells inhibitor, alpha	AI462015, Nfkbi
NM_020005	Kat2b	K(lysine) acetyltransferase 2B	A930006P13Rik, AI461839, AW536563, Pcaf
NM_011163	Eif2ak2	Eukaryotic translation initiation factor 2-alpha kinase 2	2310047A08Rik, 4732414G15Rik, AI467567, AI747578, Pkr, Prkr, Tik
NM_029780	Raf1	V-raf-leukemia viral oncogene 1	6430402F14Rik, AA990557, BB129353, Craf1, D830050J10Rik, MGC102375, Raf-1, c-Raf, v-Raf
NM_009044	Rel	Reticuloendotheliosis oncogene	c-Rel
NM_009045	Rela	V-rel reticuloendotheliosis viral oncogene homolog A (avian)	p65
NM_009046	Relb	Avian reticuloendotheliosis viral (v-rel) oncogene related B	MGC143683, MGC143684
NM_009068	Ripk1	Receptor (TNFRSF)-interacting serine-threonine kinase 1	D330015H01Rik, RIP, Rinp, Rip1
NM_138952	Ripk2	Receptor (TNFRSF)-interacting serine-threonine kinase 2	2210420D18Rik, CARD3, CARDIAK, CCK, D4Bwg0615e, RICK, RIP2
NM_015747	Slc20a1	Solute carrier family 20, member 1	AI607883, Glvr-1, Glvr1
NM_016769	Smad3	MAD homolog 3 (Drosophila)	AU022421, Madh3
NM_009283	Stat1	Signal transducer and activator of transcription 1	2010005J02Rik, AA408197
NM_019786	Tbk1	TANK-binding kinase 1	1200008B05Rik, AI462036, AW048562, MGC150301, MGC150302

Appendix Table 1 Continued

NM_009370	Tgfbr1	Transforming growth factor, beta receptor I	ALK5, AU017191, Alk-5, TbetaR-I, TbetaRI
NM_009371	Tgfbr2	Transforming growth factor, beta receptor II	1110020H15Rik, AU042018, DNIIR, RIIDN, TBR-II, TbetaR-II, TbetaRII
NM_030682	Tlr1	Toll-like receptor 1	-
NM_011905	Tlr2	Toll-like receptor 2	Ly105
NM_126166	Tlr3	Toll-like receptor 3	AI957183
NM_021297	Tlr4	Toll-like receptor 4	Lps, Ly87, Ran, M1, Rasl2-8
NM_011604	Tlr6	Toll-like receptor 6	-
NM_133211	Tlr7	Toll-like receptor 7	-
NM_133212	Tlr8	Toll-like receptor 8	-
NM_031178	Tlr9	Toll-like receptor 9	-
NM_013693	Tnf	Tumor necrosis factor	DIF, MGC151434, TNF-alpha, TNFSF2, TNFalpha, Tnfa, Tnfsf1a
NM_009397	Tnfaip3	Tumor necrosis factor, alpha-induced protein 3	A20, Tnfip3
NM_020275	Tnfrsf10b	Tumor necrosis factor receptor superfamily, member 10b	DR5, KILLER, Killer, Dr5, Ly98, MK, TRAIL-R2, TRAILR2, TRICK2A, TRICK2B, TRICKB
NM_011609	Tnfrsf1a	Tumor necrosis factor receptor superfamily, member 1a	CD120a, FPF, TNF-R, TNF-R-I, TNF-R1, TNF-R55, TNF-alphaR1, TNFAR, TNFR60, TNFRI, TNFRp55, TNFalpha-R1, Tnfr-2, Tnfr1, p55, p55-R
NM_011610	Tnfrsf1b	Tumor necrosis factor receptor superfamily, member 1b	CD120b, TNF-R-II, TNF-R2, TNF-R75, TNF-alphaR2, TNFBR, TNFR80, TNFRII, TNFalpha-R2, Tnfr-1, Tnfr2, p75
NM_011611	Cd40	CD40 antigen	AI326936, Bp50, GP39, HIGM1, IGM, IMD3, T-BAM, TRAP, Tnfrsf5, p50
NM_001033126	Cd27	CD27 antigen	S152, Tnfrsf7, Tp55
NM_009425	Tnfsf10	Tumor necrosis factor (ligand) superfamily, member 10	A330042I21Rik, AI448571, APO-2L, Ly81, TL2, Trail
NM_019418	Tnfsf14	Tumor necrosis factor (ligand) superfamily, member 14	HVEM-L, HVEML, LIGHT, LTg, Ly113
NM_023764	Tollip	Toll interacting protein	4930403G24Rik, 4931428G15Rik
NM_001033161	Tradd	TNFRSF1A-associated via death domain	9130005N23Rik, AA930854
NM_009422	Traf2	Tnf receptor-associated factor 2	AI325259
NM_011632	Traf3	Tnf receptor-associated factor 3	AI528849, CAP-1, CD40bp, CRAF1, LAP1, T-BAM, amn
NM_009539	Zap70	Zeta-chain (TCR) associated protein kinase	70kDa, AI327364, Srk, TZK, ZAP-70, mrtle, mur

Appendix B Metabolic Analysis

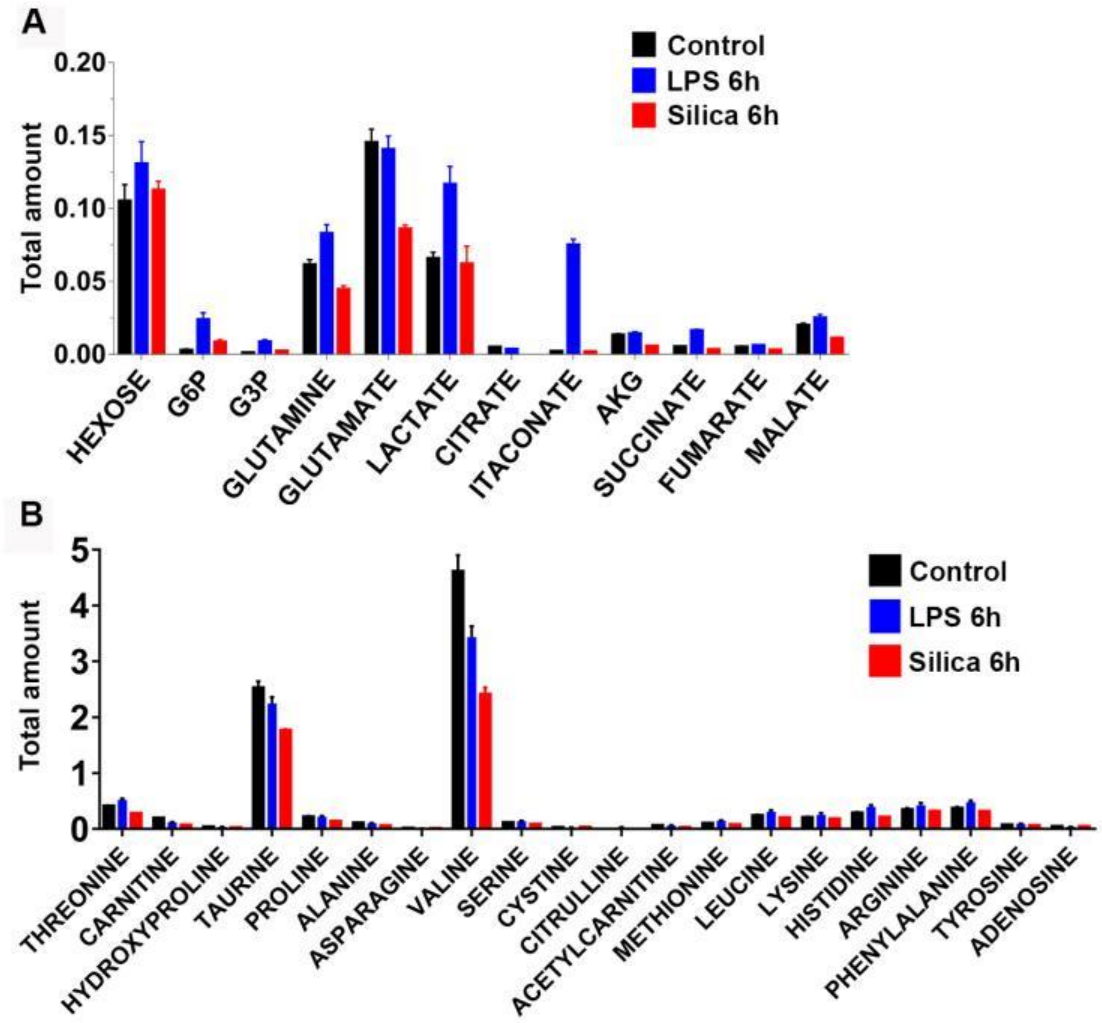

Appendix Figure 1 Schematic summarizing the key glycolysis and TCA metabolites and aminoacids significantly altered in RAW cells after LPS (blue) or Silica (red) exposure

Raw cells were exposed to vehicle, LPS (10 ng/ml) or silica (50 μg/cm^2) for 6 hours. Statistical analysis was performed on RAW cells from 6 samples for each condition. The graph shows metabolites significantly differentially regulated by LPS or Silica. Metabolites with p-value <0.05 and fold-change >10% were deemed to be statistically significant.

Bibliography

1. NIOSH, *Criteria for a recommended standard: Occupational exposure to crystalline silica. Cincinnati, OH: U.S. Department of Health, Education, and Welfare, Health Services and Mental Health Administration, National Institute for Occupational Safety and Health, DHEW (NIOSH) Publication No. 75–120.* 1974.
2. Gottesfeld, P., M. Reid, and E. Goosby, *Preventing tuberculosis among high-risk workers.* The Lancet. Global health, 2018. 6(12): p. e1274-e1275.
3. Leung, C.C., I.T.S. Yu, and W. Chen, *Silicosis.* The Lancet, 2012. 379(9830): p. 2008-2018.
4. NIOSH, *NIOSH Hazard Review; Health Effects of Occupational Exposure to Respirable Crystalline Silica. Department of Health and Human Services,CDC,NIOSH, Publication NO.2002-129.* 2002.
5. NIOSH, *Work-Related Lung Disease Surveillance System (eWoRLD). 2017-917 U.S. Department of Health and Human Services, Centers for Disease Control and Prevention, National Institute for Occupational Safety and Health, Respiratory Health Division, Morgantown, WV. Available at: <https://wwwn.cdc.gov/eworld/Data/917>*. 2017.
6. Beaudry, C., et al., *Occupational exposure to silica in construction workers: a literature-based exposure database.* Journal of occupational and environmental hygiene, 2013. 10(2): p. 71-77.
7. Yassin, A., F. Yebesi, and R. Tingle, *Occupational exposure to crystalline silica dust in the United States, 1988-2003.* Environmental health perspectives, 2005. 113(3): p. 255-260.
8. Hoy, R.F., et al., *Artificial stone-associated silicosis: a rapidly emerging occupational lung disease.* Occupational and environmental medicine, 2018. 75(1): p. 3-5.
9. NIOSH, *Occupational Safety and Health Administration; National Institute for Occupational Safety and Health. Hazard alert: worker exposure to silica during countertop manufacturing, finishing, and installation. Washington, DC: US Department of Labor, Occupational Safety and Health Administration; US Department of Health and Human Services, CDC, National Institute for Occupational Safety and Health; 2015. https://www.osha.gov/Publications/OSHA3768.pdfpdf icon.* 2015.
10. Di Giuseppe, M., et al., *Systemic inhibition of NF-kappaB activation protects from silicosis.* PloS one, 2009. 4(5): p. e5689-e5689.
11. WHO, *Elimination of silicosis, .* GOHNET news letter,, 2007: p. 1-20.
12. Chen, W., et al., *Respiratory Diseases Among Dust Exposed Workers.* Respiratory Diseases, Dr. Mostafa Ghanei (Ed.), 2012. ISBN: 978-953-307-964-6, InTech, Available from: http://www.intechopen.com/books/respiratory-diseases/respiratory-diseases-among-dust-exposed-workers.
13. Churchyard, G.J., et al., *Mycobacterial disease in South African gold miners in the era of HIV infection.* The international journal of tuberculosis and lung disease : the official journal of the International Union against Tuberculosis and Lung Disease, 1999. 3(9): p. 791-798.

14. Corbett, E.L., et al., *HIV infection and silicosis: the impact of two potent risk factors on the incidence of mycobacterial disease in South African miners.* AIDS (London, England), 2000. 14(17): p. 2759-2768.
15. Hnizdo, E. and J. Murray, *Risk of pulmonary tuberculosis relative to silicosis and exposure to silica dust in South African gold miners.* Occupational and environmental medicine, 1998. 55(7): p. 496-502.
16. Mossman, B.T. and A. Churg, *Mechanisms in the pathogenesis of asbestosis and silicosis.* Am J Respir Crit Care Med, 1998. 157(5 Pt 1): p. 1666-80.
17. ATS, *Adverse effects of crystalline silica exposure. American Thoracic Society Committee of the Scientific Assembly on Environmental and Occupational Health.* American journal of respiratory and critical care medicine, 1997. 155(2): p. 761-768.
18. Costantini, L.M., R.M. Gilberti, and D.A. Knecht, *The phagocytosis and toxicity of amorphous silica.* PloS one, 2011. 6(2): p. e14647-e14647.
19. Cassel, S.L., et al., *The Nalp3 inflammasome is essential for the development of silicosis.* Proc Natl Acad Sci U S A, 2008. 105(26): p. 9035-40.
20. Dostert, C., et al., *Innate immune activation through Nalp3 inflammasome sensing of asbestos and silica.* Science (New York, N.Y.), 2008. 320(5876): p. 674-677.
21. Beamer, C.A. and A. Holian, *Silica suppresses Toll-like receptor ligand-induced dendritic cell activation.* FASEB J, 2008. 22(6): p. 2053-63.
22. Lambeth, J.D., *NOX enzymes and the biology of reactive oxygen.* Nat Rev Immunol, 2004. 4(3): p. 181-9.
23. Hornung, V., et al., *Silica crystals and aluminum salts activate the NALP3 inflammasome through phagosomal destabilization.* Nat Immunol, 2008. 9(8): p. 847-56.
24. Piguet, P.F. and C. Vesin, *Treatment by human recombinant soluble TNF receptor of pulmonary fibrosis induced by bleomycin or silica in mice.* Eur Respir J, 1994. 7(3): p. 515-8.
25. Lassalle, P., et al., *Abnormal secretion of interleukin-1 and tumor necrosis factor alpha by alveolar macrophages in coal worker's pneumoconiosis: comparison between simple pneumoconiosis and progressive massive fibrosis.* Exp Lung Res, 1990. 16(1): p. 73-80.
26. Rokicki, W., et al., *The role and importance of club cells (Clara cells) in the pathogenesis of some respiratory diseases.* Kardiochirurgia i torakochirurgia polska = Polish journal of cardio-thoracic surgery, 2016. 13(1): p. 26-30.
27. Firth, A.L., R.A. Fernandez, and J.X.J. Yuan, *Adult Lung Stem Cells*, in *Adult Stem Cells*, K. Turksen, Editor. 2014, Springer New York: New York, NY. p. 287-318.
28. Reynolds, S.D., et al., *Secretoglobins SCGB3A1 and SCGB3A2 define secretory cell subsets in mouse and human airways.* Am J Respir Crit Care Med, 2002. 166(11): p. 1498-509.
29. Singh, G. and S.L. Katyal, *Clara cells and Clara cell 10 kD protein (CC10).* Am J Respir Cell Mol Biol, 1997. 17(2): p. 141-3.
30. Harkema, J.R., K.J. Nikula, and W.M. Haschek, *Chapter 14 - Respiratory System*, in *Fundamentals of Toxicologic Pathology (Third Edition)*, M.A. Wallig, et al., Editors. 2018, Academic Press. p. 351-393.
31. Boers, J.E., A.W. Ambergen, and F.B. Thunnissen, *Number and proliferation of clara cells in normal human airway epithelium.* Am J Respir Crit Care Med, 1999. 159(5 Pt 1): p. 1585-91.

32. Hay, J.G., et al., *Human CC10 gene expression in airway epithelium and subchromosomal locus suggest linkage to airway disease.* Am J Physiol, 1995. 268(4 Pt 1): p. L565-75.
33. Broeckaert, F., et al., *Clara cell secretory protein (CC16): features as a peripheral lung biomarker.* Ann N Y Acad Sci, 2000. 923: p. 68-77.
34. Harrod, K.S., et al., *Clara cell secretory protein decreases lung inflammation after acute virus infection.* Am J Physiol, 1998. 275(5): p. L924-30.
35. Snyder, J.C., et al., *Clara cells attenuate the inflammatory response through regulation of macrophage behavior.* Am J Respir Cell Mol Biol, 2010. 42(2): p. 161-71.
36. Guerra, S., et al., *Serum concentrations of club cell secretory protein (Clara) and cancer mortality in adults: a population-based, prospective cohort study.* The Lancet. Respiratory medicine, 2013. 1(10): p. 779-785.
37. Buendia-Roldan, I., et al., *Increased Expression of CC16 in Patients with Idiopathic Pulmonary Fibrosis.* PLoS One, 2016. 11(12): p. e0168552.
38. Doubkova, M., et al., *Prognostic significance of surfactant protein A, surfactant protein D, Clara cell protein 16, S100 protein, trefoil factor 3, and prostatic secretory protein 94 in idiopathic pulmonary fibrosis, sarcoidosis, and chronic pulmonary obstructive disease.* Sarcoidosis Vasc Diffuse Lung Dis, 2016. 33(3): p. 224-234.
39. Kokuho, N., et al., *Diagnostic Values For Club Cell Secretory Protein (CC16) in Serum of Patients of Combined Pulmonary Fibrosis and Emphysema.* COPD: Journal of Chronic Obstructive Pulmonary Disease, 2015. 12(4): p. 347-354.
40. Wang, S.X., et al., *Roles of serum clara cell protein 16 and surfactant protein-D in the early diagnosis and progression of silicosis.* J Occup Environ Med, 2007. 49(8): p. 834-9.
41. Bernard, A., et al., *Clara cell protein in human amniotic fluid: a potential marker of fetal lung growth.* Pediatr Res, 1994. 36(6): p. 771-5.
42. Boei, J.J.W.A., et al., *Xenobiotic metabolism in differentiated human bronchial epithelial cells.* Archives of toxicology, 2017. 91(5): p. 2093-2105.
43. Bernard, A.M., et al., *Early decrease of serum Clara cell protein in silica-exposed workers.* Eur Respir J, 1994. 7(11): p. 1932-7.
44. Tschopp, J. and K. Schroder, *NLRP3 inflammasome activation: the convergence of multiple signalling pathways on ROS production?* Nature Reviews Immunology, 2010. 10(3): p. 210-215.
45. Warburg, O., F. Wind, and E. Negelein, *The Metabolism of Tumors in the Body.* J Gen Physiol, 1927. 8(6): p. 519-30.
46. Mills, E.L., et al., *Succinate Dehydrogenase Supports Metabolic Repurposing of Mitochondria to Drive Inflammatory Macrophages.* Cell, 2016. 167(2): p. 457-470 e13.
47. Tannahill, G.M., et al., *Succinate is an inflammatory signal that induces IL-1beta through HIF-1alpha.* Nature, 2013. 496(7444): p. 238-42.
48. Garaude, J., et al., *Mitochondrial respiratory-chain adaptations in macrophages contribute to antibacterial host defense.* Nat Immunol, 2016. 17(9): p. 1037-1045.
49. Broeckaert, F. and A. Bernard, *Clara cell secretory protein (CC16): characteristics and perspectives as lung peripheral biomarker.* Clin Exp Allergy, 2000. 30(4): p. 469-75.
50. Morimoto, Y., et al., *Expression of clara cell secretory protein in the lungs of rats exposed to crystalline silica in vivo.* J Occup Health, 2005. 47(6): p. 504-9.
51. Reynolds, S.D., et al., *Airway injury in lung disease pathophysiology: selective depletion of airway stem and progenitor cell pools potentiates lung inflammation and alveolar dysfunction.* Am J Physiol Lung Cell Mol Physiol, 2004. 287(6): p. L1256-65.

52. Reynolds, S.D., et al., *Molecular and functional properties of lung SP cells.* Am J Physiol Lung Cell Mol Physiol, 2007. 292(4): p. L972-83.
53. Snyder, J.C., A.C. Zemke, and B.R. Stripp, *Reparative capacity of airway epithelium impacts deposition and remodeling of extracellular matrix.* Am J Respir Cell Mol Biol, 2009. 40(6): p. 633-42.
54. Fattman, C.L., et al., *Altered expression of extracellular superoxide dismutase in mouse lung after bleomycin treatment.* Free Radic Biol Med, 2001. 31(10): p. 1198-207.
55. Hong, K.U., et al., *Clara cell secretory protein-expressing cells of the airway neuroepithelial body microenvironment include a label-retaining subset and are critical for epithelial renewal after progenitor cell depletion.* Am J Respir Cell Mol Biol, 2001. 24(6): p. 671-81.
56. Giangreco, A., et al., *Stem cells are dispensable for lung homeostasis but restore airways after injury.* Proc Natl Acad Sci U S A, 2009. 106(23): p. 9286-91.
57. Rosas, I.O., et al., *MMP1 and MMP7 as potential peripheral blood biomarkers in idiopathic pulmonary fibrosis.* PLoS Med, 2008. 5(4): p. e93.
58. Saldanha, A.J., *Java Treeview--extensible visualization of microarray data.* Bioinformatics, 2004. 20(17): p. 3246-8.
59. Tusher, V.G., R. Tibshirani, and G. Chu, *Significance analysis of microarrays applied to the ionizing radiation response.* Proc Natl Acad Sci U S A, 2001. 98(9): p. 5116-21.
60. Broeckaert, F., et al., *Serum clara cell protein: a sensitive biomarker of increased lung epithelium permeability caused by ambient ozone.* Environ Health Perspect, 2000. 108(6): p. 533-7.
61. Di Giuseppe, M., et al., *Systemic inhibition of NF-kappaB activation protects from silicosis.* PLoS One, 2009. 4(5): p. e5689.
62. Dostert, C., et al., *Innate immune activation through Nalp3 inflammasome sensing of asbestos and silica.* Science, 2008. 320(5876): p. 674-7.
63. West, A.P., A.A. Koblansky, and S. Ghosh, *Recognition and signaling by toll-like receptors.* Annu Rev Cell Dev Biol, 2006. 22: p. 409-37.
64. Organization, W.H., *Silicosis.* WHO Fact Sheet 2000. 238.
65. Goodwin, S.S., et al., *Previously undetected silicosis in New Jersey decedents.* Am J Ind Med, 2003. 44(3): p. 304-11.
66. *Silicosis mortality, prevention and control - United States 1968 - 2002.* Morbidity and Mortality Weekly Report, 2005. 54(16).
67. OSHA, *Occupational exposure to crystalline silica.* Semiannual Regulatory Agenda, 2003. 68: p. 30583-30594.
68. Rosenman, K.D., M.J. Reilly, and P.K. Henneberger, *Estimating the total number of newly-recognized silicosis cases in the United States.* Am J Ind Med, 2003. 44(2): p. 141-7.
69. Yassin, A., F. Yebesi, and R. Tingle, *Occupational exposure to crystalline silica dust in the United States, 1988-2003.* Environ Health Perspect, 2005. 113(3): p. 255-60.
70. *Silicosis-related years of potential life lost before age 65 years - United States 1968-2005.* Morbidity and Mortality Weekly Report, 2008. 57(28): p. 771-775.
71. Gulumian, M., et al., *Mechanistically identified suitable biomarkers of exposure, effect, and susceptibility for silicosis and coal-worker's pneumoconiosis: a comprehensive review.* J Toxicol Environ Health B Crit Rev, 2006. 9(5): p. 357-95.
72. Bernard, A., et al., *The molecular mass and concentrations of protein 1 or Clara cell protein in biological fluids: a reappraisal.* Clin Chim Acta, 1993. 223(1-2): p. 189-91.

73. Hermans, C. and A. Bernard, *Lung epithelium-specific proteins: characteristics and potential applications as markers.* Am J Respir Crit Care Med, 1999. 159(2): p. 646-78.
74. Arsalane, K., et al., *Clara cell specific protein (CC16) expression after acute lung inflammation induced by intratracheal lipopolysaccharide administration.* Am J Respir Crit Care Med, 2000. 161(5): p. 1624-30.
75. Broeckaert, F. and A. Bernard, *Clara cell secretory protein (CC16): characteristics and perspectives as lung peripheral biomarker.* Clinical and experimental allergy : journal of the British Society for Allergy and Clinical Immunology, 2000. 30(4): p. 469-475.
76. Gilberti, R.M., G.N. Joshi, and D.A. Knecht, *The phagocytosis of crystalline silica particles by macrophages.* Am J Respir Cell Mol Biol, 2008. 39(5): p. 619-27.
77. Hamilton, M.S., V. Singh, and B.A. Warady, *Plasma cell-rich acute cellular rejection of a transplanted kidney associated with antibody to the red cell Kidd antigen.* Pediatr Transplant, 2006. 10(8): p. 974-7.
78. Fazzi, F., et al., *TNFR1/phox interaction and TNFR1 mitochondrial translocation Thwart silica-induced pulmonary fibrosis.* J Immunol, 2014. 192(8): p. 3837-46.
79. Mischler, S.E., et al., *Differential activation of RAW 264.7 macrophages by size-segregated crystalline silica.* Journal of Occupational Medicine and Toxicology, 2016. 11(1): p. 57.
80. Mischler, S.E., et al., *A multi-cyclone sampling array for the collection of size-segregated occupational aerosols.* J Occup Environ Hyg, 2013. 10(12): p. 685-93.
81. Gambelli, F., et al., *Phosphorylation of tumor necrosis factor receptor 1 (p55) protects macrophages from silica-induced apoptosis.* The Journal of biological chemistry, 2004. 279(3): p. 2020-2029.
82. Alves, T.C., et al., *Integrated, Step-Wise, Mass-Isotopomeric Flux Analysis of the TCA Cycle.* Cell Metab, 2015. 22(5): p. 936-47.
83. McKenzie, M. and M.T. Ryan, *Assembly factors of human mitochondrial complex I and their defects in disease.* IUBMB Life, 2010. 62(7): p. 497-502.
84. Guerrero-Castillo, S., et al., *The Assembly Pathway of Mitochondrial Respiratory Chain Complex I.* Cell Metabolism, 2017. 25(1): p. 128-139.
85. Nouws, J., et al., *Assembly factors as a new class of disease genes for mitochondrial complex I deficiency: cause, pathology and treatment options.* Brain, 2011. 135(1): p. 12-22.
86. Carneiro, F.R.G., et al., *An Essential Role for ECSIT in Mitochondrial Complex I Assembly and Mitophagy in Macrophages.* Cell Reports, 2018. 22(10): p. 2654-2666.
87. Fazzi, F., et al., *TNFR1/phox interaction and TNFR1 mitochondrial translocation Thwart silica-induced pulmonary fibrosis.* Journal of immunology (Baltimore, Md. : 1950), 2014. 192(8): p. 3837-3846.
88. Infantino, V., et al., *The mitochondrial citrate carrier: a new player in inflammation.* Biochem J, 2011. 438(3): p. 433-6.
89. O'Neill, L.A., *A critical role for citrate metabolism in LPS signalling.* Biochem J, 2011. 438(3): p. e5-6.
90. Mills, E.L. and L.A. O'Neill, *Reprogramming mitochondrial metabolism in macrophages as an anti-inflammatory signal.* Eur J Immunol, 2016. 46(1): p. 13-21.
91. Angajala, A., et al., *Diverse Roles of Mitochondria in Immune Responses: Novel Insights Into Immuno-Metabolism.* Front Immunol, 2018. 9: p. 1605.

92. Mills, E.L., B. Kelly, and L.A.J. O'Neill, *Mitochondria are the powerhouses of immunity.* Nat Immunol, 2017. 18(5): p. 488-498.
93. Corcoran, S.E. and L.A. O'Neill, *HIF1alpha and metabolic reprogramming in inflammation.* J Clin Invest, 2016. 126(10): p. 3699-3707.
94. Mills, E. and L.A. O'Neill, *Succinate: a metabolic signal in inflammation.* Trends Cell Biol, 2014. 24(5): p. 313-20.
95. Galvan-Pena, S., et al., *Malonylation of GAPDH is an inflammatory signal in macrophages.* Nat Commun, 2019. 10(1): p. 338.
96. Mills, E.L., et al., *Itaconate is an anti-inflammatory metabolite that activates Nrf2 via alkylation of KEAP1.* Nature, 2018. 556(7699): p. 113-117.
97. Lampropoulou, V., et al., *Itaconate Links Inhibition of Succinate Dehydrogenase with Macrophage Metabolic Remodeling and Regulation of Inflammation.* Cell metabolism, 2016. 24(1): p. 158-166.
98. Vogel, R.O., et al., *Cytosolic signaling protein Ecsit also localizes to mitochondria where it interacts with chaperone NDUFAF1 and functions in complex I assembly.* Genes Dev, 2007. 21(5): p. 615-24.
99. West, A.P., et al., *TLR signalling augments macrophage bactericidal activity through mitochondrial ROS.* Nature, 2011. 472(7344): p. 476-80.
100. Galvan-Pena, S. and L.A. O'Neill, *Metabolic reprograming in macrophage polarization.* Front Immunol, 2014. 5: p. 420.
101. Meiser, J., et al., *Pro-inflammatory Macrophages Sustain Pyruvate Oxidation through Pyruvate Dehydrogenase for the Synthesis of Itaconate and to Enable Cytokine Expression.* J Biol Chem, 2016. 291(8): p. 3932-46.
102. White, M.R. and E.D. Garcin, *The sweet side of RNA regulation: glyceraldehyde-3-phosphate dehydrogenase as a noncanonical RNA-binding protein.* Wiley Interdiscip Rev RNA, 2016. 7(1): p. 53-70.
103. Scarfi, S., et al., *Ascorbic acid pre-treated quartz stimulates TNF-alpha release in RAW 264.7 murine macrophages through ROS production and membrane lipid peroxidation.* Respir Res, 2009. 10: p. 25.
104. Naik, E. and V.M. Dixit, *Mitochondrial reactive oxygen species drive proinflammatory cytokine production.* J Exp Med, 2011. 208(3): p. 417-20.
105. Michelucci, A., et al., *Immune-responsive gene 1 protein links metabolism to immunity by catalyzing itaconic acid production.* Proc Natl Acad Sci U S A, 2013. 110(19): p. 7820-5.
106. Cordes, T., et al., *Immunoresponsive Gene 1 and Itaconate Inhibit Succinate Dehydrogenase to Modulate Intracellular Succinate Levels.* J Biol Chem, 2016. 291(27): p. 14274-84.
107. NIOSH, *NIOSH Hazard Review; Health Effects of Occupational Exposure to Respirable Crystalline Silica*. 2002, Department of Health and Human Services,CDC,NIOSH, Publication NO.2002-129.
108. WHO. *Silicosis Fact Sheet N° 238*. 2000 [cited 2013 August 6]; Available from: http://www.who.int/peh/Occupational_health/OCHweb/OSHpages/OSHDocuments/Factsheets/Silicosis.htm.
109. Centers for Disease, C. and Prevention, *Silicosis mortality, prevention, and control--United States, 1968-2002.* MMWR Morb Mortal Wkly Rep, 2005. 54(16): p. 401-5.
110. Warburg, O., *On the origin of cancer cells.* Science, 1956. 123(3191): p. 309-14.

111. Takeda, K., T. Kaisho, and S. Akira, *Toll-Like Receptors.* Annual Review of Immunology, 2003. 21(1): p. 335-376.
112. Brubaker, S.W., et al., *Innate immune pattern recognition: a cell biological perspective.* Annu Rev Immunol, 2015. 33: p. 257-90.
113. Petes, C., N. Odoardi, and K. Gee, *The Toll for Trafficking: Toll-Like Receptor 7 Delivery to the Endosome.* Frontiers in Immunology, 2017. 8(1075).
114. Leifer, C.A. and A.E. Medvedev, *Molecular mechanisms of regulation of Toll-like receptor signaling.* Journal of Leukocyte Biology, 2016. 100(5): p. 927-941.
115. Ewald, S.E. and G.M. Barton, *Nucleic acid sensing Toll-like receptors in autoimmunity.* Current Opinion in Immunology, 2011. 23(1): p. 3-9.
116. Takeda, K., T. Kaisho, and S. Akira, *Toll-like receptors.* Annu Rev Immunol, 2003. 21: p. 335-76.
117. Bao, W., et al., *Toll-like Receptor 9 Can be Activated by Endogenous Mitochondrial DNA to Induce Podocyte Apoptosis.* Scientific Reports, 2016. 6(1): p. 22579.
118. Ewald, S.E. and G.M. Barton, *Nucleic acid sensing Toll-like receptors in autoimmunity.* Curr Opin Immunol, 2011. 23(1): p. 3-9.
119. Wu, D., et al., *Type 1 Interferons Induce Changes in Core Metabolism that Are Critical for Immune Function.* Immunity, 2016. 44(6): p. 1325-1336.
120. Khoo, N.K.H., et al., *Electrophilic fatty acid nitroalkenes regulate Nrf2 and NF-κB signaling:A medicinal chemistry investigation of structure-function relationships.* Scientific reports, 2018. 8(1): p. 2295-2295.
121. Cui, T., et al., *Nitrated fatty acids: Endogenous anti-inflammatory signaling mediators.* J Biol Chem, 2006. 281(47): p. 35686-98.
122. Ambrozova, G., et al., *Nitro-oleic acid modulates classical and regulatory activation of macrophages and their involvement in pro-fibrotic responses.* Free radical biology & medicine, 2016. 90: p. 252-260.